DEVELOPMENT OF PSYCHOLOGICAL STRESS DETECTION SYSTEM USING BIO-SIGNALS

A THESIS

Submitted in partial fulfilment of the

requirements for the award of the degree

of

DOCTOR OF PHILOSOPHY

Submitted by

Amandeep Cheema

Registration number- 901504001

Under the supervision of

Dr. Mandeep Singh

Associate Professor

Department of Electrical and Instrumentation Engineering, TIET, Patiala

Department of Electrical and Instrumentation Engineering

THAPAR INSTITUTE OF ENGINEERING AND TECHNOLOGY, PATIALA

(Declared as Deemed-to-be-University u/s 3 of the UGC Act, 1956)

Punjab (India)-147004

November 2020

DECLARATION

I hereby certify that the work presented in the thesis entitled "**DEVELOPMENT OF PSYCHOLOGICAL STRESS DETECTION SYSTEM USING BIO-SIGNALS**" in the partial fulfilment of the requirements for the award of the degree of **DOCTOR OF PHILOSOPHY** submitted in the Department of Electrical and Instrumentation Engineering, Thapar Institute of Engineering and Technology, Patiala, is an authentic record of my own research work carried out under the supervision of **Dr. Mandeep Singh**, Associate Professor, Electrical and Instrumentation Engineering Department, Thapar Institute of Engineering and Technology, Patiala, India.

The matter presented in this thesis has not been submitted by me for the award of any other degree of this or any other institute.

Date : 26 Oct 2020

Amandeep Cheema

This is to certify that the above statement made by the student is correct to the best of my knowledge.

Date : 26 Oct. 2020

Dr. Mandeep Singh
Associate Professor, EIED
Thapar Institute of Engineering and Technology

ACKNOWLEDGEMENTS

First of all, I would like to thank the almighty for the strength and blessings and for letting me witness the day when I am completing my thesis.

I am thankful to **Professor (Dr.) Prakash Gopalan**, Director, Thapar Institute of Engineering and Technology, Patiala, and **Professor (Dr.) Rafat Siddique**, Dean of Research & Sponsored Projects, Thapar Institute of Engineering and Technology, Patiala, for providing me with the facilities to complete this research work. I would like to express my heartfelt gratitude towards **Professor (Dr.) R.S. Kaler**, Head, Department of Electrical and Instrumentation Engineering, Thapar Institute of Engineering and Technology, Patiala.

I would like to express my heartfelt gratitude to my supervisor **Dr. Mandeep Singh**, Associate Professor, Electrical and Instrumentation Engineering Department, Thapar Institute of Engineering for his continuous inspiration, support, guidance, motivation and patience. Sir, I will always be indebted as you helped me with all your wisdom and motivated me to achieve the research goals. You also encouraged me and introduced me to project-writing. I feel grateful and blessed to have worked under you. I am also thankful to your wife Dr. Varinderjit Kaur for helping me during project-writing and proof-reading.

I would also like to thank the esteemed members of my Doctoral Committee: **Dr. Deepti Mittal, Dr. Saurabh Bhardwaj and Dr. Siddharth Sharma** for their patience, encouragement, and constructive criticism.

This work was supported by **Department of Science and Technology (DST)**, Government of India, under the project titled "Design and development of phonocardiography based psychological stress classifier", [project number- **SR/WOS-B/202/2016**].

I am also thankful to Dr. Sarjeevan Toor, practicing physician, SPS Hospital (formerly, Apollo Hospital), Ludhiana, India for guidance during data acquisition.

I am thankful to Aman Sandhu and Alisha Malhotra for assistance during data acquisition. I am thankful to my friend Mohit for those never-ending discussions and brain-storming sessions. I am grateful to Gautam for pushing me and motivating me to achieve the goals. I am thankful to my Ph.D. friends Arun, Jitender, Arshdeep, Manjeet,

Neeru, Kriti, Kamal and Gurleen for the relaxing breaks and for helping me to work better.

I am indebted to my mother, **Jagjit Kaur**, my father Ajaib Singh Hira, my sister Preet Kamal Chima and Tippi for all the smiles you brought to my face. You are my strength and without your vision, this dream would never be a reality. Thanks for showing trust and motivating me. I am thankful to my sister for proof-reading and to my mother for being the pillar of strength who stands firmly for the family to flourish and achieve higher.

I am extremely grateful to my husband, **Amaninder Singh Brar** for showing trust in me and encouraging me. You motivate me to dream big and achieve higher. I am blessed to have you as a support.

AMANDEEP CHEEMA

Dedicated

to

my family

ABSTRACT

Psychological stress is an inevitable part of the modern-day lifestyle that affects human cognitive abilities. The relation between stress and a host of behavioural and somatic pathological conditions is well-established. The low doctor-to-patient ratio in under-developed and developing economies hinders access to expert diagnosis. This emphasizes the need for computer-aided timely detection of psychological stress. The methods like Electroencephalography (EEG) and Electrocardiography (ECG) provide important biophysical diagnostic measures for psychological stress detection, however, these methods are expensive or require a proper clinical setup. Whereas, the acoustic heart sound or Phonocardiography (PCG) signals carry significant information and can be easily acquired. The purpose of this research work is to present a novel framework for psychological stress detection using PCG signal that can serve as a first-level screening method at places where EEG or ECG are not available.

In this research work, the pre-competitive (or exam-related) psychological stress is used a as real-life stressor. For this study, the simultaneous ECG and PCG data of five minutes duration is acquired from 33 healthy male students in the age group of 18 to 25 years (mean = 20.11, standard deviation = 2.30) of Thapar Institute of Engineering and Technology, TIET campus who are attempting professional education institute examination. Two readings are acquired from every subject, one approximately two hours before the start of the exam and considered as the signals of subjects under psychological stress, whereas, second reading forms the baseline values for subject-specific template formation and recorded once the students returned from holidays after exams. In this study, the ECG signal is used as a reference signal for S1 peak detection of PCG signal and later for comparison of the results with that obtained from PCG-based method. The State-Trait Anxiety Inventory (STAI Form Y) self-report questionnaire is used in the study as the scores on the S-Anxiety scale increase when used under psychological stress and decrease after relaxation. The psychological stress is detected from the S1-S1 interval of PCG signal, referred to as an inter-beat interval (IBI) signal. The empirical mode decomposition (EMD) technique is used for decomposing IBI signal to intrinsic mode functions (IMFs). The EMD technique has been found suitable for non-linear and non-stationary signal analysis. The non-linear features namely- Area of Analytic Signal Representation (AASR), Log of Area of ellipse from Second-order Difference Plot (LASODP), Root Mean Square value of IMF (RmsIMF), Shannon Entropy (ShEnt) and

Fuzzy Entropy (FzEnt) were evaluated from IMFs of IBI signals. The first stage of this study comprises of deviation analysis in stressed signals from mean baseline values of the features in non-stressed signals. Thereafter, in the second stage of the study, Kruskal-Wallis statistical test has been used to check the significance and discrimination ability of the features. Subsequently, the features which showed maximum deviation and are statistically significant have been selected and fed to least-square support vector machine (LS-SVM) classifier. The 10-fold cross-validation has been used to make the system more reliable and robust. In this work, the average accuracy of 93.14% in classifying stressed and non-stressed signals has been achieved using Radial Basis Function (RBF) kernel. The novelty of this study is the use of PCG signals for psychological stress detection and the use of subject-specific baseline template to incorporate the individual cardiovascular characteristic behaviour and stress responses.

The applicability of another set of non-linear entropy-based features namely- Permutation Entropy (PEn), Fuzzy Entropy (FzEn) and K-Nearest Neighbour (K-NN) entropy estimator is explored in EMD domain. In order to optimise the system, the ranking methods including Entropy method, Bhattacharya space algorithm, Receiver Operating Characteristic (ROC) method and Wilcoxon method are used. The highest-ranked features are fed to LS-SVM for classification. This method showed significant improvement in accuracy and the highest accuracy, sensitivity and specificity obtained using the proposed system is 96.67%, 100% and 93.33% respectively.

The results indicate that the proposed features provide better discrimination ability than well-documented low-frequency to high-frequency power ratio (LF/HF) parameter of ECG signal on the dataset. The proposed novel methodology of using PCG signals for psychological stress detection is cost-effective and is suitable for home-care, telemedicine and in rural health care centres especially in developing countries. The proposed system opens a new research area of using PCG signal for psychological stress detection.

Table of contents

Title **Page No.**

List of Figures

List of Tables

List of Abbreviations

CVD	Cardiovascular disease
HIV	Human immunodeficiency virus
WHO	World Health Organization
NIMHANS	National Institute of Mental Health and Neuro Sciences
PCG	Phonocardiography
LAr	Left atrium
RAr	Right atrium
LVt	Left ventricle
RVt	Right ventricle
PA	Pulmonary artery
PV	Pulmonary vein
MVv	Mitral valve
TVv	Tricuspid valve
PVv	Pulmonary valve
AVv	Aortic valve
SVc	Superior vena cava
IVc	Inferior vena cava
ECS	Electrical conduction system
SA	Sino-atrial
AV	Atrioventricular
ANS	Autonomic nervous system
SNS	Sympathetic nervous system
PNS	Parasympathetic nervous system
HR	Heart rate
CNS	Central nervous system
BP	Blood pressure
ECG	Electrocardiogram
HRV	Heart rate variability
ULF	Ultra-low frequency
VLF	Very-low frequency

LF	Low frequency
HF	High frequency
S1	First heart sound
S2	Second heart sound
S3	Third heart sound
S4	Fourth heart sound
FHS	Fundamental heart sounds
IBI	Inter-beat interval
A	Aortic auscultation area
P	Pulmonary auscultation area
T	Tricuspid auscultation area
M	Mitral auscultation area
E	Erb's auscultation point
EEG	Electroencephalography
TSST	Trier social stress test
EMD	Empirical mode decomposition
AM	Amplitude modulated
FM	Frequency modulated
IMF	Intrinsic mode function
LS-SVM	Least-square support vector machine
AASR	Area of analytic signal representation
LASODP	Log of area of ellipse from second-order difference plot
RmsIMF	Root mean square value of IMF
ShEnt	Shannon entropy
FzEnt	Fuzzy entropy
PEn	Permutation entropy
K-NN	K-NN entropy
VAE	Venous air embolism
FHR	Foetal heart rate
CTG	Cardiotocograph
HS	Heart sounds
FHRV	Foetal heart rate variability
MAAS	MIT automated auscultation system
PPG	Photoplethysmography

BVP	Blood volume pulse
PD	Pupil diameter
GSR	Galvanic skin response
SVM	Support vector machine
EDR	Electrodermal response
fNIRS	Functional near infrared spectroscopy
IAPS	International Affective Picture System
EDA	Electrodermal activity
ST	Skin temperature
PRV	Pulse rate variability
F_s	Sampling frequency
STAI	State-Trait Anxiety Inventory
STFT `	Short-time Fourier transform
WT	Wavelet transform
WPT	Wavelet packet transform
CTM	Central tendency measure
ASR	Analytic signal representation
CAD	Coronary artery
S	Stressed
NS	Non-stressed
SODP	Second-order difference plot
COP	Center of Pressure
RMS	Root mean square
EMG	Electromyography
MLP	Multi-layer perceptron
RBF	Radial basis function
SD	Standard deviation
ACC	Accuracy
SEN	Sensitivity
SPE	Specificity
FzEn	Fuzzy entropy (with lower frequency IMFs retained)
ARE	Asymptotic relative efficiency
ROC	Receiver operating characteristics

CHAPTER 1 MENTAL HEALTH, STRESS AND DEPRESSION- THE CONTEXT

1.1 Mental health and mental disorders

The World Health Organization (WHO) defines mental health as a state of well-being in which an individual can realize his potential, can cope with the normal life stresses, can work productively and contribute to his community [1]. Mental health is imperative for the ability to think, emote, interact with others, earn a livelihood and enjoy life [2]. The importance of mental health is evident from the definition of health as per the constitution of the WHO, which states, health is not merely the absence of disease but a state of complete physical, mental and social well-being [3]. The physical, mental and social health of an individual has complex inter-dependence [4]. Therefore, mental health forms the basis for well-being and effective functioning of an individual and a community [1]. Neither mental health nor physical health can exist alone as most of the mental and physical illnesses can be accredited to a combination of biological, psychological and social factors [1]. It is now established that thoughts, feelings and behaviour have a significant impact on physical health and on the contrary, physical health also has an impact on mental health [4]. As mental health or psychological well-being is not merely the absence of disease, it holds importance for every individual and not only for people suffering from disorders. However, mental health is not given much importance in comparison to physical health. Globally, this has resulted in an increased burden of mental disorders and a vast treatment gap [4].

Mental disorders are generally characterized by a combination of abnormal thoughts, perceptions, emotions, behaviour and relationship with others [5]. Around 450 million

people around the world suffer from mental disorders [6]. Most of the mental disorders can be effectively treated and associated suffering can be minimized, however, between 76% and 85% of people receive no treatment for the disorder [7]. The mental disorders include:

- **Depression**: It is a common mental disorder with approximately 264 million people affected globally. The depression is mainly characterized by sadness, loss of interest, guilt feelings, low self-worth, loss of appetite or sleep, tiredness and reduced concentration [5]. Depressive disorder is among the three major causes of non-fatal health loss [8].
- **Bipolar disorder**: It consists of manic and depressive episodes separated by periods of normal mood. Nearly 45 million people are affected by this disorder worldwide [5].
- **Schizophrenia and other psychoses**: It is a severe mental disorder and about 20 million people globally are affected by this. It distorts thinking, perception, language, emotions, behaviour and sense of self. The common experiences include hallucinations and delusions. Above 69% of people suffering from schizophrenia are not receiving proper care and 90% of the people with untreated schizophrenia live in countries with low-and middle-income countries [9], [10].
- **Dementia**: It affects about 50 million people globally and mainly affects the older population. It is progressive in nature and deteriorates cognitive function. It is a major cause of disability and dependency in elderly population. Alzheimer's disease is the most common form of dementia and contributes around 60-70% of the cases [11].
- **Developmental disorders including autism**: Developmental disorders generally have an onset in early childhood and tend to persist into adulthood causing delay or impairment in central nervous system maturation [5]. It follows a steady course and approximately one in 160 children has an autism spectrum disorder [12].

A huge population suffers from mental disorders and sub-threshold mental disorders that do not reach the threshold for diagnosis as a mental disorder but lead to poor mental health [13]. These mental health problems result in an enormous socio-economic impact on society and this aspect is further elaborated in the next section.

1.2 Socio-economic impacts of mental disorders

The mental illness affects a large population of the world and impairs quality of life resulting in high socioeconomic impacts on society [14]. The mental health conditions lead to poor health, premature deaths, human rights violations and national and global economic loss. Globally, the mental health conditions impose an enormous burden on society and account for 1 in 5 years lived with disability causing more than US$ 1 trillion per year economic loss. This economic loss is due to reduced work productivity, reduced rates of labour participation, foregone tax receipts, and enhanced welfare payments [15]. The suicide mortality rates are also high, approximately 800 000 death per year, and is a leading cause of death in young people [16]. The mental, neurological and substance use disorders contribute 10% of global burden of disease and 30% of the non-fatal disease burden, thus, causing huge economic output loss [15]. The global non-fatal health loss has shown an increasing trend with depressive disorders being one of the leading causes of non-fatal disease burden measured in terms of years lived with disability (YLD). The YLDs are estimated as the product of prevalence estimate and a disability weight for health states [8]. The non-fatal health loss could ultimately lead to loss in human capital. The estimate of global cost of mental disorders in 2010 was approximately US$ 2.5 trillion and by 2030, it is projected to show an increase by 240% to reach US$ 6 trillion [15]. The social conditions associated with poverty create stress and triggers mental disorders which in return leads to mental healthcare-related costs and productivity loss that further leads to poverty. Therefore, a circular relationship exists between mental disorders and poverty and this cycle leads to rising rates for both.

As a result, mental health is a significant global concern for public health and economic development [17]. The dual aims of improving mental health and reducing personal and social cost of mental illness can be achieved through a public health approach. The WHO recognised the need for prioritising universal mental health coverage and launched a special initiative for mental health 2019-2023 [16] to ensure affordable quality care for mental health conditions.

The mental healthcare is prioritised throughout the world, however, a large number of mental disorder cases often remain unreported or untreated because of some challenges encountered in the mental healthcare delivery system that are highlighted in the subsequent section.

1.3 Major challenges in mental healthcare

Despite mental disorders exerting enormous pressure on the economy and health, there is a prevailing global mental health treatment gap of 70% [18]. This treatment gap exists because of the following major challenges in effective mental healthcare delivery systems-

- Stigma associated with mental disorders

  The stigma attached with mental disorders and discrimination faced by people suffering from mental disorders can result in social isolation, decreased self-esteem and reduced chances of employment and education. This stigma causes hindrance for patients to reach out for help regarding their mental illnesses, thereby increasing the treatment gap.
- Shortage of mental healthcare resources

  Globally, there is a shortage of mental health human resources and median number of mental health workers is 9 per 100 000 population with extreme variations between low-income countries and high-income countries (below 1 in low-income countries to 72 in high-income countries). Also, a disparity exists for median number of mental health beds available per 100 000 population. It is below 7 in low and lower-middle-income countries to over 50 in high-income countries [19].
- Expenditure on mental healthcare

  Mental disorders are among the highest contributors to global disease burden with a major burden borne by low-and middle-income countries, 54% in 2010 and projected to reach 58% by 2030. However, most low-and middle-income countries spend less than US$ 1 per person on the prevention and treatment of mental disorders. The budget allocation on mental health by low-income countries is around 0.5% of the total health budget, whereas, high-income countries allocate 5.1% [15].
- Access to mental healthcare facilities

  The difficulty in access to mental healthcare facilities is a major concern. The integration of mental healthcare at primary care and community healthcare centres can improve the outreach of mental health treatment to people living in areas with low-resource settings and thus reduce the treatment gap in mental healthcare.

The determinants of mental health and mental disorders include social, cultural, economic, political and environmental factors as well as individual attributes like the ability to manage one's thoughts, emotions, behaviours and interactions with others. The factors including stress, genetics, nutrition, perinatal infections and exposure to environmental hazards are also contributing factors to mental disorders.

As the role of stress in the onset of mental disorders and other health conditions is well-documented [20], therefore, it becomes imperative to define stress and general adaptation syndrome which is physiological response to stress.

1.4 Stress and General adaptation syndrome

1.4.1 Stress

Stress is the response of brain and body to any demand. Any challenge including performance at work, a significant change in life or a traumatic event can be perceived as stressful and are termed as stressors. A stressor may be one-time or short-term stressor or can be persistent over a long time. The body enters flight or fight mode when faced with a stressor. This survival response prepares the body to face the threat or flee to safety resulting in faster heart rate, breathing rate, tense muscles and increased consumption of oxygen by brain resulting in increased brain activity. Some people can cope with stress more effectively, thereby recovering more quickly from stressful events than others. However, long-term stress can be harmful to the body as the body never receives a clear signal to return to normal functioning. This continuous strain on the body due to stress can lead to serious health issues relating to immune system, cardiovascular health, diabetes and mental disorders [21].

1.4.2 General Adaptation Syndrome (GAS)

Hans Selye, also known as the father of stress, constructed a three-stage model of physiological response to stress called General Adaptation Syndrome (GAS). The GAS is described as the sum of all non-specific systemic reactions of the body which occur as a result of long exposure to stress [22]. This reaction is due to adaptive adjustments to the stressor.

The three stages of GAS as shown in figure 1.1 are:

- Alarm reaction
- Resistance
- Exhaustion

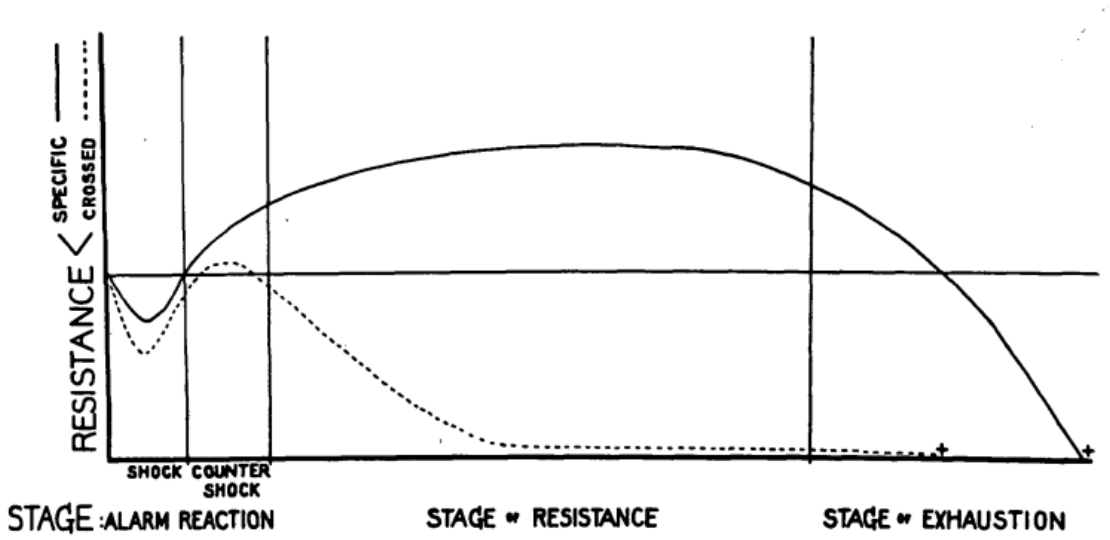

Figure 1.1 The three stages of General Adaptation Syndrome (GAS) (redrawn from [22])

Alarm reaction stage

The onset of perceived stressor leads to the activation of fight-or-flight response. The sympathetic branch of autonomic nervous system regulates the physiological changes required to deal with the perceived threat. The enlargement of adrenal cortex is the most important morphologic change that occurs in the alarm reaction stage. This stage can further be divided into two phases: shock phase and counter-shock phase [22]. In this stage, adaptation is not yet acquired.

Resistance stage

If the stress persists, the body enters the resistance stage. In this stage, the adaptation is optimal as the body tries to counteract the physiological changes of the alarm stage. This stage is regulated by parasympathetic branch of autonomic nervous system. In this stage resistance to the particular stressor is increased, whereas, resistance to other stressors is decreased [22].

Exhaustion stage

If the stress continues further and the body is unable to cope, then it goes into the final stage of GAS, known as the exhaustion stage and the body has depleted its energy resources and becomes susceptible to disease. The wear and tear is caused due to prolonged exposure to stress and the body constantly operating in fight-or-flight response. This stage is also called burnout and the acquired adaption is lost again in this stage.

These physiological changes during stress response are mediated by the endocrine system of the body that is discussed in the next section.

1.5 Endocrinology of stress

The life exists by maintaining a complex dynamic equilibrium called homeostasis, which is constantly challenged by stressors. The work of Hans Selye demonstrated that exposure to stressor leads to enlargement of adrenal cortex in the alarm reaction stage of general adaptation syndrome that indicates increased endocrine activity [22].

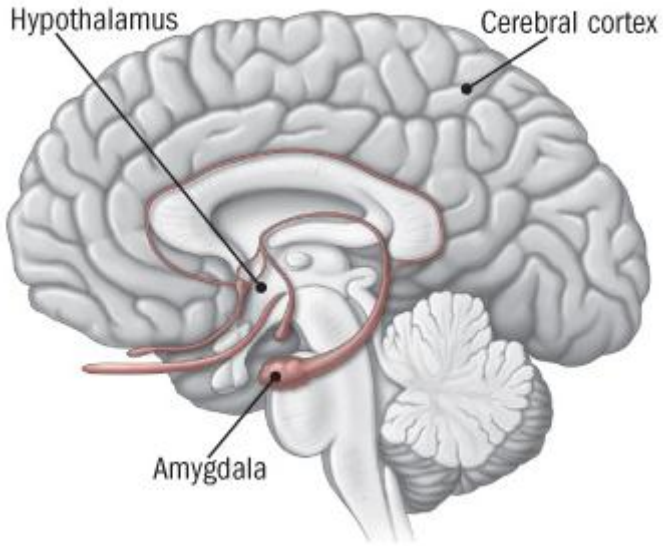

Figure 1.2 The human brain showing amygdala and hypothalamus responsible for initiation of stress response (redrawn from [23])

The onset of stressor leads amygdala, the portion of brain responsible for emotional processing, to send a distress signal to hypothalamus responsible for communication with

rest of body through nervous system. The human brain showing amygdala and hypothalamus is depicted in figure 1.2. The hypothalamus signalling results in activation of sympathetic nervous system by a rapid release of catecholamine hormones namely-epinephrine (also known as adrenaline) and norepinephrine from adrenal medulla into the bloodstream and is responsible for fight-or-flight response [23], [24]. This leads to vasoconstriction, increased heart rate, increased breathing rate, an increase in gas exchange efficiency of lungs, thereby increasing supply to brain and increasing alertness. The glucose and fats stores are released into the bloodstream to provide energy to all parts of body.

Under long-term stressful conditions, hypothalamus activates the next component of stress response termed hypothalamic-pituitary-adrenal (HPA) axis activation. In this response, hypothalamus releases corticotropin-releasing hormone (CRH) which travels to the pituitary gland, triggering the release of adrenocorticotropic hormone (ACTH) [24]. This hormone travels to the adrenal glands, prompting them to produce glucocorticoid hormones which include the release of cortisol from adrenal cortex. After the removal of the stressor, the stress responses subside and physiological functions return to normal.

Therefore, the stress responses are helpful for survival by increasing alertness in short-term stressful conditions, however, long-term stress can lead to pathological conditions. The prolonged cortisol exposure is linked to a broad range of problems including metabolic syndrome, obesity, cancer, mental health disorders, cardiovascular disease and increased susceptibility to infections [25]. The diseases of human pathology including diabetes mellitus, inflammatory bowel disease, rheumatic diseases can be regarded as by-products of the endocrine reactions which play an important role in general adaptation syndrome and stress responses [22], [26].

The most common mental disorder is clinical depression and is a major cause of non-fatal disease burden and years lived with disability. The pathophysiology of depression and relationship with stress is described in the next section.

1.6 The pathophysiology of clinical depression and its relationship with stress

The stress is useful in case of emergency situations like escaping a predator but chronic stress can manifest as illnesses. The association of stressful life events with psychiatric

illnesses is stronger in comparison to that of physical illnesses. The mental stress is considered to be central factor in the development of psychopathology. Despite some evidence for parasympathetic withdrawal and sympathetic over-activity in depression, there is no clear-cut link of psychophysiological response to stress in depression [27].

The onset of depression is often preceded by stressful life events [26]. The people who suffered through adverse life events including unemployment, bereavement, psychological trauma are more likely to develop depression whereas, depression may lead to more stress and dysfunction and worsen the situation further [28]. The depression is a result of a complex interaction of social, psychological and biological factors. The changes initiated in HPA axis and the immune system due to chronic stress can act as a trigger for depression. The concentrations of pro-inflammatory cytokines and glucocorticoids may contribute to behavioural changes associated with depression [29]. The existing evidence indicates that aberrations in immune-inflammatory pathways and activation of cell-mediated immunity represent important pathophysiological pathways for the development of major depressive disorder.

As psychological stress can substantially up-regulate inflammatory activity [20], the inflammation plays a crucial role in psychopathology of depression and is considered to be a possible cause of depression as depression usually co-occurs with inflammatory diseases including rheumatoid arthritis, inflammatory bowel disease, metabolic syndrome, coronary heart disease [20], [29].

Therefore, the biological response to stress is critical for survival during times of actual physical threat and prepares the body to deal with associated physical wounding and infection. However, in the present social environment, the associated social signal transduction pathways are most frequently activated not by approaching physical danger, but by the symbolic, anticipated or imaginary social threats. It is under these social-environmental conditions, therefore, that this biological response can lead to an increasingly pro-inflammatory phenotype that is hypothesized to be a key phenomenon driving depression pathogenesis and overlap of depression with several conditions including rheumatoid arthritis, chronic pain and cardiovascular disease [20].

Due to the global prevalence of depression and a constantly rising trend makes it imperative to detect depression at an early stage to receive proper treatment. The

spectrum of symptoms relating to clinical depression is elaborated in the subsequent section.

1.7 Symptoms of clinical depression

Depression is characterized by persistent sadness and a loss of interest in activities that the person normally enjoys, accompanied by an inability to carry out daily activities. The people suffering from depression may normally experience loss of energy, change in appetite, sleeping more or less, anxiety, reduced concentration, indecisiveness, restlessness, feelings of worthlessness, guilt, or hopelessness and thoughts of self-harm or suicide [30].

The symptoms of clinical depression may vary among individuals and can include [31]:

Psychological symptoms

The psychological symptoms of depression include:

- continuous low mood or sadness
- feeling hopeless and helpless
- having low self-esteem
- feeling tearful
- feeling guilt-ridden
- feeling irritable and intolerant of others
- having no motivation or interest in things
- finding it difficult to make decisions
- not getting any enjoyment out of life
- feeling anxious or worried
- having suicidal thoughts or thoughts of self-harm

Physical symptoms

The physical symptoms of depression include:

- moving or speaking more slowly than usual
- changes in appetite or weight (usually decreased, but sometimes increased)
- constipation
- unexplained aches and pains

- lack of energy
- low sex drive
- changes in menstrual cycle
- disturbed sleep – for example, finding it difficult to fall asleep at night or waking up very early in the morning

Social symptoms

The social symptoms of depression include:

- avoiding contact with friends and taking part in fewer social activities
- neglecting hobbies and interests
- having difficulties in home, work or family life

According to the number and severity of the symptoms experienced, the depression can be classified as mild, moderate or severe.
The huge population is suffering from depression which is a treatable mental disorder. In order to reduce the socio-economic impact it is exerting on the society, the WHO and countries are working in tandem to prioritise management of depression as explained in the subsequent section.

1.8 Current management of depression

The community-based approaches effective for prevention of depression include enhancing positive thinking patterns in children and adolescents in school-based programmes and interventions for parents of children with behavioural problems. The exercise programmes for elderly can also be effective in prevention of depression.

The effective treatments for moderate and severe depression include psychological treatments like behavioural activation, cognitive behavioural therapy (CBT) and interpersonal psychotherapy (IPT) or antidepressant medications like selective serotonin reuptake inhibitors (SSRIs) and tricyclic antidepressants (TCAs).

The various talking therapies for psychological treatments are discussed below [32] –

Cognitive behavioural therapy (CBT)

The aim of cognitive behavioural therapy (CBT) is to help the patient understand their thoughts and behaviour, and the associated effect. The CBT recognises that events in past may have shaped the patient, but it mainly concentrates on how the patient can change the way of thinking, feeling and behaving in the present. It also teaches about overcoming negative thoughts – for example, being able to challenge hopeless feelings.

Interpersonal psychotherapy (IPT)

This therapy focuses on the relationship problems of the patient including difficulties in communication or coping with bereavement. In some cases, it is found to be as effective as antidepressants.

Counselling

In this therapy, the counsellor supports the patient in finding solutions to the problems they are facing and to find new ways of dealing with them.

The psychosocial treatments are also found to be effective for mild depression, whereas, antidepressants are an effective form of treatment for moderate and severe depression. The antidepressants may have associated adverse effects and are not the first line of treatment for adolescents, mild depression and should not be used for treating children [28].

The WHO recognised depression as a priority condition covered under mental health gap action programme. The various programmes including Problem Management Plus, Group Interpersonal Therapy and Thinking Healthy by WHO aims to help countries in increasing mental health services by health workers not specialised in mental health using brief psychological intervention manuals for depression that may be delivered by lay workers. The mental disorders are now considered to be of prime importance due to the associated socio-economic impact on society.

As per the scenario in India, a study conducted by Indian Council of Medical Research (ICMR) reported 197.3 million people in India suffering from mental disorders in 2017 and the total disease burden due to mental disorders approximately doubled since 1990

[33]. The National Institute of Mental Health and Neuro Sciences (NIMHANS), India in National Mental Health Survey 2015-2016 [34] reported a treatment gap of 74% to 90% for common mental disorders. The shortage of mental healthcare professionals in the health care delivery system of India is the major reason for this treatment gap as India has only 3800 psychiatrists, 898 clinical psychologists and 1500 psychiatric nurses [35] for mental healthcare.

The WHO mental health action plan 2013-2020 has recently been extended till 2030 recognising the need for further emphasis on mental health. The WHO recognised the need for prioritising universal mental health coverage and launched a special initiative for mental health 2019-2023 [16].

Moreover, experts warn about an unprecedented wave of the mental health crisis due to the pandemic as it has resulted in increased psychological stress and a spike in people seeking help regarding mental health issues [36]–[39]. The role of digital technology in mental health interventions to provide better access to tele-health services is emphasized [36], [40].

This study presents a cardiac sounds based framework for computer-aided psychological stress detection and is a step in the direction of using machine learning, signal processing techniques and digital technologies to provide tele-mental health services.

CHAPTER 2 INTRODUCTION AND OBJECTIVES

2.1 Psychological stress

Psychological stress occurs when the complex dynamic equilibrium called homeostasis is threatened or perceived to be threatened by internal or external adverse forces termed as stressors [41]. Homeostasis is a self-regulating mechanism that maintains critical systems of the body, important for the survival of the organism, within their narrow range of operation [42]. The association of psychological stress with pathogenesis is well-established and the contribution of stress in progression of diseases like cardiovascular disease (CVD), cancer, human immunodeficiency virus (HIV) and clinical depression is well-documented [43]. According to a World Health Organization (WHO) report, depression is among the single largest causes of disability worldwide [44]. This emphasizes the need for timely detection of psychological stress.

According to National Mental Health Survey, 2015-2016 [34] by National Institute of Mental Health and Neuro Sciences (NIMHANS), India, an increase is reported in Indian population suffering from mental illness from 7.5% in 2014 to 10.6% in 2016 and the treatment gap of 74% to 90% exists for common mental disorders. The major reason for this treatment gap can be attributed to the shortage of mental healthcare professionals in health-care delivery system as India has only 3800 psychiatrists, 898 clinical psychologists and 1500 psychiatric nurses [35] for mental healthcare. Therefore, low doctor-to-patient ratio in developing and under-developed economies impedes access to expert clinical diagnosis and healthcare. The solution to the above-stated problem could be a computer-based automated system of psychological stress detection that is cost-

effective and suitable for use in home-care and telemedicine. The stethoscope is an important diagnostic tool as it is available at rural primary health care centres. The proposed system uses electronic stethoscope for Phonocardiography (PCG) signal acquisition and thereafter, psychological stress is detected from the acquired PCG signal. In some diseases, use of cardiovascular signals is confirmed to be a reliable and inexpensive method for early diagnosis. However, the diagnostic ability and accuracy of cardiac auscultation depend on the experience of the physician. The human audibility range also limits the diagnostic potential of cardiac auscultation [45], as shown in figure 2.1. Moreover, storing the records for follow-ups and future references is also not feasible with conventional auscultation. Therefore, a computer-aided methodology for using PCG signals for psychological stress detection is proposed in this work.

The PCG signals are heart sound signals, therefore, an introduction to the anatomy and physiology of human heart and the physics of heart sounds are discussed in subsequent sections.

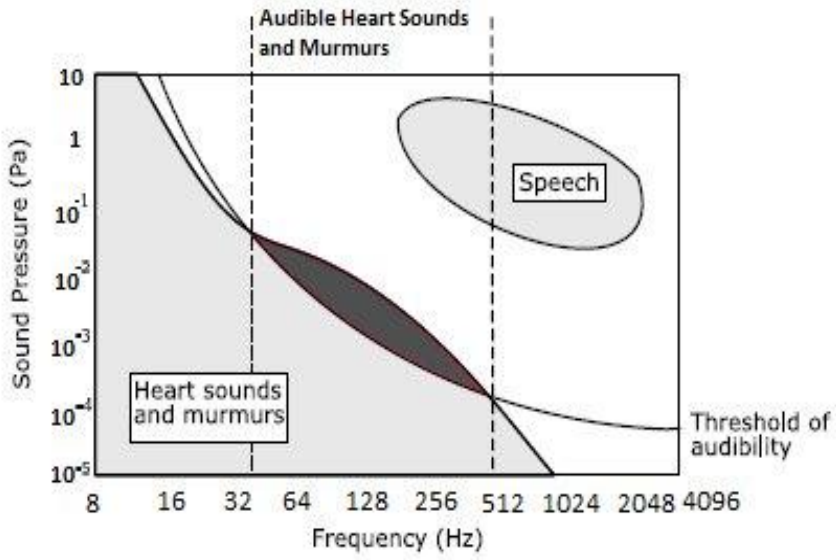

Figure 2.1 Relationship between acoustic range of heart sounds and threshold of audibility (redrawn from [46]**)**

2.2 Human heart- Anatomy and Physiology

Human heart acts as a muscular pump for circulation of blood throughout the body. The muscle wall of heart consists of three layers. The inner layer that lines heart chambers is

called endocardium, the middle layer is myocardium which provides sufficient force for the pumping action of heart and the outermost layer is pericardium which consists of fluids that decreases friction against heart movements during heartbeats [47]. The thickness of muscular wall of left ventricle is about three times as compared to the muscular wall of right ventricle. This is due to the heavier workload of left ventricle to pump blood to rest of the body as compared to right ventricle workload of pumping blood to the lungs [47]. The anatomy of human heart is shown in figure 2.2.

Blood carries oxygen and nutrients to tissues of the body and also carries away carbon dioxide and metabolic waste for excretion through lungs and kidneys respectively [47]. The heart has four chambers- two upper chambers are left atrium (LAr) and right atrium (RAr) while two lower chambers are left ventricle (LVt) and right ventricle (RVt). The muscular wall, septum, divides right side of heart from left side [47]. The deoxygenated blood from superior vena cava (SVc) and inferior vena cava (IVc) enters right atrium, flows into right ventricle and is pumped to lungs through pulmonary arteries for oxygenation [48]. The oxygenated blood received from the lungs through pulmonary veins enters left atrium, flows to left ventricle and then the ventricular contraction pumps oxygenated blood to the rest of the body through aorta [47], [48]. The blood vessels that carry blood to the heart are called veins and that carry blood away from heart are called arteries with pulmonary artery (PA) and pulmonary vein (PV) being exceptions [49].

The heart has four valves- two atrioventricular valves and two semilunar valves that allow unidirectional blood flow. The atrioventricular valve between LAr and LVt is mitral valve (MVv) and between RAr and RVt is tricuspid valve (TVv). These atrioventricular valves allow blood to flow from atria to ventricles when pressure in atria exceeds pressure in ventricles. The semilunar valve located between RVt and PA is pulmonary valve (PVv) and between LVt and aorta is aortic valve (AVv). The PVv and AVv control blood flow out of ventricles.

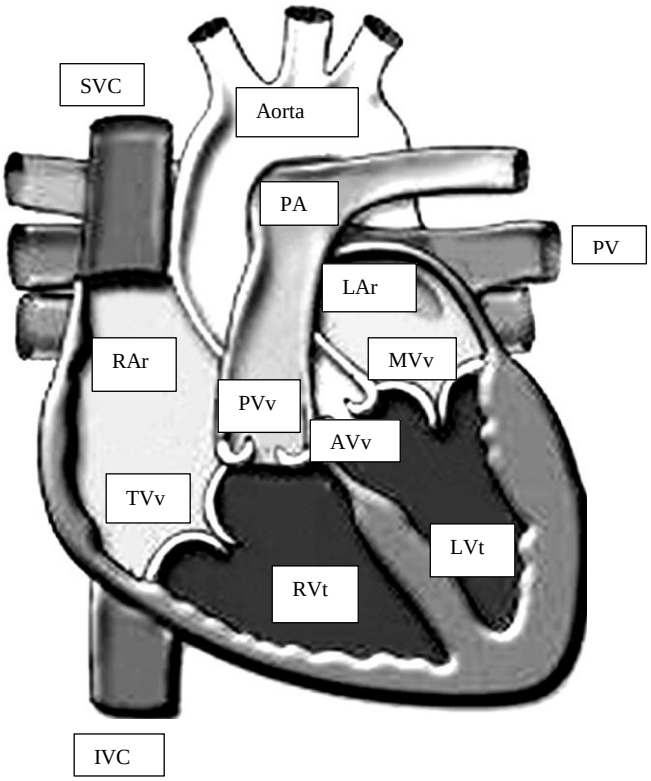

Figure 2.2 Anatomical structure of heart (adapted from [47]**)**

The time duration of ventricular contraction is termed as ***systole*** and time duration of ventricular relaxation is ***diastole*** [48]. The cardiac cycle consists of systole and diastole and generally, systole is shorter than diastole. The steps involved in a cardiac cycle can therefore be summarized as [50]:

- The deoxygenated blood enters RAr through superior SVc and IVc
- When pressure gradient develops across RAr and RVt, TVv opens and deoxygenated blood passes to RVt. Thereafter, RAr contracts and passes all deoxygenated blood to RVt
- The RVt contracts to pump blood to lungs, TVv shuts to prevent blood from flowing back to RAr. The PVv opens to pass blood through PA to the lungs for oxygenation. When pressure in RVt falls and pressure in PA increases, PVv shuts to prevent blood from flowing back from PA to RVt
- The oxygenated blood from lungs comes to LAr through PV
- The blood enters LAr and passes to LVt through MVv

- The LVt contracts to open AVv and oxygenated blood is pumped to the whole body through aorta. During LVt contraction, MVv shuts to prevent blood from flowing back to LAr, whereas, when pressure in LVt decreases than pressure in aorta, AVv shuts to prevent blood from flowing back to LVt

For the heart to function properly, the heart chambers must contract in a synchronised manner. The pumping of heart is synchronised with atria contracting in unison for force-filling the ventricles and thereafter, ventricles contracting in unison for supplying blood to lungs and rest of body. This synchronisation is achieved through electrical conduction system (ECS) of the heart. The sino-atrial (SA) node, also called natural pacemaker, located in upper wall of RAr, initiates the ECS [51]. The SA node exhibits automaticity property as it periodically generates electric impulse even without external stimulus. The electrical impulse originated at SA node spreads via myocardium to RAr and LAr and results in their contraction. The non-conducting tissues electrically separate atria from ventricles. The electrical impulse traverses from atria to ventricles through atrioventricular (AV) node with short time delay for LVt and RVt to fill with blood before contraction [47]. The bundle of His transmits an electrical impulse from AV node to myocardium of ventricles leading to ventricular contraction.

The ECS explains the electrical activity of heart that leads to mechanical activity of heart. The mechanical activity of heart comprises of contraction and expansion of heart chambers and opening and closure of heart valves. The electrical activity of heart is recorded as ECG signals, whereas, mechanical activity of heart is recorded as PCG signals. In order to analyse the PCG heart sound signals, it is important to emphasize on physics of heart sounds which is presented in the next section.

2.3 Physics of heart sounds

A sound signal is generated as a wave of alternating pressure by a vibrating object. The vibrating source sets each particle moving in back and forth motion with the frequency of the tone and pushing nearby particles causing a chain effect and resulting in compression and rarefactions. Therefore, a pressure wave consists of alternating areas of compression and rarefaction moving away from the source of sound [52]. These pressure variations are detected using mechanical impact they create on membranes like diaphragm of

stethoscope. The source of sound vibrating in an irregular manner will produce a complex sound wave. If a sound wave is non-stationary, the measures to describe such a signal have to be time-varying in order to give significant information [52].

The complex relationship between blood volume, flow and pressure within the heart regulates opening and closing of heart valves. The fundamental heart sounds occur during closure of heart valves but the actual cause of heart sounds is still debatable. According to valvular theory, the heart sounds originate from point source located near heart valves. This theory is considered to be a simplistic viewpoint. Whereas, according to the cardiohemic theory, heart and blood are interdependent systems that vibrate as a single unit [52].

The relationship between autonomic nervous system, accountable for maintaining homeostasis and heart is described in the next section.

2.4 Autonomic nervous system and heart

The autonomic nervous system (ANS) involuntarily controls organs and systems of human body. The ANS is responsible for regulation of homeostasis function [53]. The ANS has central components located in brain stem and peripheral components comprising efferent fibers, afferent fibers and peripheral ganglia exerting control over all internal organs. The ANS has two branches- sympathetic nervous system (SNS) and parasympathetic (vagal) nervous system (PNS). The SNS stimulates functioning of the organs, whereas, PNS inhibits their functioning. An increase in sympathetic stimulation increases HR, stroke volume and systemic vasoconstriction, in contrast, increase in parasympathetic stimulation decreases HR, stroke volume and systemic vasoconstriction. The PNS and SNS regulate the target organs that include eyes, salivary glands, sweat glands, heart, lungs, intestines and kidneys. The PNS promotes growth and restoration, whereas, SNS deals with increased metabolic output to cope with challenges outside the body. In response to SNS activation, pupil dilate, heart-rate and force of heart contractility increases, blood vessels constrict, blood pressure increases and movements of intestines are inhibited [53]. The complex and opposing interaction between sympathetic and parasympathetic (vagal) nervous system is termed as sympathovagal

balance whereas, increase in sympathetic activation leads to sympathovagal imbalance [54].

The field of neurocardiology explores the interconnections between heart and brain. The heartbeat originates at SA node, which generates around 100-120 electrical impulses per minute, whereas, the resting heart rate (HR) of a healthy subject is between 50-70 beats per minute. This is because of continuous control of ANS over SA node output and the real HR is the output of net regulatory effect of ANS on heart [47].

At resting conditions, both parasympathetic and sympathetic nervous systems are active and parasympathetic system is dominant [47]. When HR increases to about 100 bpm, the balance shifts and sympathetic activity dominates [55]. The actual balance between PNS and SNS is dynamic and is optimised based on internal and external stimuli. The response time of heart for sympathetic activation is relatively slow in comparison to instantaneous response time of heart for parasympathetic activation [48]. Therefore, during mental-stress, the consequences of central nervous system (CNS) lead to increase in HR and blood pressure (BP) that defines hemodynamic reactivity [56] and this is useful in this research of stress detection.

The cardiac signals useful in this study of psychological stress detection are discussed in the following section.

2.5 Cardiovascular signals

The cardiovascular signals are signals originating from heart. The analysis of cardiac signals forms important non-invasive diagnostic tool to monitor and assess cardiac health and overall health of an individual. In some diseases, use of cardiovascular signals is confirmed to be a reliable and inexpensive method for early diagnosis. The cardiovascular signals used in this work are:

2.5.1 Electrocardiogram

The Electrocardiogram (ECG) is a graphical recording of the electrical activity of heart. The cardiac muscles depolarize in response to electrical impulses generated by pacemaker

cells resulting in generation of ECG signal [47]. A typical ECG signal is shown in figure 2.3.

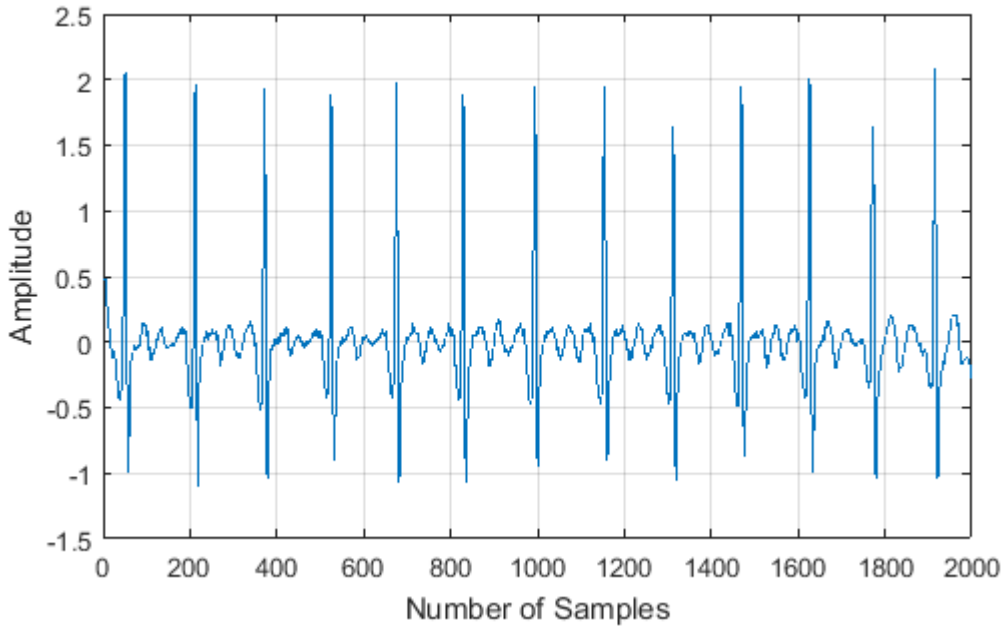

Figure 2.3 A plot of ECG signal

An ECG beat comprises of P-wave, QRS complex, T-wave and U-wave as shown in figure 2.4. The significance of these waves is:

- P-wave signifies depolarisation of atrial myocardium, start of atrial contraction to pump blood into ventricles
- QRS-complex corresponds to depolarisation of ventricular myocardium, start of ventricular contraction to pump blood to lungs and rest of the body
- T-wave reflects repolarisation of ventricular myocardium which is an essential recovery process for myocardium to depolarise and contract again
- The origin of U-waves is uncertain and is believed to correspond to late depolarisation. These waves are <10% height of QRS complex and prominent in abnormal conditions

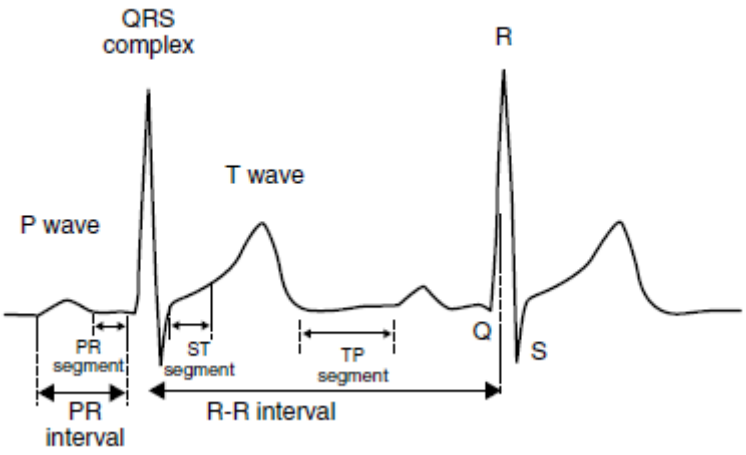

Figure 2.4 An ECG signal showing P wave, QRS complex and T-wave (adapted from [47]**)**

The heart rate variability signals, derived from the R-R interval information of ECG signals are described below.

2.5.2 Heart rate variability

The heart rate variability (HRV) is the variation in time interval of consecutive R-peaks of ECG signal. A plot of typical HRV signal is shown in figure 2.5. As the HR of a healthy subject is not steady, HRV depicts the capability of heart in adapting to changing conditions by swiftly responding to stimuli [47]. The beat-to-beat variability is due to ANS modulation of cardiac pacemaker and hence, the HRV depicts sympathovagal balance. A low HRV suggests an increased sympathetic dominance or reduced parasympathetic dominance [57]. Therefore, HRV is considered as a measure of neuro-cardiac function that reflects interactions of heart-brain and ANS dynamics [55].

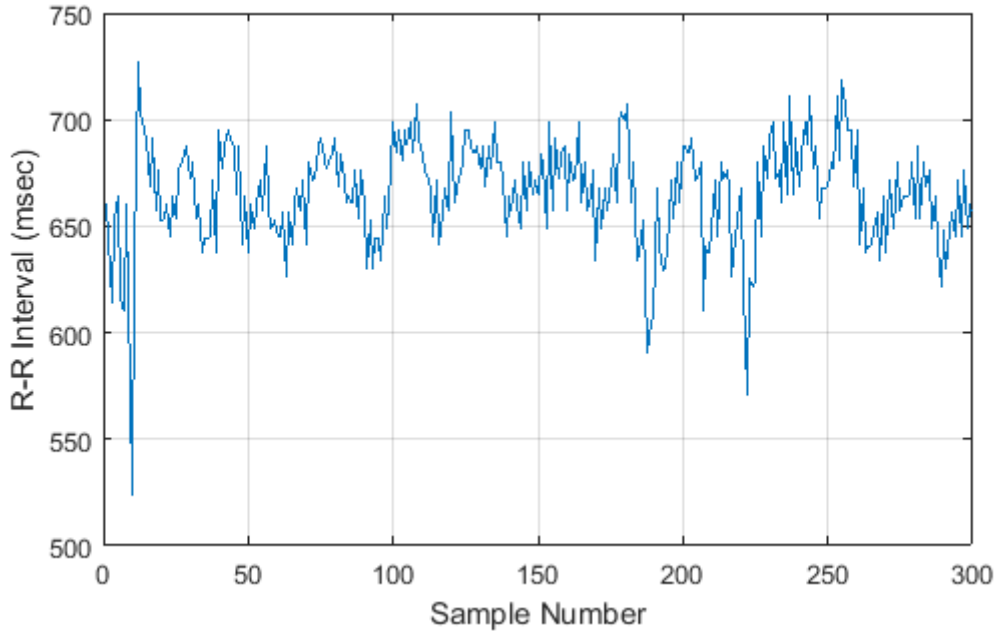

Figure 2.5 A plot showing HRV signal

According to Task Force of European Society of Cardiology and North American Society of Pacing and Electrophysiology [58], the frequency domain (power spectrum density) analysis of HRV has four frequency bands as shown in figure 2.6:

ULF- This is ultra-low frequency (ULF) band. The frequency range of this band is less than 0.003 Hz.
VLF- This is very-low frequency (VLF) band. The frequency range of this band is 0.003 Hz to 0.04 Hz.
LF- This is low frequency (LF) band with frequency range of 0.04 Hz to 0.15 Hz.
HF- This is high frequency (HF) band with frequency range of 0.15 Hz to 0.4 Hz.

The LF/HF power ratio is considered as sympathovagal balance indicator. An increase in this index indicates a shift towards sympathetic dominance whereas the decrease of this index indicates a shift towards parasympathetic dominance [59]–[63].

However, concept of LF, HF and LF/HF ratio for sympathovagal balance indication is challenged in many studies [64]–[66].

Therefore, this research work proposes the use of PCG signals for psychological stress detection. The PCG signals are described in the following section.

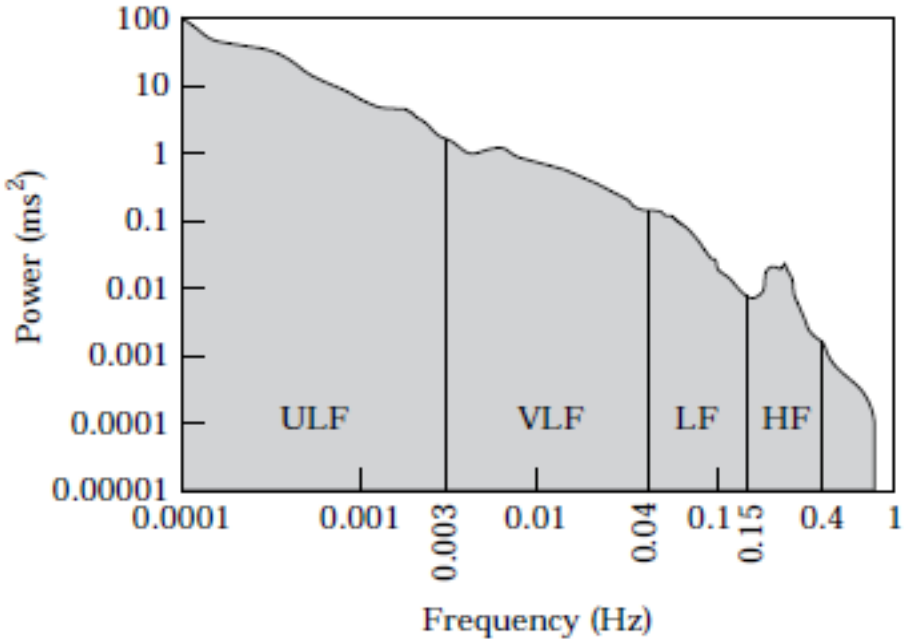

Figure 2.6 Estimate of Power spectral density of HRV signal showing UHF, VLF, LF and HF bands (adapted [67]**)**

2.5.3 Phonocardiography signals

Phonocardiography (PCG) is graphical recording of mechanical activity of heart. The heart sounds are generated due to blood flow and valve closure. The complex interplay between pressure gradients in atria, ventricles and arteries changes the heart sound morphology thereby affecting timing and magnitude of heart sounds [68]. These heart sounds when recorded and plotted electronically are called PCG signals. A typical PCG signal is shown in figure 2.7.

The PCG signal is acquired using an electronic stethoscope. The heart sounds are described as follows:

S1- It is termed as first heart sound and is a low-frequency, low pitch and longer duration acoustic signal [69]. The ventricular systolic contraction triggers cardiohemic system vibrations that include heart chambers, valves and blood. These vibrations are transmitted through thoracic cavity and received at chest wall [70]. The S1 occurs during systole, at the end of isometric contraction period [71] due to closure of tricuspid and mitral valves [72].

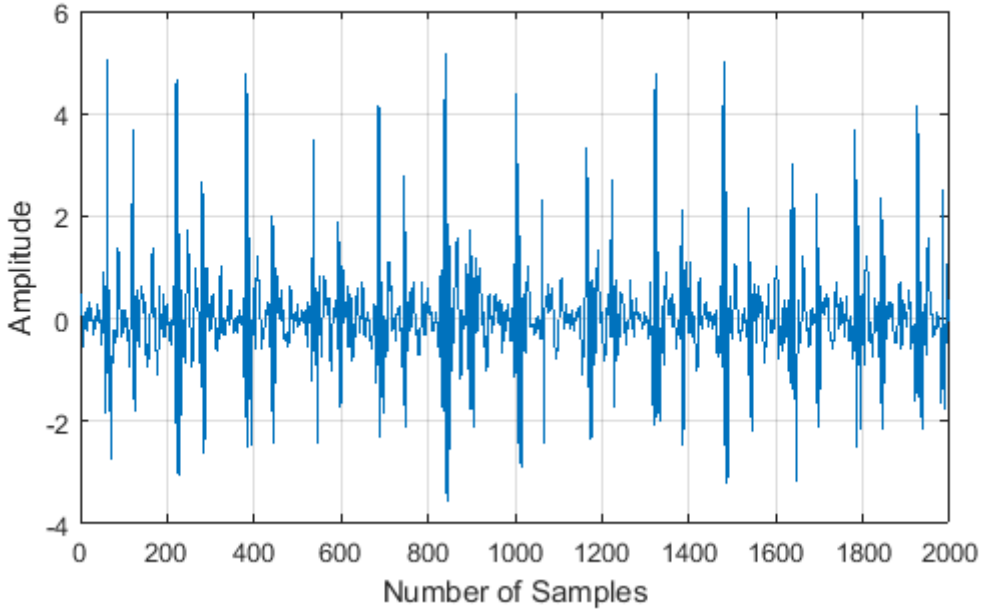

Figure 2.7 A plot of PCG signal

S2- It is termed as second heart sound and is a high-pitch, shorter duration acoustic signal [69]. The S2 occurs during diastole, after isovolumetric relaxation period [71] because of closure of pulmonary and aortic valves [72].

Under normal or pathological conditions, some extra sounds including third heart sound (S3), fourth heart sound (S4), murmurs and clicks can also be present in a PCG signal [69], [73]. The fundamental heart sounds (FHS) are S1 and S2. In a PCG signal, the interval between S1 to subsequent S2 is systole whereas, the interval between S2 to subsequent S1 is diastole. In normal conditions, systole is shorter than diastole [69]. The systole and diastole together form a cardiac cycle. The S1 peaks, S2 peaks, systole and diastole of PCG signal are shown in figure 2.8.

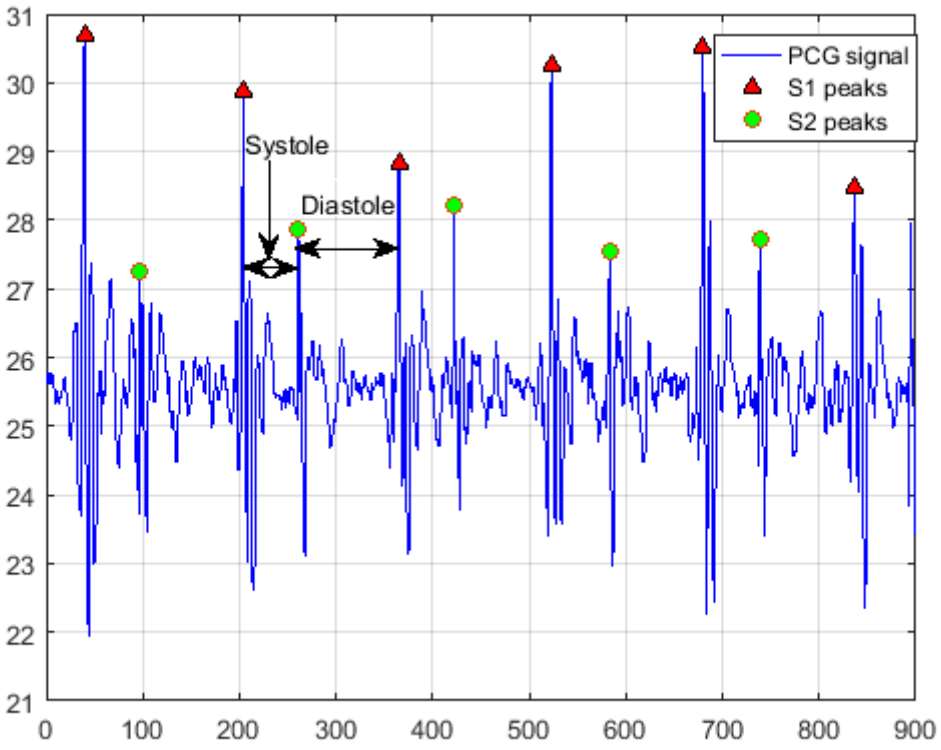

Figure 2.8 A PCG signal depicting S1 peaks, S2 peaks, systole and diastole

The interbeat interval signals that are derived from PCG signals are explained in the following section.

2.5.4 Inter-beat interval signal

The inter-beat interval (IBI) signal is derived from PCG signal by extracting the time interval between consecutive S1 peaks. Due to variability in HR, the time interval between S1 peaks is also dynamic so as to adapt to changing requirements of the individual and in response to the stimuli. It is analogous to HRV derived from ECG signals. A plot of typical PCG-derived IBI signal is shown in figure 2.9.

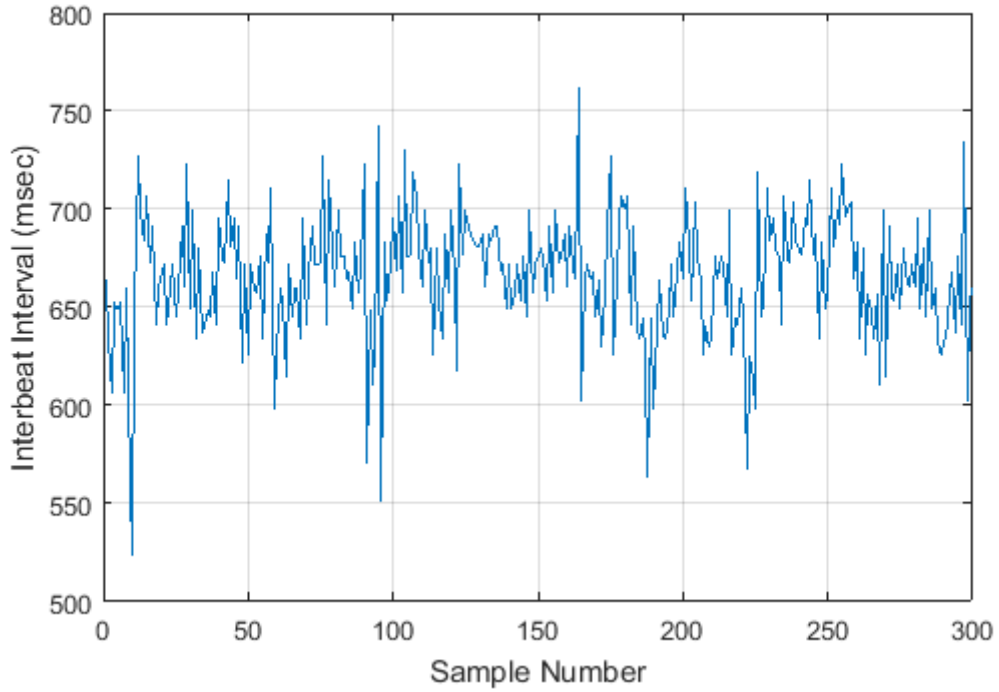

Figure 2.9 A plot of IBI signal

In order to properly acquire PCG signals, the electronic stethoscope chest-piece is to be placed at appropriate sites on the chest. The sites best suitable for auscultation and acquisition of cardiac sound PCG signals are called auscultation sites and are described in the next section.

2.6 Auscultation sites

The heart sounds originate due to the closure of valves and vibrations in cardiohemic system. These vibrations travel to the chest wall and microphone can be placed at these sites for auscultation. The auscultation sites and their respective anatomical landmarks are given below [72] and are shown in figure 2.10.

Aortic auscultation area (A) - It is located at 2nd intercostal space along right sternal border

Pulmonary auscultation area (P) - It is located at 2nd intercostal space along left sternal border

Tricuspid auscultation area (T) - It is located at 4th intercostal space along left sternal border

Mitral auscultation area (M) - It is located at 5th intercostal space along left midclavicular line

Erb's auscultation point (E) - It is located at 3rd intercostal space along left sternal border

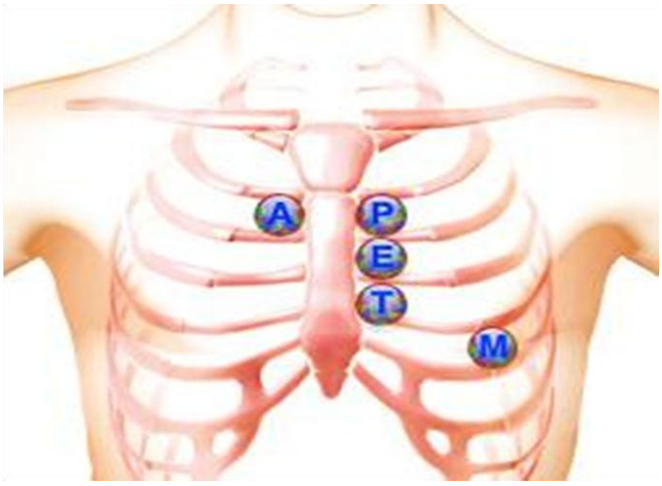

Figure 2.10 Auscultation sites for heart sound acquisition (adapted from- [74]**)**

2.7 Motivation

The traditional cardiac auscultation is listening to acoustic heart sounds using stethoscope, whereas PCG is electronic recording and graphical representation of heart sounds using electronic stethoscope. A stethoscope is very important diagnostic tool as it is available at primary healthcare centres, making auscultation an important diagnostic measure. The accuracy and diagnostic capability of cardiac auscultation are dependant on experience of the physician. The human audibility range also limits the diagnostic potential of cardiac auscultation [45]. Whereas, the diagnostic capability of PCG signals is independent of human audibility range. The PCG signal acquisition is cost-effective and does not require proper clinical setup as compared to Electroencephalography (EEG) and Electrocardiography (ECG) signals and hence is suitable for areas where sophisticated equipment and trained physicians are not available. Therefore, PCG-based psychological stress detection is suitable for computer-aided diagnosis, telemedicine, rural areas and homecare.

The psychological stress detection using ECG-based HRV signals is well-documented [59]–[63]. The LF/HF power ratio feature extracted from HRV signals is used as sympatho-vagal balance indicator. The increase in this feature indicates a shift towards sympathetic dominance whereas the decrease in this feature indicates a shift towards parasympathetic dominance. ***A temporal relation exists for simultaneously recorded ECG and PCG signals. The R-wave of ECG signal appears just before S1 peak of PCG signal*** [71] ***as shown in figure 2.11. This relationship between the two signals gives an insight for using PCG instead of ECG for psychological stress detection.***

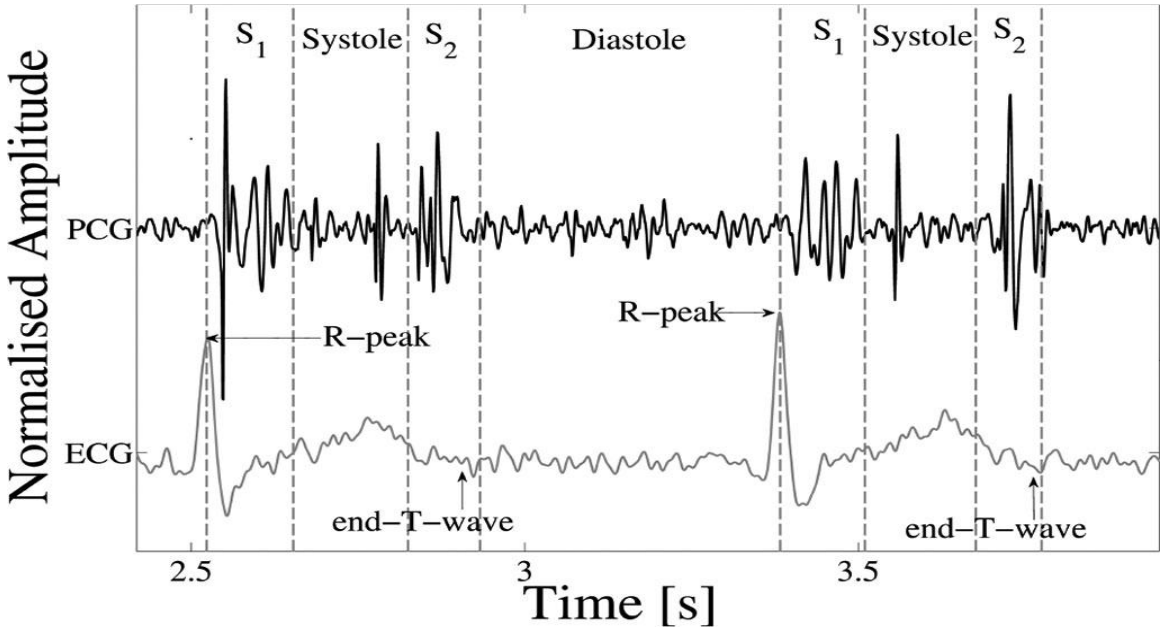

Figure 2.11 A plot showing simultaneously recorded PCG and ECG signals and depicts their temporal relationship (redrawn from [73]**)**

The bio-signals generally exhibit non-linear and non-stationary behaviour. Therefore, extraction of significant diagnostic information from these signals is a challenging task. Due to the non-linear and non-stationary characteristics of cardiac signals [47], the conventional signal processing techniques that impose crucial restrictions of linearity and stationarity of data are inadequate to capture complex dynamics of heart. Therefore, a technique that can deal with non-linear and non-stationary nature of cardiac sound signals will yield more significant results. The Empirical mode decomposition (EMD) is an adaptive and data-dependent time-frequency domain signal processing technique suitable

for non-stationary and non-linear signals [75]. The EMD technique decomposes a signal without making *a priori* assumptions on the input data. The EMD technique decomposes any temporal signal into a set of amplitude and frequency modulated (AM-FM) mono-component sub-band signals called Intrinsic Mode Functions (IMFs). The information present in these sub-bands can then be extracted using non-linear features as cardiac signals have non-linear characteristics. Thereafter, these non-linear features can be fed as an input to classifiers for decision-making. In this research work, non-linear features have been investigated in EMD domain for psychological stress detection using PCG signals.

The conventional state-of-technologies including ECG and EEG provide important biophysical measures for psychological stress detection. However, the present study proposes a novel application of PCG signals for psychological stress detection.

The motivations for developing PCG-based framework for psychological stress detection include:

- The studies [64]–[66] indicate that the well-documented ECG-based LF/HF ratio method for psychological stress detection is not accurate and may not efficiently indicate sympathovagal imbalance

- Stress manifestation on heart rate forms the basis for ECG-based LF/HF ratio method for psychological stress detection. The ECG signals are temporally related to simultaneously acquired PCG signals but as yet, there has been no systematic investigation of the possible use of PCG for psychological stress detection.

- The EEG signals provide important diagnostic measures for psychological stress detection but are expensive, require proper clinical setup and training for data acquisition thus making it unsuitable as homecare-based first-level timely screening method

- The non-availability of proper cost-effective home-care based methods for psychological stress detection and challenges in commercial wearable devices like frequent movement of data acquisition site, improper placement of sensors that can also lead to unreliable data and high cost emphasize on the need for reliable data-acquisition, alternate measurement site and cost-effective solution for psychological stress detection

- The easy availability of stethoscope at primary health care centers makes stethoscope an important diagnostic tool. The easy acquisition of PCG signals makes PCG-based method appropriate as a first-level screening method at places where a specialized physician/equipment is not available. The easy to acquire PCG signals make it suitable for telemedicine and can possibly increase the outreach of timely expert diagnosis and reduce the urban-rural divide in healthcare

- Understanding and developing PCG-based psychological stress detection framework may lead to better, early diagnosis at homecare and greater effectiveness in healthcare delivery system using telemedicine due to shortage of mental healthcare workers and psychiatrists in low and middle-income countries like India

The above-mentioned motivations and research problems formed the basis of the present study that explores the applicability of PCG signals for psychological stress detection. The objectives of the study are defined in the subsequent section.

2.8 Objectives

The objectives of this research work are:

1.) To acquire the bio-signals, pre-process the signals and extract the features for psychological stress detection

2.) To identify the most discriminating features of bio-signals for stress detection

3.) To develop a bio-signals based stress detection system

4.) To test and validate the developed system

2.9 Steps involved in PCG-based psychological stress detection

In order to accomplish the above-mentioned research objectives for psychological stress detection using PCG signals the following steps are involved as shown in figure 2.12:

- Signal Acquisition

  The PCG and ECG signals are simultaneously recorded as per the guidelines of Task Force by European Society of Cardiology and North American Society of Pacing and Electrophysiology.

- S1 peak detection and Interbeat Interval (IBI) signal formation

  The S1 heart sounds are detected from PCG signals using ECG-gating method. The interval between consecutive S1 heart sounds is computed and interbeat interval signal (IBI) is formed. This IBI signal is used for further signal analysis to detect psychological stress.

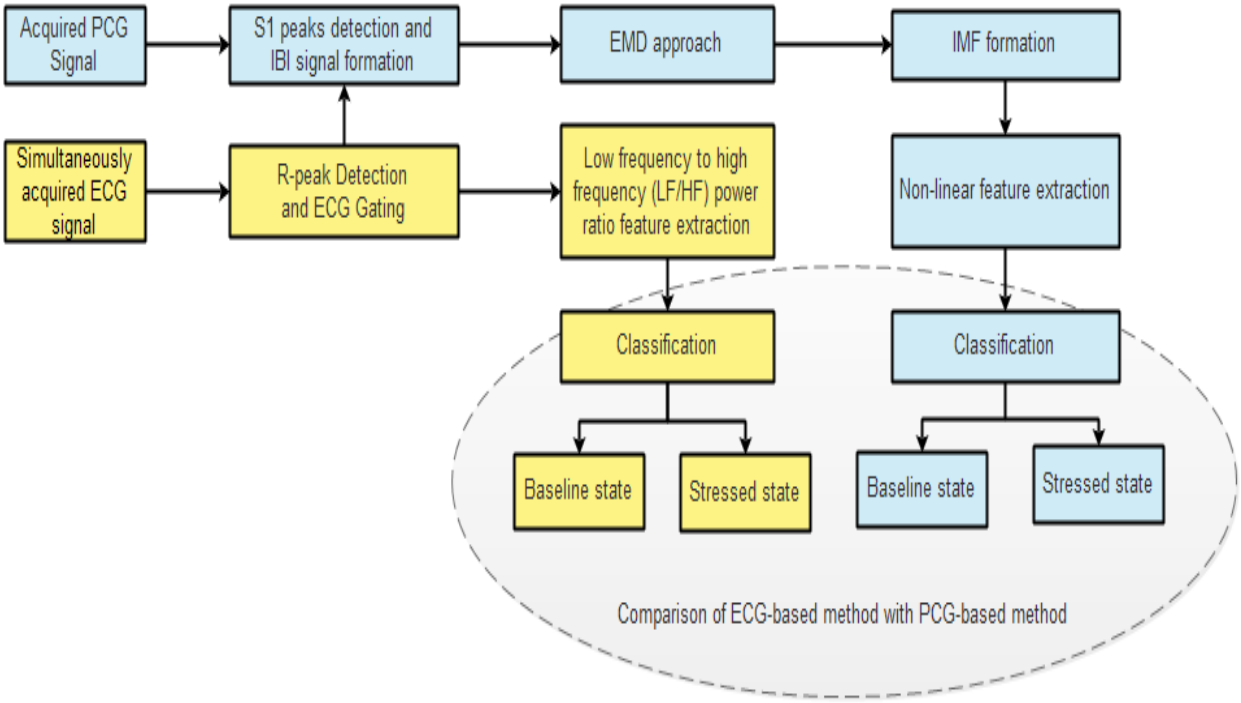

Figure 2.12 Steps involved in PCG-based psychological stress detection

- Empirical Mode Decomposition

  The EMD method is a time-frequency domain signal analysis method that is applicable for non-linear and non-stationary data. The bio-signals are generally non-linear and non-stationary, therefore, use of EMD is suitable for signal decomposition.

- Intrinsic Mode Functions formation

  The application of EMD on IBI signals leads to formation of mono-component sub-band signals known as intrinsic mode function (IMFs) using an iterative process called sifting.
- Non-linear feature extraction

  In order to detect psychological stress, the complex non-linear dynamics of cardiac signals are captured using non-linear features. The IMF signals are used for extracting the non-linear features.
- Classification

  The classification of signals as stressed state and non-stressed baseline state is done using Least-Square Support Vector Machine (LS-SVM) classifier.
- Comparison with ECG-based LF/HF power ratio feature method

  The results of the developed method are then compared with well-documented ECG-based LF/HF power ratio sympathovagal balance indicator method.

2.10 Contributions

The contributions of this thesis are summarized as:

- A novel method of using PCG signals for psychological stress detection has been developed
- The time-interval between consecutive S1 heart sounds of acquired PCG signal is computed to form IBI signal. The IBI signal is decomposed to IMFs using EMD method. These IMFs were used to compute non-linear features namely-Area of Analytic Signal Representation (AASR), Log of Area of ellipse from Second-order Difference Plot (LASODP), Root Mean Square value of IMF (RmsIMF), Shannon Entropy (ShEnt), Fuzzy Entropy (FzEnt), Permutation Entropy (PEn) and K-NN Entropy (K-NN). The maximum classification accuracy on the dataset is achieved using LS-SVM classifier
- The developed method uses subject-specific baseline template analysis to cater to varied stress responses and characteristic cardiac behaviour of every individual
- The developed PCG-based method of psychological stress detection is cost-efficient, suitable for home-care, telemedicine, rural-areas and performed better

than well-documented ECG-based LF/HF power ratio sympathovagal balance indicator method on the available dataset

- This work opens a new research area of psychological stress detection using PCG signals

2.11 Organization of the thesis

The remaining portion of this thesis is organized as follows:

Chapter 3 Literature review

This chapter elaborates the prior-work available in this research area. The works done in the field of PCG signals and the studies for psychological stress detection are included in this chapter and based on this, the research gaps have been identified.

Chapter 4 Data acquisition and pre-processing

This chapter explains the method and protocol of data acquisition for this study and the related guidelines of Task Force by European Society of Cardiology and North American Society of Pacing and Electrophysiology. This is followed by the steps involved in pre-processing of acquired signals. This involves detecting S1 peaks in PCG signals using simultaneously acquired ECG signals and formation of IBI signal. This IBI signal is then used for decomposition and further analysis.

Chapter 5 Empirical mode decomposition

This chapter describes the importance of using empirical mode decomposition method for time-frequency domain signal analysis. The EMD technique is suitable for non-linear and non-stationary signal analysis. The bio-signals are generally non-linear and non-stationary in nature making EMD a justified choice for signal decomposition and analysis. The steps for implementation of EMD on IBI signals and formation of IMFs that are mono-component sub-band signals are also discussed in this chapter.

Chapter 6 Proposed method 1

This chapter investigates the relevance of five non-linear features namely- AASR, LASODP, RmsIMF, ShEnt and FzEnt for PCG-based psychological stress detection. The

classification results using this method are discussed in detail and compared with existing ECG-based method.

Chapter 7 Proposed method 2

In this chapter, clinical relevance and diagnostic importance of three non-linear entropy-based features namely- Permutation entropy (PEn), Fuzzy entropy (FzEn) and K-NN entropy (KNN) is explored. Thereafter, the classification parameters obtained using this method are discussed and compared with existing well-documented ECG-based method.

Chapter 8 Conclusion and future scope

This chapter concludes the experimental work and summarizes major research contributions of this work. This chapter also elaborates on major findings from this research along with advantages and limitations of the proposed method. The possible extensions and applications of this work are also discussed in this chapter as future scope.

CHAPTER 3 LITERATURE REVIEW

3.1 Literature review on PCG

The PCG signals are heart sound signals and have been extensively used in studies for cardiac anomalies detection. The major work on PCG signals is done on heart sounds segmentation that leads to cardiac cycle segmentation and detection of S1, S2, systole and diastole. The PCG signals are widely used in literature for murmur detection and pathological abnormal cardiac sound detection. The PCG is also useful for foetal heart rate monitoring as there is no acoustic energy transferred to the foetus, making it a safe long-term cardiac monitoring method [76]. However, as per the extensive literature survey, the authors did not come across any prior-work focussing on PCG-based psychological stress detection.

The contributions in the field of using PCG signal for the applications mentioned above along with techniques applied for signal analysis are reported here in chronological order:

Lehner *et al.* [77] developed a microcomputer-based system to segment PCG signals and characterize murmurs using ECG and carotid pulse as reference signals. The study acknowledged the appearance of murmurs long before appearance of other signs and symptoms of cardiovascular system malfunction. The study proposed the use of carotid pulse as a reference signal for PCG analysis lead to reliable detection of S2 heart sound in PCG signals. Thus combined use of ECG signal for S1 heart sound detection and carotid pulse for S2 heart sound detection resulted in proper and reliable segmentation of PCG signal in systole and diastole. This resulted in an accurate characterization and localization of the murmurs. This study used 47 phonocardiogram signals for the analysis. The use of PCG energy curve is suggested for diagnosis of valvular and septal heart defects and presence of murmurs is indicated if significant energy appears after S1 during

systole or after S2 during diastole. The use of PCG energy spectrum indicated presence of high-frequency murmurs. This study implemented on a dedicated microcomputer resulted in fast analysis of PCG signals.

Khadra *et al.* [78] suggested the use of wavelet transforms for signal analysis of phonocardiogram signals. The study highlights the disadvantages of using methods like fast fourier transform for non-stationary heart sound signal analysis. Further, the limitations of using spectrogram and Wigner distribution in tracking sudden changes and transients that are characteristic to heart sound PCG signals. The study emphasized applicability of time-frequency domain wavelet transform method in extracting clinically useful information particularly for exact measurement of the time difference between A2 and P2 components of S2 heart sound in PCG signals as this time difference can be widened due to pathological conditions.

Zhang *et al.* [79] used 11 PCG signals to test the applicability of time-frequency domain scaling transformation based on matching pursuit method which makes use of an iterative method for decomposing a signal into a series of time-frequency atoms. The two components of a signal becomes difficult to distinguish if there is a small time-interval and hence, the difficulty increases when the heart rate increases. These limitations of auscultation are removed through time-frequency scaling of the PCG signal based on the matching pursuit method. In this method, the time scale is changed without changing the spectral properties and for frequency scaling the frequency band of the signal can be compressed or expanded and frequency band can be shifted up or down to a desired frequency range without changing the temporal properties of the signal. This technique is found to be useful for applications like- detecting heart and heart-valve diseases and teaching auscultation.

Kovács *et al.* [76] developed PCG-based long-term foetal heart rate (FHR) monitoring method. The use of acoustic approach for FHR does not transmit any energy to foetus and feasibility of using low-power electronic instrumentation makes this method suitable for long-term foetal heart rate monitoring. This study analysed simultaneous acoustic FHR and ultrasound cardiotocograph (CTG) recordings of 80 patients for 10 minutes duration. The study reported that for approximately 90% of total time, findings from PCG-based FHR agreed with that of ultrasound CTG. This study also highlights the challenges of foetal heart sound (HS) detection and analysis as described below:

- The foetal HS signal is recorded from maternal abdomen. Therefore, it is a low-intensity signal in comparison to the interference signals originating from the organs of the mother.
- The acquired foetal HS signal depends on foetus position in mother's womb and hence it may vary in intensity, spectra and in time. This leads to changes in the amplitude and frequency characteristics thereby, significantly modifying the waveform of the foetal heart sound signal.
- Double peaks may appear in the foetal HS signal owing to temporal delay between aortic and pulmonary components.

Guillén *et al.* [80] designed a tele-homecare system using integrated services digital network and internet protocol using videoconferencing standards and standard TV set to interact with patient and monitor ECG, heart sounds and blood pressure remotely. The specifications and requirements for home-care and telemedicine are discussed in this study. The usability, cost-effectiveness, and interoperability of the designed system were the salient features. This system was evaluated for 52 patients and 10 university students and emphasized the importance of feeling of virtual presence. The virtual presence tends to provide psychological perception of empathy between physician and patient. This leads to trustworthy assessment by medical staff and reliable outcomes of the interventions. This is particularly useful in the scenario where a large number of patients need health monitoring and support at home and for places with high patient-to-doctor ratio in order to increase outreach of expert diagnosis and healthcare.

Ortiz *et al*. [81] studied differences in foetal heart rate variability (FHRV) from abdominal electrocardiography and phonocardiography in 15 pregnant women. The duration of antepartum phocardiograms and abdominal electrocardiograms is reported to be 3 minutes. This work depicted that mean heart rate from both the methods are similar but differences exist for FHRV indices extracted from PCG and abdominal ECG. The FHRV indices including root mean square of the difference between sequential intervals (RMSSD), short term variability (STV) computed as the mean of the difference between consecutive intervals, and power of high frequency (HF) component showed higher values in case of PCG in comparison to ECG. A significant lineal correlation was observed between R-R spectrum of ECG and S-S spectrum of PCG within the low-

frequency components; however, a non-significant correlation was reported at high frequencies.

Vàrady *et al*. [82] emphasized the importance of long-term variability of foetal heart rate in accessing the foetal health status. The study suggested use of two-channel phonocardiography with wavelet-based advanced signal processing techniques for low-cost, standalone, battery-operated long-term foetal heart rate monitoring as an alternative to expensive ultrasound cardiography for home-care use. The study used wavelet-based denoising with adaptive cross channel coefficient adjustment for efficient cancellation of external noise in comparison to other methods examined in the study. The bursts are identified with cross-correlation based amplitude burst detection which may correspond with the highest probability to an S1 or S2 beat. Thereafter, the rule-based selection of the S1 and S2 beats is accomplished by finite state machine and physiological timing rules. This method is implemented on acoustic sound signal heavily loaded with noise as it is recorded from maternal abdomen and yielded 83% accuracy in comparison to simultaneously recorded ultrasound measurements on 16 pregnant women in 28^{th} to 40^{th} week of pregnancy.

Syed *et al*. [83] used actual patient data of 30 to 40 second duration from 39 adult subjects out of which 11 suffered from mitral regurgitation, 15 subjects had benign murmurs and the remaining 13 were normal control subjects. This study made an attempt to approximate steps of cardiologist-based auscultation, which include discarding the clinically irrelevant beats, selectively tuning in to particular frequencies and gathering information across time in order to make a diagnosis, for making an automated computer-based auscultation system named MIT automated auscultation system (MAAS) for cardiac sound analysis. This framework provides noise isolation, automatic cardiac sound segmentation, high diagnostic content interval isolation and statistically significant feature extraction corresponding to pathological signals. The stages involved in this framework include interval segmentation, interval selection, time-frequency decomposition using wavelet-based approach, clustering, construction of prototypical intervals and cluster selection. The results of the classifier used are reported to be comparable to best-published results.

Amit *et al.* [70] proposed a computational analysis framework for continuous non-invasive monitoring of cardiac and respiratory functions consisting of hierarchical

clustering, compact data representation in the feature space of cluster distances and a classification algorithm for identification of distinct morphologies of heart sounds and further classifying them into the physiological states. This study used time-frequency domain signal representation, hierarchical clustering on two datasets to classify two physiological states using morphological changes in S1. The data in the first dataset was acquired from 12 subjects while modulating the respiratory pressure and an average accuracy of 82±7% is achieved in classifying the breathing resistance level. This algorithm estimated the instantaneous breathing pressure with an average error of 19± 6% and a strong correlation of 0.92 was reported between the estimated and the actual breathing efforts. The data of second dataset from 11 subjects was acquired during pharmacological stress tests and the average accuracy of 86±7% was reported in classifying the pharmacological stress stage.

Tang *et al.* [84] dealt with impulsive noise or interference in heart sounds that is inevitable due to friction between chest-piece of stethoscope and patient's skin, lungs sounds and noisy hospital environments. Firstly, the quasi-cyclostationary nature of heart sounds is discussed, then consistency of S1 and S2 heart sounds is established using nine different clinical cases. Thereafter, non-linear time scaling is suggested in cycle-frequency domain for reducing noise and disturbances in heart sounds. This method achieved good performance even with five cycles and results showed clearer and more discernible recovered heart sounds. Tang *et al.* [85] used fuzzy detection in joint cycle frequency-time-frequency domain for impulsive noise reduction in heart sounds. The heart sound atoms congregated whereas, noise atoms dispersed on joint plane. This method attained good performance even for five cardiac cycles.

Mandal *et al.* [86] designed a point-of-care cardiac pre-screening hand-held, low-power device suitable for providing heart-care services to rural areas of the developing countries. This study used adaptive multi-resolution signal processing techniques for acquisition, wavelet-based denoising, segmentation and classification of heart sounds and murmurs using ultra low-power embedded processor TI-MSP 430. The presence of cardiac abnormality in the patient leads to alteration in the temporal domain signature of the heart sounds and it can be sensed by the device. The device can categorize a subject in normal, abnormal, valvular abnormalities or ischemic classes and can be useful in early detection of common congenital heart diseases. The device showed good performance on

72 samples taken from 17 volunteers. The system developed in this study used a special colour scheme for indication of the risk and also, a networked cardiologist is alerted if any abnormalities are detected in the recorded heart sounds in order to provide proper point-of-care leading to increased expert outreach in rural areas.

Kovàcs *et al.* [87] worked in the field of foetal heart rate variability and detection of foetal heart murmurs. The work also contributed to accessing useful parameters of foetal cardiac operation in addition to cardiotocographic examination. The study used 3000 acoustic recordings from the maternal abdomen for detection of S1 heart sound in foetal PCG. This study used multimodal algorithms namely- autocorrelation, wavelet transform, matching pursuit algorithm and model-based correlation algorithm for S1 foetal heart sound detection. The autocorrelation has proven to be the most efficient algorithms, however, if it fails to identify an S1 sound with acceptable certainty, a combination of two additional methods are applied consecutively for detecting heartbeats. This complex combination of these methods provided an improved accuracy, even in case of noisy records, as compared to individual methods at the cost of increased computation demand. The framework suggested in the study is suitable for long-term foetal heart monitoring.

Patidar *et al.* [88] contributed towards heart sounds segmentation using tunable-Q wavelet transform (TQWT) by working on dataset of heart sounds pod-cast series 2011 by the Robert J. Hall Heart Sounds Laboratory of Texas Heart Institute at St. Luke's Episcopal Hospital, containing 50 abnormal cardiac sound signals. The murmurs present in the PCG signal are removed using decomposition based on constrained TQWT and reconstruction with adaptive selection of input variables. The study suggests adjusting Q-factor, redundancy parameter and number of stages of decomposition of the TQWT to desired statistical properties in order to obtain murmur-free reconstructed cardiac sound signals. The values used in this study for reconstruction of signal are r = 11 and j = 11 at Q = 1. Thereafter, low energy components are removed from reconstructed signal to extract envelope based on cardiac sound characteristic waveform. The timing information from characteristic waveform is used to extract heartbeat cycles from original cardiac sound signals. This study showed promising results in FHS detection even in presence of overlapping murmurs of comparable magnitude.

Patidar *et al.* [89] used data from five different sources to form a more generalized dataset for septal defect detection from cardiac sound signals using TQWT based feature

approach. The constrained TQWT is used for heartbeat cycle extraction and thereafter, TQWT based decomposition is used for decomposing extracted heartbeat cycles in sub-bands. The combinations of sub-bands are used for diagnostic feature extraction. The decomposed sub-bands are reconstructed to compute sum of average magnitude difference function (SAMDF). The feature set was obtained with SAMDF to represent murmurs in heart sound signals. The classifier used in the study is LS-SVM with different kernel functions. The study reported significant classification accuracy of 98.92% with sensitivity of 98.80%, specificity of 99.29% at tenth level of decomposition with Q=6.

Watanabe *et al.* [90] made a significant contribution in the field of ubiquitous health monitoring by suggesting the use of bi-directional microphone for mobile phone having pressure detecting film that receives differential pressure between ports. This microphone can be used for bio-signal measurement and can serve as a sphygmograph, a stethoscope or a bed-side health monitor. The findings suggested that this set-up can be used as a sphygmograph and detects the wave similar to the second derivative of the conventional optical pulse oximeter output wave and the correlation of 0.92 is reported with pressure pulse wave. The set-up when used as a stethoscope detects cardiac sound and pulse wave and respiration. The use of two microphones allows computation of delay time from neck carotid to the fingertip. The approach of this study was to make the audio microphone a low-frequency microphone with high sensitivity by setting one pressure-detecting port in one closed space and this lead to expansion of cut-off frequency from 200 to 0.5 Hz or less and the gain increased by more than 50 dB in the low-frequency range.

Papadaniil *et al.* [91] worked in the field of automatic heart sound segmentation for localization of S1 and S2 heart sounds and used ensemble empirical mode decomposition with kurtosis feature for the investigation. This study was conducted on 43 heart sound recordings from 11 normal subjects, 16 subjects with mitral regurgitation and 16 patients with aortic stenosis recorded in real clinical environment and achieved 94.56% accuracy in determining heart sounds location and 83.05% in heart cycle segmentation. The results from noise stress test with additive Gaussian noise and respiratory noise suggests the superiority of this technique in comparison to other efficient methods employing wavelet transform, energy, simplicity and frequency measures. This work also suggested that the improvement is due to more effective decomposition of the PCG signals into the distinct components in comparison to the wavelet transform decomposition.

Springer *et al.* [73] contributed in the field of automated heart sounds segmentation using hidden semi-Markov model with *a priori* information about the duration of states, the use of logistic-regression for emission probability estimation and modified Viterbi algorithm for decoding the most-likely sequence of states. The study is conducted using 30-40 s duration noisy real-world PCG signals of 112 patients and the F1-score of 95.63±0.85% is achieved as compared to F1-score of 86.28±1.55% using state-of-art method based on duration-dependent hidden Markov model [92]. The greater discrimination between the states is achieved due to logistic regression in comparison to Gaussian distribution-based emission probability estimation and the proposed method of the study significantly outperformed the state-of-the-art method due to the use of an extended Viterbi algorithm.

Liu *et al.* [93] conducted a significant study to enlist all the available open PCG databases and describes a public heart sound database, assembled for an international competition, the PhysioNet/ Computing in Cardiology (CinC) Challenge 2016. This work is necessary for comparative evaluations of heart sound algorithms for heart sound segmentation and classification. The study comprises of nine databases acquired across the seven countries and three continents over the period of a decade so this lead to a large variation in hardware, recording locations, data quality and patient types. Therefore, the study incorporated the sensor used, recording duration, recording position, sampling rate and sensor frequency bandwidth. The databases included 2435 heart sound recordings from 1297 patients and healthy subjects. This study does not report any database for PCG-based psychological stress detection.

Zhang *et al.* [94] investigated use of scaled spectrogram with partial least squares regression for classifying heart sounds in categories namely- normal, murmur, extra heart sound and artefact. This study is performed on PASCAL classifying heart sounds challenge. The four stages of the study included heart cycle estimation using short-time average magnitude difference of Shannon energy envelope, spectrogram scaling using bilinear interpolation for obtaining equal length spectrograms, dimension reduction accomplished using partial least squares regression and classification using support vector machine classifier. The proposed method outperformed the baseline methods of the challenge. Zhang *et al.* [95] used scaled spectrogram with tensor decomposition method for classifying heart sounds using support vector machines classifier. The main contribution of this study is use of tensor decomposition to extract the intrinsic structure

of the scaled heart cycle spectrograms. The method proposed in the study is evaluated on three public datasets by the PASCAL classifying heart sounds challenge and 2016 PhysioNet challenge and yielded competitive results.

Chen *et al.* [96] investigated the feasibility of reliable S1 and S2 heart sound recognition without using duration of heart sounds information and heart interval information. The study proposed conversion of heart sound signals to Mel-frequency cepstral coefficients (MFCC) and K-means algorithm for clustering MFCC features and thereafter, using a deep neural network classifier for S1 and S2 recognition. This study achieved 91% accuracy in S1 and S2 fundamental heart sounds recognition using Mel-frequency cepstral coefficients based only on acoustic characteristics and without ECG as a reference signal. The high recognition accuracies of individual S1 and S2 heart sounds, even in the absence of duration and interval information makes this method suitable for patients with arrhythmia due to irregular S1 and S2 time intervals.

Latif *et al.* [97] recommended the use of recurrent neural networks for automated cardiac auscultation and abnormalities detection. This study used Logistic Regression-Hidden Semi-Markov Models [73] for heart states identification and the overall PCG waveform is segmented into shorter instances by locating the beginning of each heartbeat. The Mel-frequency cepstral coefficients are used for representing PCG signal in compact representation and thereafter, recurrent neural network model is trained. The database used is Physionet Computing in Cardiology Challenge. The results of the study outperformed AdaBoost-CNN model which was placed as rank 1 in the PhysioNet Computing in Cardiology Challenge 2016.

Omari *et al.* [98] reported another application of PCG signals for blood pressure estimation. The correlation between pulse transit time and diastolic duration S21 is explored in this study for PCG-based blood pressure measurement. The developed artificial neural network used systolic duration, diastolic duration, heart rate, sex, height and weight as input data and as per the NN decision, the mean blood pressure was measured and thereafter, the systolic and the diastolic pressures were estimated. This method was evaluated on 37 subjects and results are reported to be satisfactory as error in estimation lies very close as per AAMI standard. This study shows the feasibility of PCG-based blood pressure estimation.

Ghosh *et al.* [99] worked in the field of automated heart valve disorder detection including mitral stenosis, aortic stenosis and mitral regurgitation on a public database by segmenting PCG signal into cycles based on formation of Shannon-entropy envelope and approaches for heart sound cycle extraction. Thereafter, a time-frequency matrix is obtained using wavelet synchrosqueezing transform and magnitude and phase features are computed from the matrix. The seven features extracted from magnitude component are mean, standard deviation, entropy, skewness, kurtosis, median, and energy and similarly, from phase component six features namely- mean, standard deviation, entropy, skewness, kurtosis, and energy are computed. The classifier used is random forest classifier and the average individual accuracy values for normal, aortic stenosis, mitral stenosis, and mitral regurgitation classes obtained are 98.83%, 97.66%, 91.16%, and 92.83%. This reported methodology is suitable for real-time detection of PCG-based heart valve disorder detection and an overall accuracy value of 95.12% as classification performance is reported using proposed method. The study also verified the method on 15 recorded PCG signals and achieved 93.33% accuracy.

Thanaraj *et al.* [100] proposed method for abnormal heart sound detection from unsegmented phonocardiogram using deep neural network architectures such as a one-dimensional convolutional neural network and feed-forward neural network. The feature engineering and feature selection process is automated to reduce the analysis time of screening the PCG records for heart disease identification. In this study, the challenge 2016 dataset was used with sampling frequency of 2000 Hz, and down-sampled to 500 Hz. The signal is then divided into small time-segments of 6 s epochs and Savitzky–Golay filter is used for suppressing high-frequency noises. The processed data was provided as an input to the proposed deep neural network architectures. The study used 1081 PCG records for training and validation and the feed-forward neural network model with five hidden layers provided overall accuracy 0.8565, sensitivity 0.8673 and specificity 0.8475.

Chien *et al.* [101] made an important contribution by presenting a deep convolutional autoencoder for compressing PCG signals to reduce the bandwidth requirements for transmission to remote sites for telecare applications. The hidden semi-Markov model is used for heart sound segmentation. The seven convolution layers at encoder side compress PCG signals into feature maps and at decoder site, other seven convolution layers decompress feature maps and PCG signal is reconstructed for doctors to perform

diagnosis. The proposed system was tested on Dalian University of Technology heart sounds database of Physionet dataset and achievable compress ratio is reported to be 32 under a constraint that percent root-mean-square difference is less than 5%.

Altuve *et al.* [102] worked in the field of S1 and S2 heart sound analysis using intrinsic mode decomposition from empirical mode decomposition and improved complete ensemble empirical mode decomposition with adaptive noise. The two fundamental heart sounds exhibit similarity in morphology, duration and superposition in frequency domain, thereby making automated diagnosis difficult. This study uses two parameters for heart sounds analysis in different IMFs- variance as power of S1 and S2 and Shannon entropy as a measure of complexity in terms of information content. The study is performed on 2732 recordings of PhysioNet Computing in Cardiology Challenge 2016 database.

The study of existing literature shows that the prior-work involving PCG signals primarily focussed on the fields including foetal heart rate monitoring [76], [81], [82], [87], fundamental heart sounds segmentation [73], [83], [91], [96], abnormal heart sound murmur detection [94], [97], [103] and noise reduction [84], [85]. Whereas, the field of using PCG signals for psychological stress detection is unexplored. Therefore, this research work focuses on the applicability of PCG signals in psychological stress detection.

3.2 Literature review on stress detection

The major work on psychological stress detection using bio-signals is often divided into two categories [104]:

1) Physical signals: These measures change as a result of muscle activity due to psychological stress like- eye movements, pupil size, speech, respiration and facial expressions.

2) Physiological signals: The change in vital functions of body due to psychological stress is covered under this category. Examples include- changes in cardiac activity, brain activity, Blood Volume Pulse, exocrine activity and electrodermal activity.

The contributions in the field of psychological stress detection are described in chronological order as follows:

Shusterman *et al.* [105] studied three methods for detection of sympathetic activation as indicator of stress on ten healthy subjects (three females and seven males). The methods included skin temperature variability, photoplethysmography (PPG) and HRV. The study showed insensitivity of temperature variability to noise or other mechanical factors and hence suitability for detection of sympathetic activation. The loss of correlation in temperature variability of right hand and left hand and a significant reduction in pressure wave envelope indicate sympathetic tone. This study also documented changes in HRV and temperature variability in response to mental stress in eighteen (sixteen males and two females) Coronary Artery Disease (CAD) patients and ten normal subjects. In controls, both temperature variability and HRV in very low-frequency range decreased, whereas, no changes occurred in spectral HRV power of CAD patients during stress.

Zhai *et al.* [106] experimented on Blood Volume Pulse (BVP), pupil diameter (PD) and Galvanic Skin Response (GSR) data acquired from six subjects. The stressor used for this study is Stroop test. The study used ten attributes for stress detection. The accuracy achieved is 80% using Support Vector Machine (SVM) classifier and sigmoid kernel function in differentiating stressed and non-stressed mental states of computer users. The study also demonstrated the hardware, software and signal processing requirements involved in this study of stress detection.

Kumar *et al.* [107] used HRV data of 38 (26 male, 12 female) physically fit volunteers during air traffic control task simulation and subjective stress rating was evaluated using NASA Task Load Index. The continuous wavelet transform was used to compute features of HRV signals and fuzzy clustering and fuzzy-based identification techniques were utilized to eliminate the effect of uncertainties because of individual variations in HRV for ANS assessment. The participants of the study were asked to refrain from use of coffee and nicotine before and during the conduct of experiment. This study contributed in quantifying mental stress and establishing a direct functional relationship between ANS activities and mental stress.

Choi *et al.* [108] suggested removal of respiratory influences from HRV signals as residual signals showed more discriminating power for monitoring mental stressed state in four subjects. This is because the breathing may fall in LF or HF band of HRV signal, reducing the diagnostic ability of HRV-based LF/HF ratio feature. The extracted residual signal for the stress condition had more spectral power as compared to relaxed condition

depicting better discriminatory power of residual signal. The dual-task for mental stress used in the study was tracking the target and memory search while following the pacing signal. The classifier used is quadratic classifier and classification performance of extracted residual signal outperformed the traditional HRV analysis method. The study also proposed a normalization method for compensating the ventilation differences between paced and spontaneous breathing.

Li *et al.* [109] reported superiority of Hilbert marginal spectrum based on EMD as compared to conventional power spectrum density estimation for assessment of ANS. The data used in this study is simulated HRV signals and real-HRV data from 7 healthy subjects. The selective blocking drugs namely atropine and metoprolol are used for this study. The R-R signal is interpolated and resampled to make R-R interval a function of time. The analytic signals obtained by using Hilbert transform is used for feature extraction. The frequency behaviours are then analysed to estimate spectral traits of HRV signal. The system proposed in the study is more sensitive in identifying low-frequency and high-frequency bands of HRV.

Sharma *et al*. [110] collected data from 35 (22 males, 13 females) graduate students while they watched stressed film clip and non-stressed film clip. The videos having facial regions in visible spectrum and thermal spectrum were acquired. The features used in the study are spatio-temporal features from thermal and visible spectrum videos. The study also contributed towards a new feature for thermal spectrum videos to capture dynamic thermal patterns in histograms. The fusion of thermal and visible spectrum facial patterns yielded 72% stress recognition rate using SVM classifier.

Chen *et al.* [111] contributed in the field of contact-less stress detection and suggested the use of hyperspectral imaging technique for extraction of tissue oxygen saturation value in 21 volunteers. The stressor used for the study is Trier Social Stress Test and stress detection accuracy achieved is 88.1% with manual selection of classifier threshold. For this study, the participants with a 125% higher cortisol level and a 6 bpm higher heart-rate were regarded as stressed candidates. This method can serve as a non-contact type stress detection modality.

Lanata *et al.* [112] accessed the changes in ANS and style of driving due to an incremental increase in stress. This experiment was performed on 15 subjects and parameters like HRV, respiration and electrodermal response (EDR) and parameters from

steering wheel like change in velocity, angle and time response were monitored during simulated driving. The stressors used in the study included unpredictable skids of vehicle during simulated driving and a further increase in stress, induced by time-based arithmetic questions along with unpredicted skids. The accuracy achieved is greater than 90% in discriminating three driving sessions- simple driving, stressed driving, and increased stress-level driving.

Al-Shargie *et al.* [113] proposed fusion of EEG and functional near-infrared spectroscopy (fNIRS) data acquired from prefrontal cortex showed improvement of 3.4% and 11% in classification accuracy of mental stress as compared to unimodal EEG and fNIRS modalities respectively. This study was conducted on 22 healthy male participants and experiment was conducted based on Montreal Imaging Stress Task and mental arithmetic task. The alpha amylase measurement was also conducted on the participants. The SVM classifier was used in this study.

Baltaci *et al.* [114] acquired pupil diameter and thermal data from 11 (2 females, 9 males) healthy subjects. The stress is induced by viewing pictures from International Affective Picture System (IAPS). The classifiers used in the study included decision tree classifier and Adaboost with random forest classifier. The performance of Adaboost with random forest was better than decision tree classifier. The features extracted from pupil diameter and periorbital temperature yielded the best accuracy as 83.8%. The best sensitivity and specificity reported in the study is 83.9% and 83.8%. The study showed that entropy in a pre-defined time window offers useful features for combining with actual measurements.

Giannakakis *et al.* [115] contributed in contact-less stress detection and used video-recorded facial cues extracted from mouth activity, eye activity, head movements and heart rate estimate through camera-based PPG as indicators of stress and anxiety. The data from 23 adults (7 women, 16 men) and stressors used included social exposure, emotion recall, stressful images from IAPS and stressful video. The study also used self-report in order to correlate facial parameters to perceived stress. During stress, eye blink rate increased, small rapid head movements indicated by head movement amplitude and velocity and heart rate increased. The highest classification of 91.68% is achieved during social exposure phase by Adaboost classifier.

Anusha *et al.* [116] acquired electrodermal activity (EDA), skin temperature (ST) and ECG from 34 (20 males, 14 females) subjects. The stressor used in the study is laboratory

intervention that matches with real-life job stress by combining mental workload, performance pressure and time pressure. The stress response validation was done using salivary cortisol level. This work used 61 features and four classifiers namely- Linear Discriminant Analysis, Quadratic Discriminant Analysis, Support Vector Machine with Radial Basis Function kernel and k-Nearest Neighbour classifier with k=3 are used in this study. The analysis in the study was conducted on ECG of 300 s duration as per international guidelines for short-term HRV analysis, whereas, EDA and ST data segments of 300 s, 180 s, 60 s and 30 s were examined. The EDA performed well for 60 s data segments and ST for 30 s data segments. The study showed EDA as the best single modality, whereas, highest accuracy of 97.13% is achieved for stress recognition with combination of EDA and ST.

Xia *et al.* [117] worked on early detection of mental stress using both EEG and ECG signals acquired from 22 male subjects. This study emphasized on performing predictions not on accuracy but for treatment efficacy by defining four stress levels and creating models for individual levels. The accuracy, sensitivity and specificity achieved using this method is 79.54%, 81%, and 78% respectively. The stressors used in the study are Montreal Imaging Stress Task and arithmetic questions. The study also highlighted significant neurophysiological differences at individual level between stress and stress-free conditions. The features computed for this study are- relative power, power ratios, coherence, amplitude asymmetry and phase lag and SVM classifier with RBF kernel and sigmoid kernel are utilized in this study.

Asif *et al.* [118] studied effect of music tracks on human mental-stress levels. In this study, EEG signals from 27 (14 males, 13 females) subjects were acquired using MUSE headband while listening to different music tracks. The subjects were asked to fill self-report state and trait anxiety questionnaires. The features computed from acquired EEG signal for this study included- absolute power, relative power, coherence, phase lag and amplitude asymmetry. The classifiers used in the study are sequential minimal optimization, stochastic decent gradient, logistic regression, and multilayer perceptron. The performance of logistic regression classifier was better and reported classification accuracy of 98.76%. It is also concluded from the study that music tracks lead to reduction in stress levels and stress response of females is more sensitive for music tracks as compared to males.

Castaldo *et al.* [119] made an important contribution by suggesting the use of ultra-short HRV features extracted from duration of less than 5 min as valid surrogates for short-term HRV features extracted from 5 min duration. These findings can be helpful in real-time e-health monitoring where 5-min recordings might be unsuitable. The ECG signals used for the study are acquired from 42 healthy subjects during university exam and resting phase. The 23 features from ultra-short length were compared with the standard short HRV features. The results of the study indicate that 6 features out of 23 showed consistency across all durations from 5 min to 1 min, whereas, 3 out of the selected 6 ultra-short HRV features namely- MeanNN, StdHR, and HF achieved accuracy above 88% using Neighbour Search (IBK) classifier.

Mejia *et al.* [120] conducted a whole-body cold exposure study on 20 healthy subjects for assessment of autonomic responses. This study extracted Pulse rate variability (PRV) data from ear canal, ear lobe and peripheral sites such as fingers and toes from photoplethysmography signals. In addition to this, HRV data was also acquired. The study aimed to explore the effect of cold exposure on autonomic control and on the relationship between HRV and PRV signals. The findings of the study showed an increase in PRV time-domain and Poincaré plot indices, differences were also observed in frequency-domain indices; however, relative-power parameters remain unaltered. The HRV-indices showed similar trends but were less impacted than PRV. The study showed promising results for PRV-based autonomic activity assessment on different body locations thus giving insights on localized autonomic nervous system responses.

Zubair *et al.* [121] also contributed in multi-level stress detection using ultra short-term PPG recordings of a low-cost wearable sensor for PRV estimation. The stressor used in the study is mental arithmetic task and subjective validation of stress was done. The study used beat-to-beat interval series estimated from PPG signals of 60 seconds duration and features are proposed in the study captured temporal information of PPG quantify it in Poincare plot. The classifiers used in the study are quadratic discriminant analysis and SVM. The findings of the study reported 94.33% accuracy of proposed method with SVM for five-level identification of mental stress. This study is also validated on a dataset using a different Stroop test as stressor.

The above mentioned studies show the applicability of ECG-based HRV signals [107]–[109], [119], EEG signals [113], [118] and imaging [110], [111], [114], [115], PPG and

PRV [115], [121] for stress detection. The fusion of various modalities including skin temperature variability, photoplethysmography, BVP, pupil diameter, electrodermal activity, EEG and ECG are used in various studies for psychological stress detection [105], [106], [112], [116], [122]. The prior-work showed no considerable effort towards PCG-based psychological stress detection. As the ECG signal is temporally related with PCG signal [71], it is proposed that the latter can be used for psychological stress detection.

3.3 Commercial wearables for stress detection

The rising levels of stress on a global level and increase in the knowledge regarding the harmful effects of stress on physical health and well-being lead to an increase in emphasis on stress monitoring. In order to explore this field, commercially available wearables including smartwatches and fitness bands provide unobtrusive, non-invasive continuous stress monitoring. These wearables provide physiological measurements and analytics for gauging the state of mind. The important contributors in wearable stress monitors include Garmin, Apple and Fitbit.

Figure 3.1 The commercial wearable smartwatches depicting stress (image from [85])

The Garmin devices use HRV for stress level detection computed from heart rate data. In case of higher stress levels, there is less variability between beats, whereas less stress is

indicated by an increase in variability between beats. The stress score between 1 to 100 on Garmin devices, as shown in figure 3.1, is the result of a three-minute test performed while standing still for analysing HRV, where 1 is very low-stress state and 100 is very high-stress state [123].

The Apple watch and Samsung galaxy watch also utilizes heart data acquired from the wrist in order to compute stress level and provide early detection of increased stress. The optical heart sensor in smartwatch heart rate monitor generally uses photoplethysmography. The sensors are generally located in back-panel of the watch as shown in figure 3.2. This technology uses an optical LED light source and an LED light sensor and as the light shines through the skin, the sensor measures the amount of light reflected back. The reflections of light reflections vary as blood pulses under the skin of wrist pass the light. These variations in light reflections are interpreted as heartbeats [124]. The reason for colour of blood appearing red is that it reflects red light and absorbs green light, therefore, Apple watch uses green LEDs and light-sensitive photodiodes for detection of amount of blood flowing through wrist. During heartbeat, blood flow in the wrist and leads to more absorption of green light, whereas, in between the beats lesser amount of green light absorption takes place. The LEDs are flashed hundreds of times every second to compute number of heartbeats per minute and range of heartbeats supported is 30-210 beats per minute and the low-level signal is compensated by an increase in brightness of LED and sampling rate [125]. However, the Fitbit sense uses electrodermal activity for stress detection.

Figure 3.2 The image showing sensor placement on a smartwatch (image from [88])

Another wearable device, Muse is an EEG-based headband and has seven calibrated sensors for detection and measurement of the brain activity and is shown in figure 3.3. This device translates brainwaves to guiding weather sounds, for instance, if the mind is in calm state, peaceful weather sound is heard and if the mind is busy and distracted, stormy weather sound is heard [126].

Figure 3.3 The wearable EEG-headband (image from [90])

The recovery process during sleep is also a significant feature in wearable technology for stress monitoring. The wearables are also moving further by providing meditation sessions, recommending deep breathing in order to lower the stress levels and return to a calm mental state.

A study [127] summarized the major contributions in stress detection using wearable technologies and useful physiological signals for stress detection. This study also identified data acquisition challenges in wearable technologies that include frequent movement of data acquisition site, for instance, the wrist movement during data acquisition by smartwatch sensor. The improper placement of sensors can also lead to unreliable data. The need for wearables to be charged several times for recording a single day data as the battery life is generally 3-4 hours when all sensors are active, the big data problem and difficulty in data fusion from different sensors are also significant challenges during data acquisition using wearable sensors.

3.4 Research gaps

The research gaps identified during the study of existing literature and state-of-art technologies include:

- The existing studies mainly focussed on psychological stress detection using EEG or ECG signals that are expensive or require proper clinical setup, but no significant efforts have been done towards the detection of psychological stress using PCG signals
- The mental health problems are prevalent globally, with India alone having 197.3 million mental health patients. Despite this, the problem of low-cost home-care based solutions for timely detection of psychological stress is not addressed
- The methods suitable for telemedicine and computer-aided psychological stress diagnosis are not available
- Most significant features for psychological stress detection have not been identified

Based on the aforementioned problem definitions, the goal of this research is to develop a low-cost PCG-based framework for timely detection of psychological stress that is suitable for home-care and telemedicine and can serve as an alternative to well-documented ECG-based method.

3.5 Summary

The studies done on PCG signals mainly focussed on fundamental heart sounds detection, foetal heart rate monitoring and murmur detection. The psychological stress prevailing globally needs timely detection and home-care based pre-screening to prevent manifestation of diseases. The methods available for psychological stress detection like EEG and ECG signals are not suitable for this purpose. The easy to acquire PCG signals are temporally related to ECG signals and this provided the insight of using PCG for psychological stress detection. The hidden diagnostic information from non-linear and non-stationary dynamics of cardiac signals can be extracted using non-linear features computed from PCG signals in EMD domain. This time-frequency domain signal

decomposition and analysis technique is suitable for non-linear and non-stationary data. This study explores PCG-based non-linear features to find the most discriminating features for psychological stress detection. This is a new research area for application of PCG signals.

CHAPTER 4 DATA ACQUISITION AND PRE-PROCESSING

4.1 Data acquisition

4.1.1 Introduction

A comprehensive list of accessible databases for PCG signals is available at [93]. These databases are available for fundamental heart sound segmentation and abnormal heart sound murmur detection but no database is reported for PCG-based psychological stress detection. As per the extensive literature survey, the authors did not come across any prior-work that addresses the issue of psychological stress detection using PCG signals. Hence no publicly accessible dataset was available for psychological stress detection using PCG signals. Therefore, the challenges of this study were more as dataset under the guidance of physician needs to be acquired for psychological stress detection using PCG signals.

In this study, the ECG and PCG signals were simultaneously acquired as shown in figure 4.1, so that the ECG signal is used as a reference signal for S1 peak detection of PCG signal and later for comparison of the results with that obtained from PCG-based method. The ECG and PCG signals are not used directly in this study but instead, HRV and IBI signals derived from the timing information of respective signals are used for further analysis and psychological stress detection. For this study, the data was acquired from 33 healthy male students in the age group of 18 to 25 years (mean = 20.11, standard deviation = 2.30) of Thapar Institute of Engineering and Technology, TIET campus who were to attempt the professional education institute examination. The readings of this study are taken as per guidelines of Task Force by European Society of Cardiology and

North American Society of Pacing and Electrophysiology. In case of ECG signals, the optimum sampling rate between 250 Hz-500 Hz and 5-minute duration of recording is suggested to capture proper diagnostic information and fiducial point estimation [67], [128]. Thereafter, ECG R-wave fiducial point information is used to detect S1 peaks of PCG signal. The S1 peak frequency in normal subjects was reported at 46±2Hz [129] and the spectrum of S1 is reported up to 120 Hz [130]. Therefore, simultaneous PCG and ECG signals of five minutes duration were recorded using Medicaid's dual-channel PhysioPac having sampling frequency (F_s) 256 Hz. In this study, the simultaneous ECG and PCG signal recordings of duration five minutes, approximately two hours before the start of the exam were considered as the signals of subjects under psychological stress. The baseline values for subject-specific template formation were recorded once the students returned from holidays after exams under similar environmental conditions.

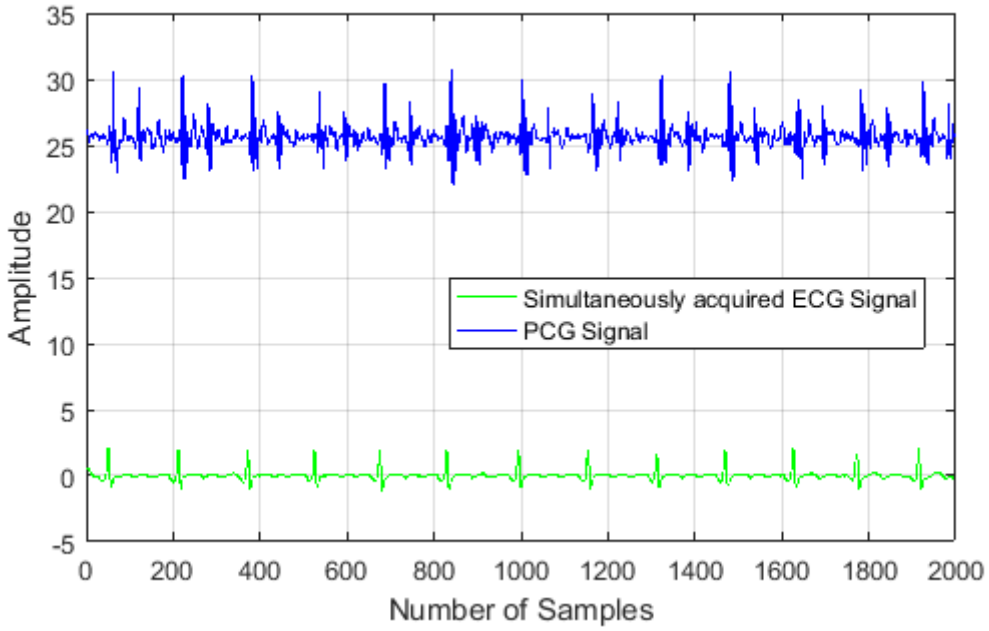

Figure 4.1 Simultaneously recorded PCG and ECG signals

4.1.2 Stressors- Laboratory induced and real-life stressors

The studies for stress detection using laboratory-induced stress show increased sympathetic activity and reduced baroreflex gain but their efficacy is limited due to intrinsic artificiality [131]. The models like public speaking can affect respiration due to speaking and may interfere in the interpretation of results [131]. Therefore, the real-life

stressors might involve negative emotions and can be more clinically relevant for psychological stress detection [131], [132]. The real-life psychological stress occurs when the complex dynamic equilibrium called **homeostasis** is threatened by real-life forces or situations termed as real-life stressors. The real-life stressors used in various studies include- examination stress [119], [131]–[133], stress due to dental procedures [134] and job interviews [135]. The stress in this study is not laboratory-induced [136], [137], rather real-life examination stress [131]–[133]. The data for this study is acquired from students approximately two hours before the institute examination and another reading as baseline is acquired from the same subjects after they return from holidays as done in studies [131], [132].

4.1.3 Duration of data acquisition

The duration of simultaneous ECG and PCG data acquisition for this study is 5-minute and rationale behind this is explained ahead. In the present study, stress is not induced using cold pressor test, colour stroop test and trier social stress test (TSST) as the intrinsic artificiality of these tests may not elicit negative emotions otherwise experienced during a real-life stressful situation. The students of the institute undergoing examination are already stressed, so the designed study protocol did not require the time for inducing stress using a task. Additionally, the baseline readings are taken on another day, when the participants of the study returned from home after exams, therefore, recovery period is also not the requirement of the study protocol.

The requirement of the study is to compute LF/HF ratio parameter of ECG-HRV signal as sympathovagal indicator and on similar lines developing a novel PCG-IBI based psychological stress detection method as ECG and PCG signals are temporally related. Therefore, as per the guidelines of Task Force by European Society of Cardiology and North American Society of Pacing and Electrophysiology involved in standardization of measurement methods for HRV analysis, a 5 minute ECG recording is sufficient for short-term frequency-domain HRV analysis. As LF/HF ratio is a frequency domain parameter, a 5-minute recording is sufficient.

Moreover, on similar lines, the studies [132], [138] conducted using examination as real-life stressor, used 5-minute ECG signal acquisition. The novel PCG-based psychological

stress detection method proposed in this work required simultaneous signal acquisition of ECG and PCG signals as these signals are temporally related. Therefore, signal acquisition duration of 5-minutes is sufficient for this study. In addition to this, a recent study [119] for mental stress assessment during university examination also highlighted the use of ultra short-term HRV signals of duration less than 5 minutes for stress detection.

4.1.4 Sampling frequency for the study

The sampling frequency used for this study is 256 Hz and the reason for this is explained ahead. A study [139], is conducted on ECG signals originally sampled at 1 kHz and down-sampled to 500 Hz, 250 Hz, 100 Hz and 50 Hz for determining acceptable ECG sampling frequency range for HRV analysis. It concluded that ECG sampling frequency of 250 Hz ensures sufficient R-R interval precision and is acceptable for HRV analysis. However, if frequency-domain analysis of HRV signals is not required then a sampling frequency of 100 Hz is also acceptable, but, in this study, LF/HF ratio is required which is a frequency domain measure, therefore, minimum acceptable sampling frequency required is 250 Hz. Additionally, readings are taken as per the guidelines of Task Force by European Society of Cardiology and North American Society of Pacing and Electrophysiology. In case of ECG signals, the optimum sampling rate between 250 Hz-500 Hz and 5-minute duration of recording is suggested to capture proper diagnostic information and fiducial point estimation [67], [128].

In case of PCG signals, we need to detect S1 peaks using ECG R-peak fiducial point as a reference. The S1 peak frequency in normal subjects was reported at 46±2Hz [129] and the spectrum of S1 was reported up to 120 Hz [130]. Therefore, the sampling frequency of 256 Hz is sufficient for this study.

The protocol adopted for data acquisition of this study is explained in the next section.

4.1.5 Data acquisition protocol

The protocol adopted for this study of psychological stress detection using PCG signals is explained as follows:

The data acquisition is done about two hours before the start of institute exam, at around 11 am, for institute exam starting at 1 pm. In order to avoid diurnal variations, the baseline readings were also recorded around 11 am on another day when the participants of the study returned from home after exams.

Inclusion criteria

{1} Any adult male student of Thapar Institute of Engineering and Technology having institute examination the next day

{2} Agrees to give two readings: R1- approximately 2 hours before the institute exam conducted the next day; R2- baseline reading recorded once participant returns to institute from home after exams

{3} Eligible and willing to participate in the study

{4} No medical history

{5} Not currently on any type of medications

The primary outcome of the study is detecting psychological stress using PCG signals and secondary outcome of the study includes a comparison of obtained results with ECG-based LF/HF ratio sympathovagal indicator method. The primary end-point is recording R2 baseline readings.

The State-Trait Anxiety Inventory (STAI- Y1) self-report questionnaire was filled by each participant before the data acquisition. The STAI form has twenty statements to evaluate how the participant feels right now (in the present moment). It is a 4-point scale where 1 indicates “not at all”, 2 indicates “somewhat”, 3 stands for “moderately so” and 4 stands for “very much so” pertaining to the statements. It deals with the state anxiety and showed high alpha reliability coefficients under unavoidable conditions of psychological stress. This STAI S-Anxiety questionnaire used in this study is reported to show high reliability when used under psychological stress conditions and has been found suitable in real-life stressors such as job interviews, important examination and dental procedures [140]. The scores on the S-Anxiety scale increase when used under psychological stress and decrease after relaxation [140]. As per the developers of this STAI scale, the affective states considered under stress class are tension, nervousness, apprehension and worry [140]. The examination is a prominent real-life stressor for the students of age-group 18 to 25 years. The non-stress baseline in this study is when the students return from holidays after the exams as suggested by the clinical psychologist of the institute and used in previous studies [131], [132].

As per the recommendation of the supervisor of this study, the data acquisition was done at the waiting lounge of the hostel of the participating students, where the students reside and prepare for exams in order to avoid laboratory settings for real-life examination stressor based data acquisition. The students from various disciplines of engineering including mechanical, electrical, computer sciences and electronics engineering participated in the study.

The steps included during data acquisition procedure are as follows:

- The subjects were informed about the purpose of the study and written consent was taken
- The subjects were asked to fill a declaration form about any medications recently used or any medical history
- The subjects were asked to answer State-Trait Anxiety Inventory (STAI Form Y) self-report questionnaire for evaluation of their present psychological state
- The subjects were asked to lie in the supine position and breathe normally
- The PCG sensor was placed on fifth intercostal space along the left mid-clavicular line
- ECG strap electrodes were attached to limbs of the subjects after applying bio-electrode gel for better conductivity
- The simultaneous PCG and ECG signals of five minutes duration were acquired

This protocol of signal acquisition was approved by a practising physician and the readings for this study were taken under his guidance. The records of the subjects on medications were removed from the study. The study has ethical clearance from the institution ethics committee.

The study design has certain limitations and compromises as in this study, the difficulty level of the examination, the subjective understanding and interpretation of the STAI questionnaire presented to the participants is not considered. In addition to this, the dataset is small and only male participants are included in this study making the findings gender-specific. The dataset needs to be increased and include female data analysis to make it a robust generalized system. The individual trait interpretations cannot be gauged from this data as the study deals with state data. The other real-life stressors are not included in this study and the present study does not explore the chronic stressful conditions that are believed to cause pathological issues.

The acquired signals need to be pre-processed to make them suitable for further analysis and psychological stress detection. The pre-processing of signals performed in this study is explained in the following section.

4.2 Pre-processing of signal

The acquired ECG and PCG signals are not used directly in this study but instead, HRV and IBI signals derived from the timing information of respective signals are used for further analysis and psychological stress detection. The time duration of cardiac cycles consisting of consecutive S1 peaks is computed from acquired PCG signals to form IBI signals. The extracted IBI signals are used for further analysis and psychological stress detection.

In order to form IBI signal, FHS segmentation is to be done, which requires identifying fundamental heart sounds S1 and S2 of the PCG signals. The methods reported in literature for FHS segmentation can be divided into two categories. The first set of studies [71], [84] used simultaneously recorded ECG signal as a reference for FHS segmentation. This method is called ECG gating and depends on the timing information provided by R-peak of ECG signal. These methods locate R-peak in the ECG signal and the corresponding peak in PCG signal will be S1, thus leading to reliable detection of S1, S2, systole and diastole [70]. The second set of studies [73], [91], [94], [96] focuses on FHS detection without simultaneous ECG signal. These methods have also shown reliable results. The primary motive of the developed methodology is to emphasize the use of PCG for psychological stress detection, thus in this study, ECG is used as a reference signal for FHS detection.

The acquired ECG signal has baseline wander as shown in figure 4.2. The baseline wander is removed from the acquired ECG signals $e(i)$, for reliable detection of R-peaks using a bandpass filter of lower cut-off frequency 0.3 Hz and higher cut-off frequency of 15 Hz [141]. Thereafter, Pan-Tompkins algorithm [142] is applied for peak detection and location identification of R-peaks in baseline wander removed signal $\hat{e}(i)$. Then, the resulting signal $\hat{e}(i)$ is normalized by

$$\bar{e}(i) = \frac{\hat{e}(i)}{\max(|\hat{e}(i)|)} \tag{4.1}$$

where $e(i)$ is the acquired ECG signal, $\hat{e}(i)$ is the filtered signal and $\bar{e}(i)$ is the normalized signal to the fixed scale of [-1,1].

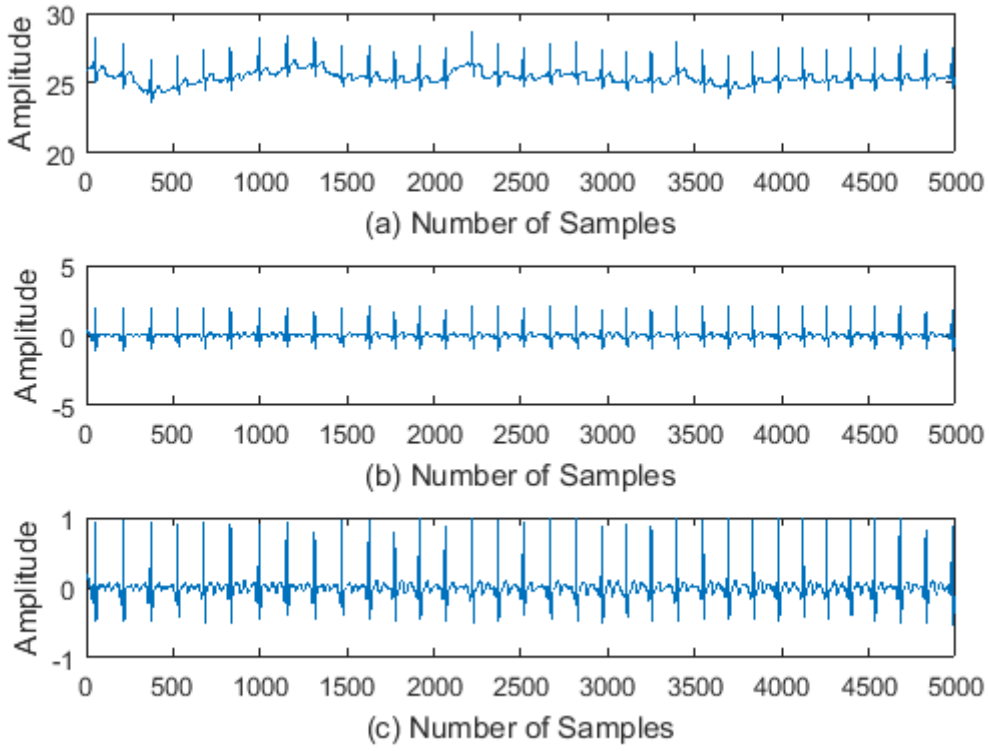

Figure 4.2 a) ECG signal with baseline wander b) ECG signal with baseline wander removed c) Normalized ECG signal

The acquired ECG signal with baseline wander and corresponding corrected ECG signal are shown in figure 4.2. This corrected ECG signal is then used for S1 peak detection of PCG signals. The peak occurring in PCG signal, corresponding to R-peak of simultaneously acquired ECG signal will be S1 peak. Firstly, the R-peak of processed ECG signal is detected. Thereafter, windowing method is used to select a portion of PCG signal $p(i)$ where the probability of finding S1 peak is maximum. Then the peak detected in this portion of PCG signal is S1 peak. Then this is repeated for the next identified R-peak of ECG signal till all the R-peaks in ECG signal and corresponding S1 peaks of PCG signal are identified. The algorithm 1 is used and all the S1 peaks of PCG were detected as shown in figure 4.3, but for uniformity in signal analysis, a total of 300 S1-S1 peaks were considered. The algorithm used for S1 peak detection is provided below:

Algorithm1: Windowing Technique for PCG peak detection

Variables: E_p = *Number of R-peaks of ECG*

k = Location of i^{th} *R-peak*

n = Average number of samples depicting duration of S1 peak (based on dataset template)

for i = 1 to E_p

pcgWindow = PCG signal from k to k+n samples

Find Peaks in pcgWindow

maxP = maximum of peaks detected in pcgWindow corresponding to the i^{th} *R-peak*

location of i^{th} *PCG peak = location of maxP + k - 1*

end

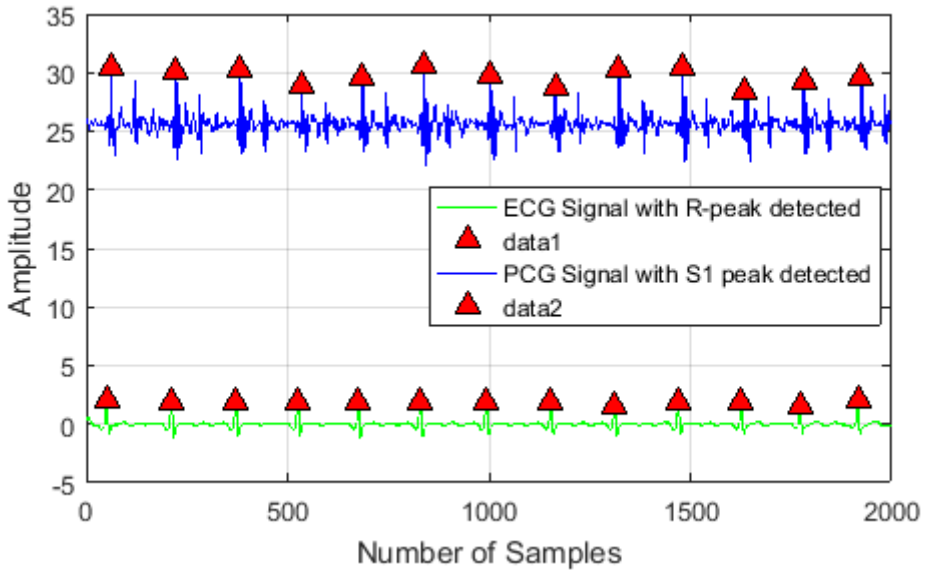

Figure 4.3 Simultaneous ECG and PCG signals with peaks detected

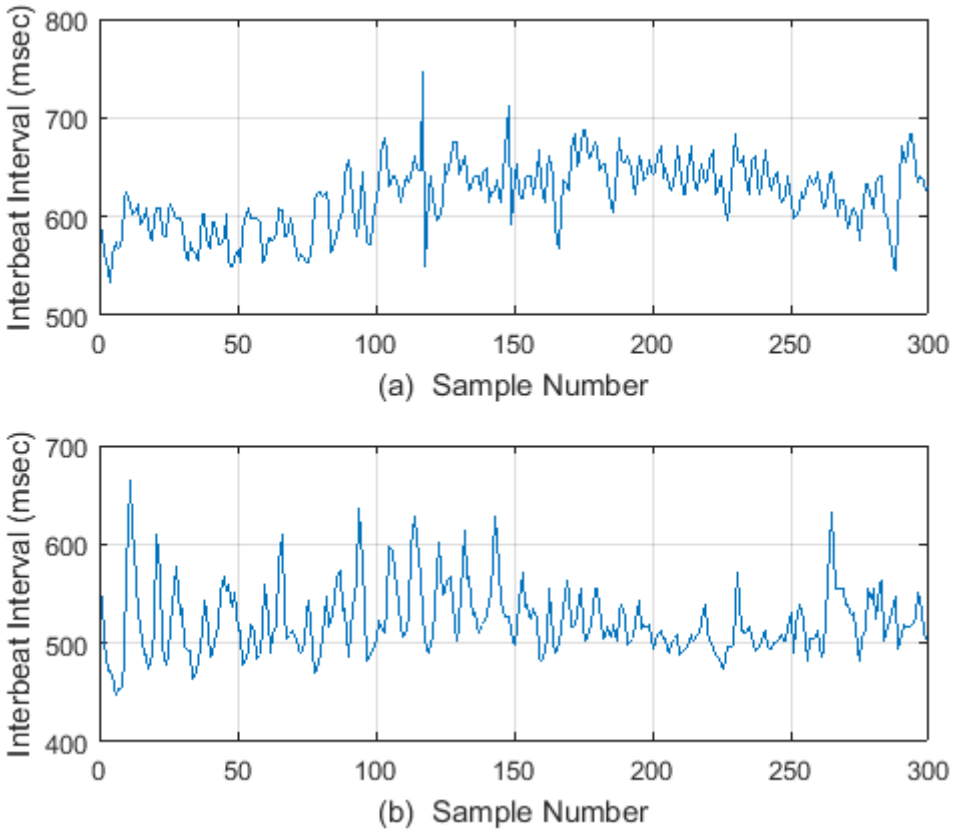

Figure 4.4 Plots of Interbeat Interval (IBI) signal a) Baseline state b) Stressed state

The peak detection algorithm when implemented detects the S1 peaks in PCG signal by the technique of ECG gating as shown in figure 4.3. The duration between two consecutive S1 peaks, t_{SS} is calculated to form IBI signal $s(i)$. The IBI signals for baseline non-stressed state and stressed state are shown in figure 4.4. This IBI signal will be further used for signal analysis and psychological stress detection.

The specifications of the computational facilities used for this study include signal processing and analysis using MATLAB 2016a installed on HP Pavilion dv6 notebook PC with Intel core i5 – 2430M CPU with 2.4GHz processor base frequency, 4 GB RAM, 64-bit operating system. In addition to this, data acquisition was done using Medicaid's dedicated software for Physiopac ECG and PCG data acquisition device.

4.3 Summary

The simultaneous ECG and PCG signals were acquired as per the guidelines of Task Force by European Society of Cardiology and North American Society of Pacing and

Electrophysiology. The simultaneously acquired ECG signal serves two purposes- firstly, S1 peak detection in PCG signals using ECG-gating method and secondly, the ECG signals will also be used for comparing the results with PCG-based method. The stressor used in this study is real-life examination stress and not laboratory-induced stress as their efficacy is limited due to intrinsic artificiality. The IBI signal is derived from the timing information of consecutive S1-peaks. Therefore, acquired PCG signal is not used directly for psychological stress detection but the inter-beat interval signal derived from PCG signal will further be used for signal decomposition and analysis to detect psychological stress.

CHAPTER 5 EMPIRICAL MODE DECOMPOSITION

5.1 Introduction

The signal decomposition is often a pre-requisite for useful feature extraction and classification problems. The signals acquired from biological systems like humans are generally non-linear and non-stationary. The analysis of these signals require information of both time and frequency domain. The time-frequency domain techniques like Fourier spectral analysis are available, but they impose crucial restrictions of linearity and stationarity of data. The time-frequency domain non-stationary signal processing techniques like short-time Fourier transform (STFT), Wavelet transform (WT) and Wavelet packet transform (WPT) have been applied for biomedical signals, but the drawbacks of these methods include linear data assumption and the requirement of *a priori* designed basis functions for signal decomposition [143], [144]. Therefore, the above methods are inadequate to capture the complex non-linear dynamics of cardiac signals.

In STFT method, the width of window remains constant for signal analysis and hence, the time and frequency resolution cannot be altered. The selection of wide window in time-domain results in fine resolution in frequency-domain and poor resolution in time-domain [145]. For non-stationary analysis, good time resolution is required at the event of high frequency and fine frequency resolution is required at the occurrence of low-frequency [146]. Therefore, fixed resolution limits the performance of STFT. The scaling parameter of WT allows multi-resolution signal analysis. The study [147] used WT on ECG signals for detection of premature ventricular contractions and [148] used WT for patient-specific

ECG signal classification. The analysis using wavelets is linear and the selection of one basic wavelet for data analysis makes wavelet-based analysis non-adaptive in nature.

The Empirical mode decomposition is a time-frequency domain signal processing method which is applicable to non-stationary and non-linear signals. This adaptive and data-dependent technique makes no *a priori* assumptions on the input data for signal decomposition and hence found to be useful in many biomedical signal processing applications. The EMD technique has a limitation of mode-mixing when the signal to be decomposed has frequencies that are too close. The S1 and S2 heart sounds of PCG signals have overlapping spectra. However, in this study, the EMD technique is not applied on PCG signals directly, but on inter-beat interval signals derived from respective PCG signals, so this problem does not have a significant effect on this study. Moreover, on similar lines, EMD has been used in the analysis of various studies involving inter-beat RR-interval signals derived from ECG signals [149], [150]. The EMD has also been applied on EEG signals for analysing open eye and closed eye [151], normal and epileptic seizure EEG signals [152]–[155]. In addition to this, the EMD technique has also been used on PCG signals for heart sounds classification [156], heart sounds segmentation [91], heart sound analysis [102]. In this study, we are using EMD technique on PCG signals for analysis of stressed and non-stressed subjects.

The motivation behind using EMD for signal decomposition of PCG signals for psychological stress detection is the applicability of EMD technique on non-linear and non-stationary data. The data from biological systems generally violates conditions of stationarity and linearity. Therefore, techniques like STFT and Fourier spectral analysis are insufficient to capture the complex non-linear dynamics of cardiac sound PCG signals. The EMD technique works without defining a basis function and without setting *a priori* the level of decomposition whereas, defining a mother wavelet function is a pre-requisite before applying time-frequency domain wavelet transform method. Moreover, the EMD has been previously used on PCG signals [91], [156] and showed better decomposition of PCG signals in comparison to wavelet transform signal decomposition technique [91]. Therefore, in the present study, the EMD method has been used for signal decomposition and analysis.

5.2 Signal decomposition and analysis using EMD technique

In this study, EMD technique is used for decomposition of signals to mono-component sub-band signals. The EMD technique decomposes non-stationary and non-linear signals into a set of AM and FM mono-component signals called IMFs. In this study, EMD technique is used on IBI signal to form IMFs. These IMFs fulfil two basic conditions [143]:

i. The number of extrema and number of zero crossings must be the same or differ at the most by one within the entire dataset.
ii. The mean value of the envelope defined by local maxima and the envelope defined by local minima is zero at any point.

The decomposition of signal $g(t)$ into IMFs is done using an iterative process named as sifting process and is summarized as [143]:

1) Extract all the extrema of signal $g(t)$
2) Interpolate all maxima to form an upper envelope $Emax(t)$ and all minima to form lower envelope $Emin(t)$
3) Compute the average value of upper and lower envelope by:

$$c(t) = \frac{Emax(t) + Emin(t)}{2} \tag{5.1}$$

4) Find the difference between $g(t)$ and $c(t)$

$$d(t) = g(t) - c(t) \tag{5.2}$$

5) Check whether $d(t)$ fulfils the two basic conditions of IMFs mentioned above, if it does, go to step (7)
6) If $d(t)$ does not satisfy above-stated conditions for IMFs, repeat step 1 to step 4 till the conditions are met
7) After obtaining the IMF, $I_1(t) = d(t)$
8) Calculate the residue as:

$$R_1(t) = g(t) - I_1(t) \tag{5.3}$$

9) Rest of the IMFs will be obtained from the residue $R_1(t)$ by repeating step 1 to step 6

The above-described sifting operation is repeated until no more IMFs can be obtained from the final residue function. In this study, the stopping criterion used for sifting

process limits the standard deviation between two consecutive sifting results to typical value of 0.3 [107].

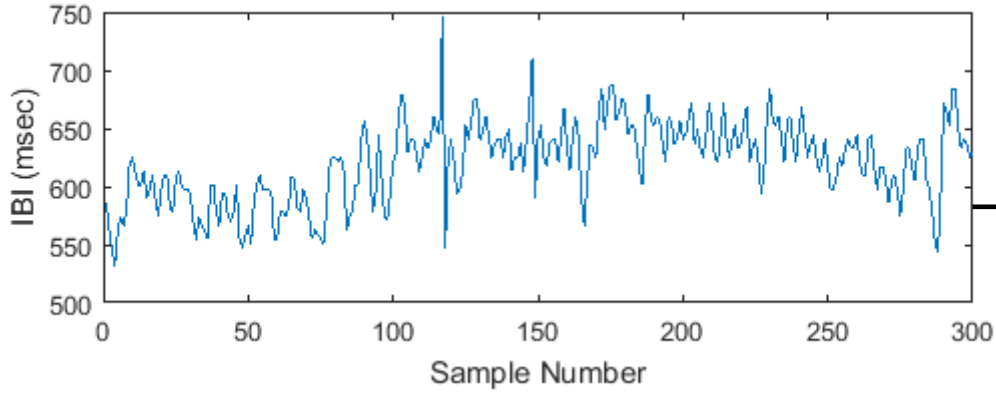

Figure 5.1 IBI signal of non-stressed subject

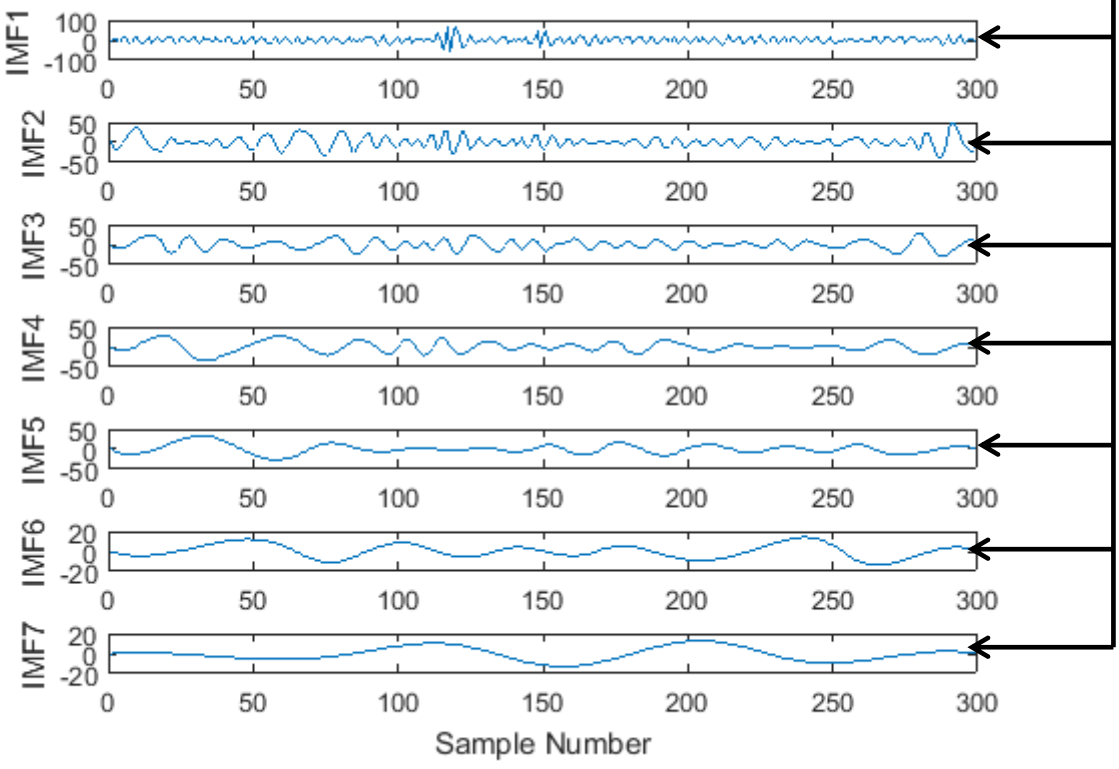

Figure 5.2 IBI signal of non-stressed subject decomposed to IMFs after application of EMD technique

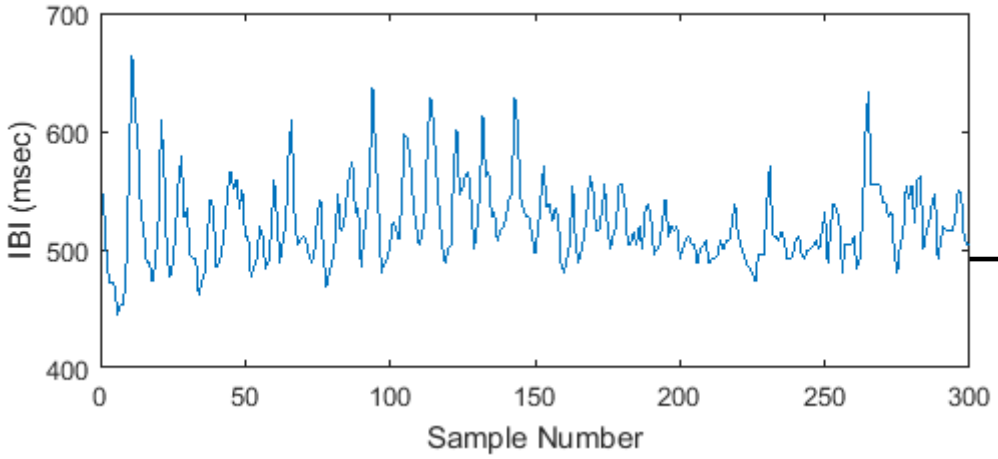

Figure 5.3 IBI signal of stressed subject

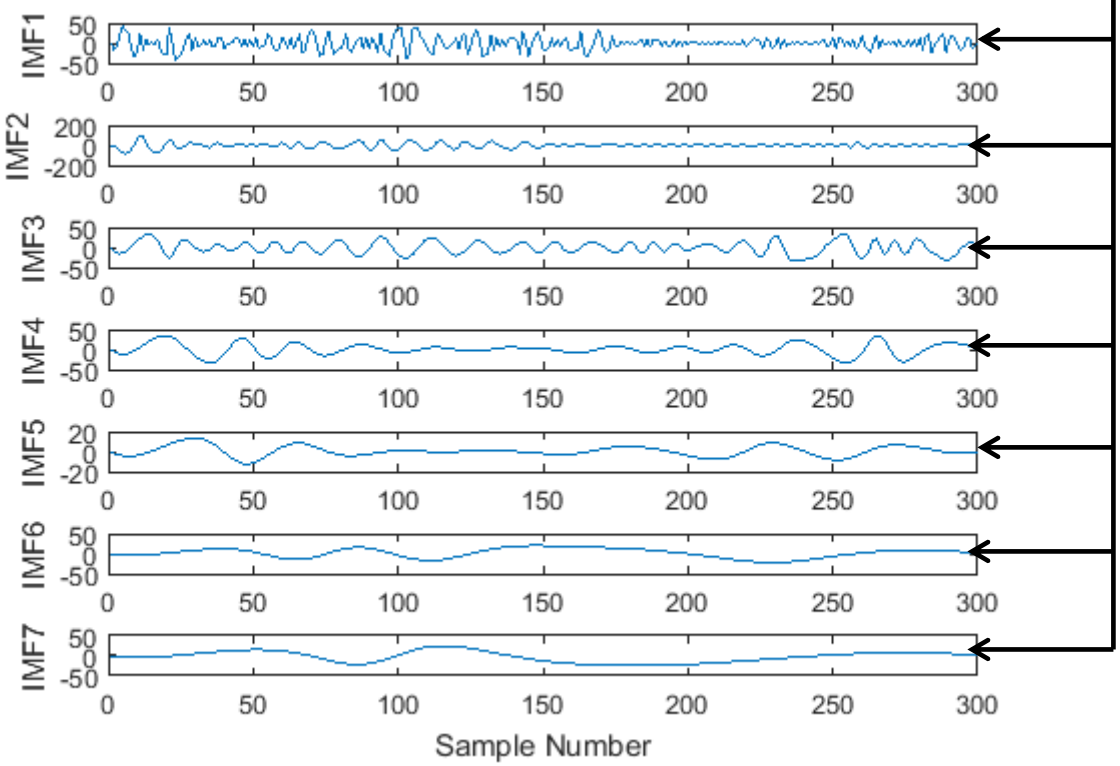

Figure 5.4 IBI signal of stressed subject decomposed to IMFs after application of EMD technique

The signal $g(t)$ after decomposition can be represented as:

$$g(t) = \sum_{m=1}^{M} I_m(t) + R_M(t) \tag{5.4}$$

where, $I_m(t)$ is the *m*th IMF, $R_M(t)$ is the final residue and M is the total number of IMFs extracted. The signal approximation of signal $g(t)$ is given by:

$$g(t) \approx \sum_{m=1}^{M} A_m(t) \cos\big(\varphi_m(t)\big) \tag{5.5}$$

The timing information of consecutive S1 peaks of acquired PCG signals is extracted to form IBI signals. The EMD technique is applied to decompose IBI signals to IMFs for signal analysis and feature extraction. The IBI signals decompose to different number of IMFs on application of EMD technique. In the present study, all the IMFs of the acquired signals were extracted. Each IBI signal of the dataset had atleast seven IMFs, so for uniformity in signal analysis, seven sub-band decomposition was selected as done in studies [149], [150], [157]. The MATLAB code for signal decomposition using EMD technique is available at **http://www.mit.edu/~gari/CODE/HRV/emd.m**

The IBI signal from non-stressed subject as shown in figure 5.1 is decomposed to IMFs on application of EMD technique as shown in figure 5.2. The IBI signal from subject in stressed state is shown in figure 5.3 and is decomposed to corresponding IMFs using EMD technique as shown in figure 5.4. The highest frequency components of the signal are captured in IMF1, subsequent lower frequency components are captured in IMF2 and lowest frequency components are in IMF7 as shown in figure 5.2 and figure 5.4. These IMF signals obtained by decomposition of PCG-derived IBI signals of non-stressed and stressed subjects are then used for feature extraction and detection of psychological stress.

5.3 Summary

The EMD is a convincing technique for time-frequency domain signal analysis. It often decomposes a signal into finite and small number of mono-component sub-band IMFs. The main advantage of EMD is the applicability on non-linear and non-stationary signals and hence is suitable to capture non-linear characteristics of cardiac signals.

CHAPTER 6 PROPOSED METHOD 1

6.1 Introduction

The goal of this research work is to develop a psychological stress detection system that is cost-effective, suitable for homecare and telemedicine using easy to acquire PCG signals. As discussed in the previous chapters, firstly, the S1 peaks are detected from the acquired PCG signals (described in chapter 4). Then the time interval between successive S1 peaks is computed in order to form IBI signals (described in chapter 4). Thereafter, the EMD technique for signal decomposition and analysis is applied on IBI signal to decompose it into mono-component sub-band IMF signals (described in chapter 5).

The next step is to extract non-linear features from the IMFs. The non-linear features have been widely used in the analysis of cardiac signals [158], [159]. These features unearth the underlying non-linear nature of PCG signals and are able to capture complex non-linear characteristics of cardiac signals. This PCG-based psychological stress detection method uses five non-linear features extracted using EMD approach namely- Area of Analytic Signal Representation (AASR), Log of Area of ellipse from Second-order Difference Plot (LASODP), Root Mean Square value of IMF (RmsIMF), Shannon Entropy (ShEnt) and Fuzzy Entropy (FzEnt). The explanation of these features is given in the next section.

The remaining chapter is organized as: section 6.2 describes non-linear feature extraction and feature selection is explained in section 6.3. The section 6.4 of this chapter describes the classifier used and the results and discussions are provided in section 6.5. The proposed method is summarized in section 6.6 of this chapter.

6.2 Feature extraction

The complex non-linear dynamics of PCG signals are explored using five non-linear features namely- AASR, LASODP, RmsIMF, ShEnt and FzEnt. The details of these non-linear features are discussed in this section.

6.2.1 Area of analytic signal representation

The analytic signal representation (ASR) of the IMF is obtained using Hilbert transformation [143]. The ASRs of the IMFs possess a unique center and proper structure of rotation [152]. The original IBI signals do not satisfy these conditions but the mono-component IMFs calculated using EMD technique satisfy these conditions as shown in figure 6.1. Therefore, the area of ASR plot of IMF signal can be evaluated and can be used as a feature for differentiating different classes.

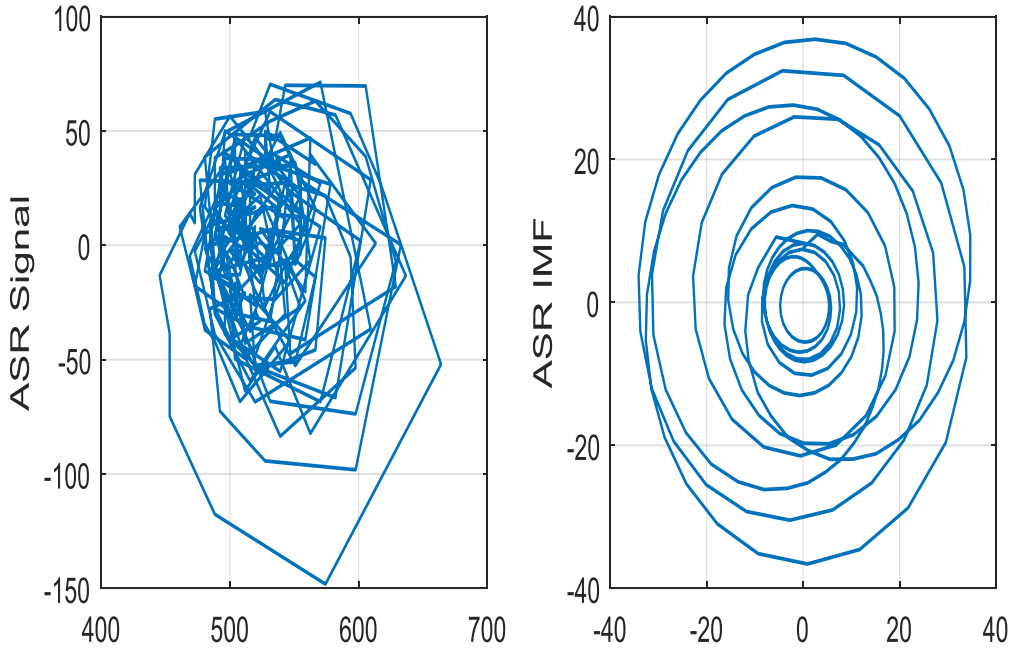

Figure 6.1 ASR of IBI signal and IMF signal

The Hilbert transform of a real signal $g(t)$ is given by:

$$g_H(t) = g(t) * \frac{1}{\pi t} \tag{6.1}$$

Therefore, the Hilbert transform of IMF $I(t)$ is given by:

$$I_H(t) = I(t) * \frac{1}{\pi t} \tag{6.2}$$

The ASR of the IMF is computed as:

$$a(t) = I(t) + jI_H(t) \tag{6.3}$$

Alternatively, the signal $a(t)$ in equation (6.3) can also be represented as:

$$a(t) = B(t)\exp\big(j\varphi(t)\big) \tag{6.4}$$

where, $B(t)$ is the amplitude of the analytic signal $a(t)$ and $\varphi(t)$ is the instantaneous phase and are calculated as follows:

$$B(t) = \sqrt{I^2(t) + I_H^2(t)} \tag{6.5}$$

$$\varphi(t) = tan^{-1}\left[\frac{I_H(t)}{I(t)}\right] \tag{6.6}$$

The ASR plot of signal $a(t)$ is obtained by plotting the imaginary part of signal $a(t)$ (i.e. $B(t)\sin(\varphi(t))$) against the real part, $B(t)\cos(\varphi(t))$. The ASR plots for seven IMFs of a non-stressed subject are shown in figure 6.2 (a) and for a stressed subject are shown in figure 6.2 (b).

Then the central tendency measure (CTM) has been used to compute the area of circle of ASR plots of IMFs in the complex plane. The radius corresponding to 95% CTM has been used to compute the area of ASR plot in the complex plane.

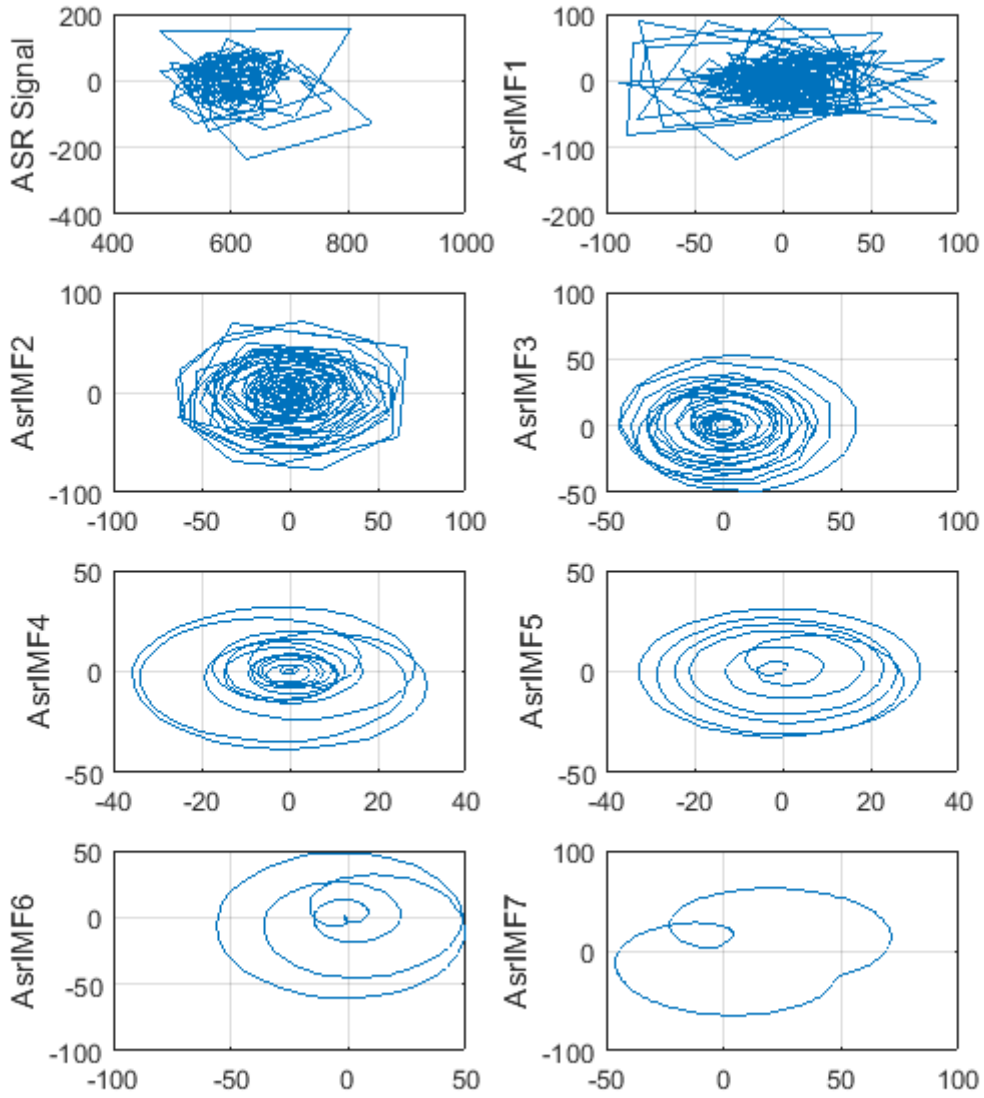

Figure 6.2 (a) ASR plots of IBI signal from non-stressed subject and seven IMFs

The CTM for ASR plot is computed by selecting a circular region of radius r, around the origin, then counting the points that fall within that radius, and dividing by total number of points [160]. Let N be the total number of points in analytic signal $a(n)$ and r is the chosen radius, then CTM for ASR plot is calculated as [152]:

$$CTM = \frac{\sum_{n=1}^{N} F(n)}{N} \tag{6.7}$$

Where,

$$F(n) = \begin{cases} 1 \; if \; ([Re\{a(n)\}]^2 + [Imag\{a(n)\}]^2)^{0.5} < r \\ 0 \; otherwise \end{cases} \tag{6.8}$$

The area of ASR plot is calculated using:

$$Area \; ASR = \; \pi r^2 \tag{6.9}$$

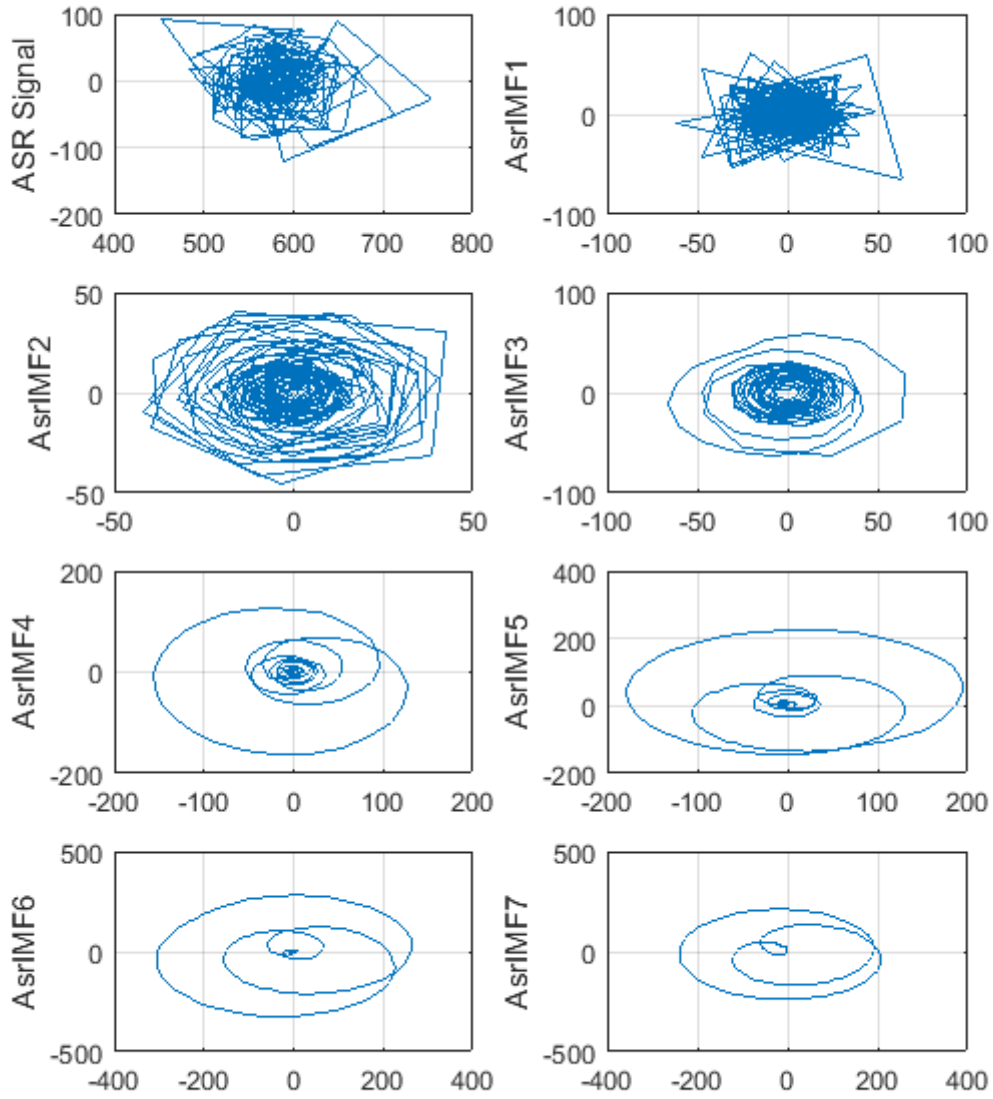

Figure 6.2 (b) ASR plots of IBI signal from stressed subject and seven IMFs

This feature has been used for epileptic seizure detection in EEG signals [152], [154]. It has also been used on ECG signals for normal and diabetic RR-interval analysis [149] and normal and coronary artery disease (CAD) heart rate signals [157]. In this study, this complex plane area feature is used on PCG signals to discriminate between the stressed and non-stressed (S and NS) subjects.

6.2.2 Area of second-order difference plot

The second-order difference plot (SODP) feature provides graphical representation of variability of the IMF signal. The SOD plot of IMF $I(n)$ can be obtained by plotting $K(n)$ against $J(n)$ where $J(n)$ and $K(n)$ are defined as [151]:

$$J(n) = I(n+1) - I(n) \tag{6.10}$$

$$K(n) = I(n+2) - I(n+1) \tag{6.11}$$

The plot obtained by plotting $K(n)$ as vertical axis and $J(n)$ as horizontal axis follows an elliptical pattern as shown in figure 6.3. The 95% confidence ellipse area is used to quantify the variability of signals. This parameter has been used in this study to discriminate between stress and non-stressed subjects in this study. It can be calculated as follows [151]:

Firstly, the means of $J(n)$ and $K(n)$ are calculated as:

$$M_J = \sqrt{\frac{1}{N}\sum_{n=1}^{N-1} J(n)^2} \tag{6.12}$$

$$M_K = \sqrt{\frac{1}{N}\sum_{n=1}^{N-1} K(n)^2} \tag{6.13}$$

$$M_{JK} = \frac{1}{N}\sum J(n)K(n) \tag{6.14}$$

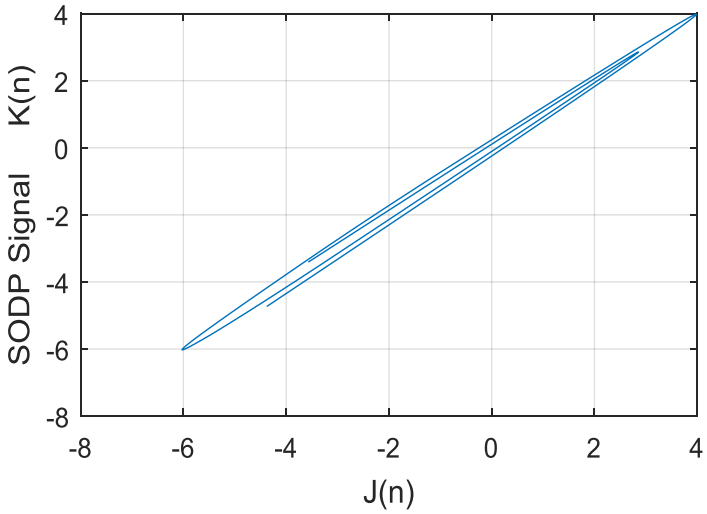

Figure 6.3 An elliptical pattern obtained using second-order difference plot (SODP)

Then, d parameter is computed as:

$$d = \sqrt{\left({M_J}^2 + {M_K}^2\right) - 4(M_J^2 M_K^2 - M_{JK}^2)} \tag{6.15}$$

The a and b parameters are computed as:

$$a = 1.7321\sqrt{\left(M_J^2 + M_K^2\right) + d} \tag{6.16}$$

$$b = 1.7321\sqrt{\left(M_J^2 + M_K^2\right) - d} \tag{6.17}$$

Now, the ellipse area of SODP is computed as:

$$Area\ SODP = \pi ab \tag{6.18}$$

The SOD plots for seven IMFs of a non-stressed subject are shown in figure 6.4 (a) and for a stressed subject are shown in figure 6.4 (b).

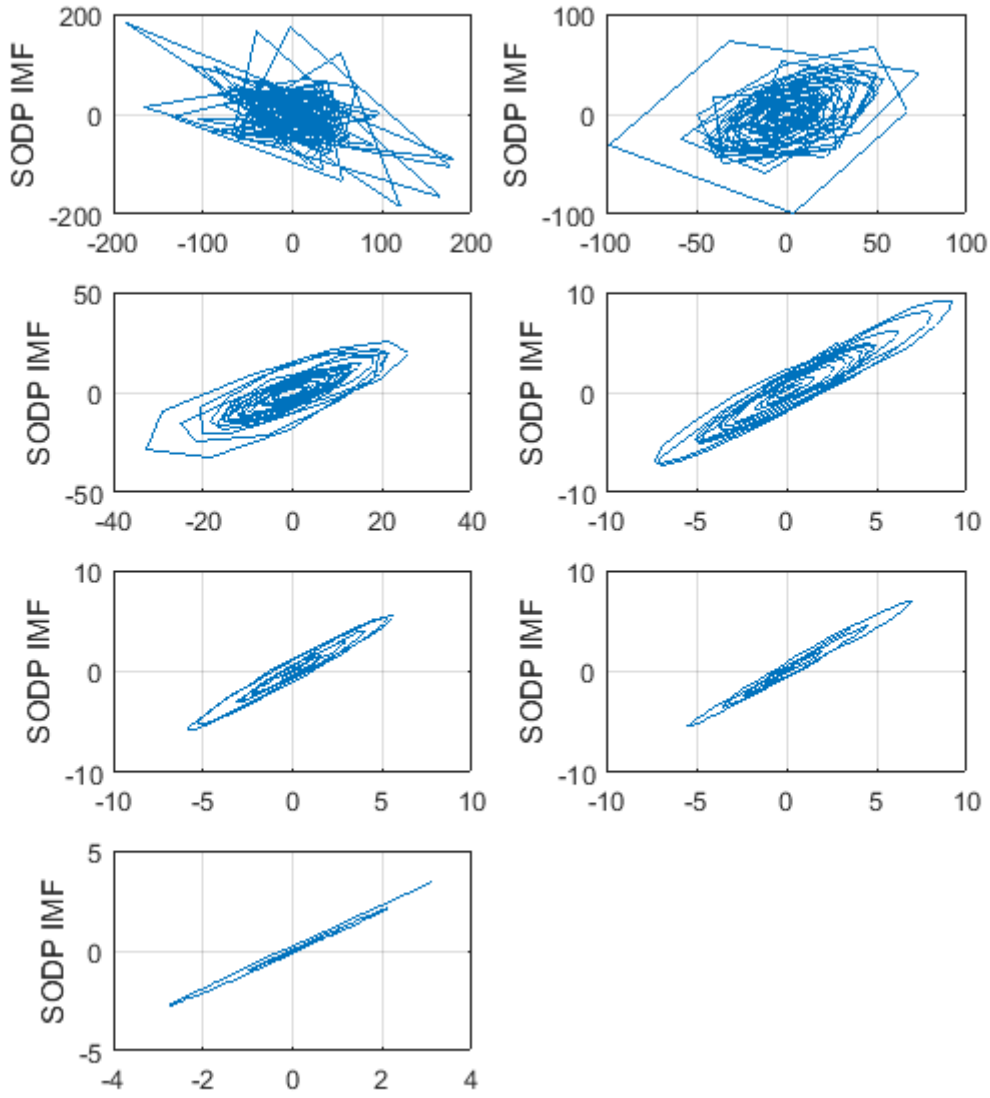

Figure 6.4 (a) SOD plots of seven IMFs of non-stressed subject

This parameter has been recently used in the analysis of EEG signals [155], ECG signals [149], [150] and in Center of Pressure (COP) signals [161]. In this research work, the significance of this parameter to provide important diagnostic information for discriminating stressed and non-stressed subjects is explored.

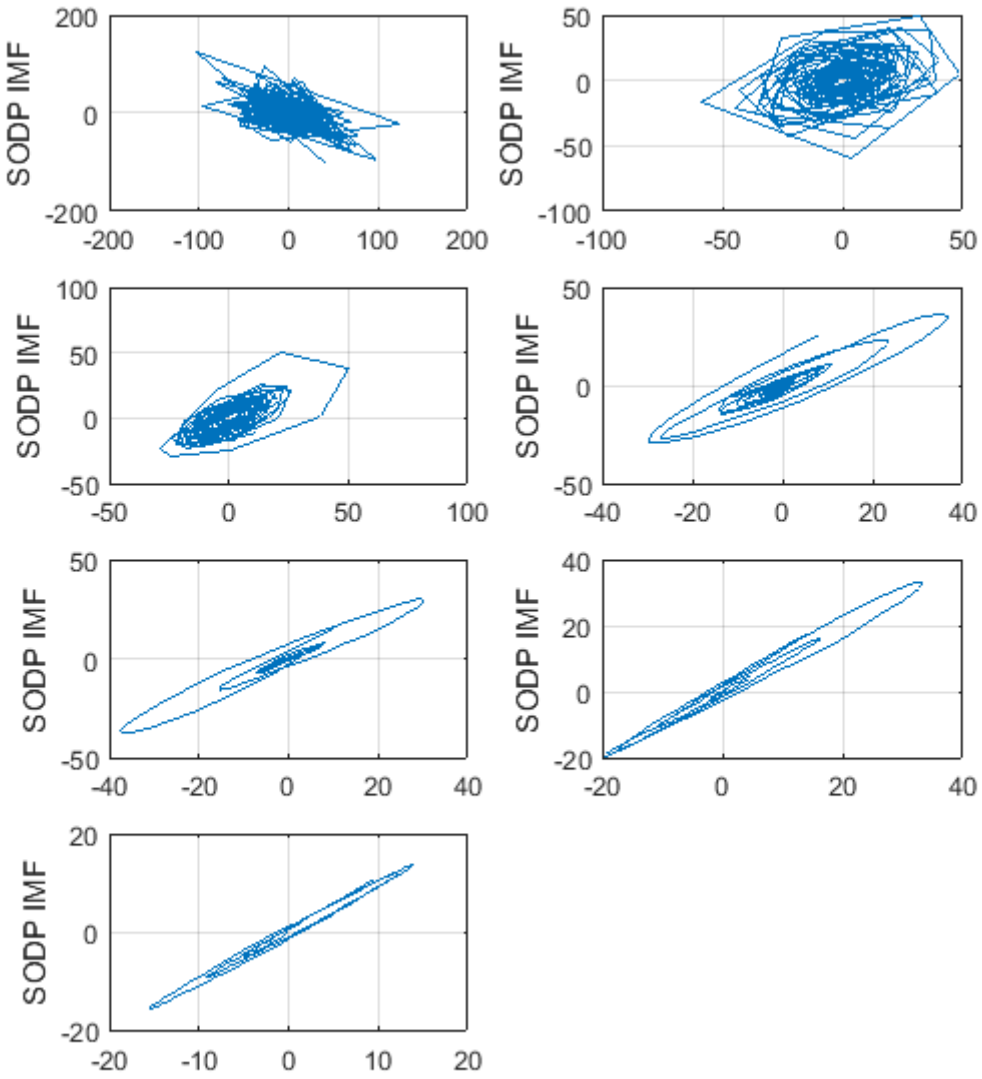

Figure 6.4 (b) SOD plots of seven IMFs of stressed subject

6.2.3 Root mean square value of IMF

The root mean square (RMS) value of the IMFs is used as a parameter to differentiate between stressed and non-stressed signals of the subjects in this study. As the IMF signals shown in figure 6.5 have zero-crossing, this parameter is valuable for calculating the amplitude of each IMF signal.

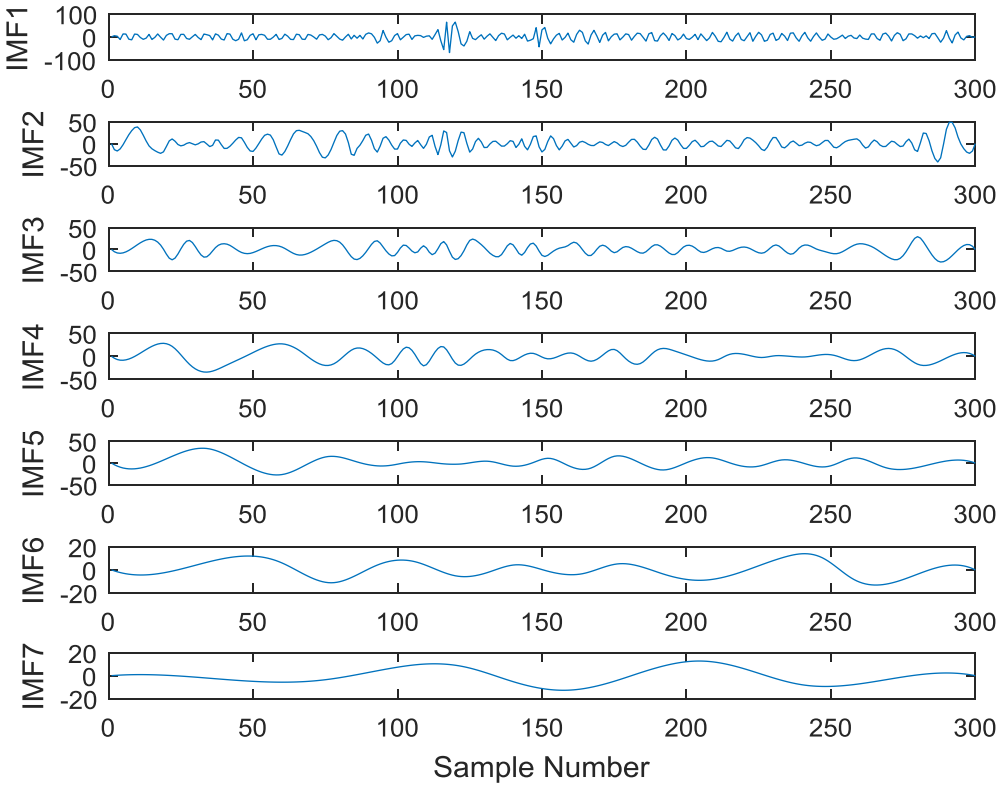

Figure 6.5 IMF signals showing zero-crossing

It is computed as square root of arithmetic mean of squares of a set of values of IMF signal. The RMS value of an IMF signal $I(n)$ with n values can be computed as:

$$RmsIMF = \sqrt{\frac{1}{n}(I_1^2 + I_2^2 + I_3^2 + \cdots + I_n^2)} \tag{6.19}$$

The RMS value has been used in ECG signal analysis for ischemia monitoring [162] and in individual identification [163]. This study uses this parameter extracted from IMFs of PCG-based IBI signals to find significant diagnostic information to differentiate stressed and non-stressed signals.

6.2.4 Shannon entropy

This parameter is evaluated on the IMFs obtained from IBI signal of PCG. The entropy in information theory is the measure of disorder or uncertainty. The Shannon entropy associated with each data value is calculated as negative of logarithm of probability mass

function of the value. Therefore, the Shannon entropy (in bits) of an IMF signal $I(n)$ with n values can be computed as:

$$H(I) = -\sum_{k=1}^{n} P(I_k) log_2 P(I_k) \tag{6.20}$$

where, $I(n) = \{I_1 + I_2 + I_3 + I_4 + \cdots + I_n\}$ be the n values of IMF signal and $P(I_k)$ is the probability of a random phenomenon I_k.

Shannon entropy has been used for detection of epilepsy in EEG signals [164] and also recently used on IMFs for identification of focal EEG signals [165]. In this study, this feature has been used on IMFs obtained from PCG signals for psychological stress detection.

6.2.5 Fuzzy entropy

The concept of fuzzy sets is imported and applied to measure the similarity of vectors on the basis of an exponential function and their shapes. It is defined as natural logarithm of conditional probability that two vectors similar for *m* points will remain similar for *m+1* points [166]. This parameter is calculated as follows [166]:

For an *N* sample time-series $I(k): 1 \leq k \leq N\}$, given *m*, form vector sequences $\{X_k^m, k = 1, \ldots, N - m - 1\}$, where X_k^m represents *m* consecutive *I* values starting from *k*th point.

For given *n* and *r* values, compute the similarity degree, L_{kj}^m between two sequences (*k*th and *j*th) using fuzzy function $\mu\left(l_{kj}^m, n, r\right)$

$$L_{kj}^m(n, r) = \mu\left(l_{kj}^m, n, r\right) \tag{6.21}$$

where, l_{kj}^m is the maximum absolute difference of two sequences (*k*th and *j*th) and fuzzy function $\mu\left(l_{kj}^m, n, r\right)$ is an exponential function

$$\mu\left(l_{kj}^m, n, r\right) = \exp(-\left(l_{kj}^m\right)^n / r) \tag{6.22}$$

The use of an exponential fuzzy function has two main advantages: 1) the function is continuous so that the similarity does not change abruptly; 2) the function is convex so that the self-similarity is maximized. Therefore, fuzzy entropy uses soft boundary for

similarity measurement whereas other entropy measures use hard-boundary which can lead to abrupt changes in entropy values with small changes in tolerance limit [159].

Define the function φ^m as follows:

$$\varphi^m(n,r) = \frac{1}{N-m}\sum_{k=1}^{N-m}\{\frac{1}{N-m-1}\sum_{j=1,j\neq k}^{N-m}(l_{kj}^m)\} \tag{6.23}$$

Similarly, form $\{X_k^{m+1}\}$ and compute $\varphi^{m+1}(n,r)$

Then, Fuzzy entropy is computed as:

$$FzEnt(m,n,r,N) = \ln[\varphi^m(n,r)] - \ln[\varphi^{m+1}(n,r)] \tag{6.24}$$

Here, *m* is the embedding dimension, *n* is gradient and *r* is width of boundary of fuzzy function. Typically, small integer values are chosen for *n* and value of *r* is computed using standard deviation of the dataset [166]. In this study we have taken, *n*=2, *r*=0.2*standard deviation of dataset and *m*=2,3,4,5. For this study, *m*=4 has been selected using false nearest neighbour algorithm. Larger *m* values allow more detailed reconstruction of the dynamic process but too large *m* values will impose a need of a very large N (10^m-30^m), which is generally not feasible for a physiological dataset, or the need of a very broad boundary that can lead to information loss [166].

This parameter has been used for characterization of electromyography (EMG) signals [166], to identify focal EEG signals [167] and for detection of congestive heart failure in ECG based HRV signals [159]. In this study, the significance of this parameter to provide important diagnostic information for discriminating stressed and non-stressed subjects has been analysed.

6.3 Feature Selection

All the features extracted for the study may not be significant and can lead to decrease in classification accuracy of the classifiers. The relevant feature selection becomes fundamental [168]. A systematic approach for selecting the features is used in this study. As the objective of feature selection in this study is to select the features that remain consistent during subject-specific and across subject analysis so, the intersection of

significant features from experiment 1 and experiment 2 are selected and fed to the classifier.

The experiment 1 of this study comprises of deviation analysis in stressed signals from mean baseline values of the features in non-stressed signals. Each subject in experiment 1 is compared to his own baseline reading. This technique incorporates individual variations in stress responses. The experiment 2 of the study focuses on extracting significant features that are comparable across the subjects. In experiment 2, Kruskal-Wallis non-parametric statistical test is used for evaluating *p*-value for checking significance and discrimination ability of extracted features. The features that exhibit maximum deviation and are statistically significant are selected for psychological stress detection. The selection of the common features from subject-specific and across subjects feature analysis ensures that the selected features are statistically significant and gives high discrimination between the stressed and non-stressed category of signals. The selected features are then fed to the classifier.

6.4 Least squares support vector machine classifier

Support vector machine (SVM) is a machine learning and data mining technique effectively used for pattern recognition. It has been successfully applied in many real-world applications such as biomedical signal classification, bioinformatics, image classification and hand-written character recognition. The SVM is based on structural risk minimization and provides better generalization ability than empirical risk minimization based traditional learning methods [169]. As SVM is based on structural risk minimization and not on empirical risk minimization which works by minimising number of misclassified training data, therefore, SVM is less vulnerable to over-fitting [170]. It constructs separating hyperplane in higher dimension input space to identify different classes of data [171]. It involved quadratic programming with inequality constraints. This study uses least-square version of SVM called LS-SVM. It involves linear equations with equality constraints in order to achieve better performance with faster computation speed. Mathematically, LS-SVM is represented as [171]:

$$H(x) = sign\left[\sum_{k=1}^{p} \alpha_k t_k R(z, z_k) + b\right] \tag{6.25}$$

where $R(z, z_k)$ is kernel function, α_k is Lagrangian multiplier, t_k is the target class vector, z_k denotes *D*-dimension *k*-th input vector and b represents the bias-term. In this study, LS-SVM with linear, quadratic, polynomial (order 3), Multi-layer Perceptron (MLP) and Radial Basis Function (RBF) kernels are used. The RBF kernel is mathematically represented as [172]:

$$R(z, z_k) = e^{\frac{-\|z-z_k\|^2}{2\gamma^2}} \tag{6.26}$$

where, $-\|z - z_k\|^2$ represents squared Euclidean distance between two feature vectors and width of RBF function is controlled by γ parameter.

The motivation of using LS-SVM for classification in this study is that it is based on a well-established mathematical model and is suitable for linear and non-linear classification problems. The LS-SVM works with equality constraints and sum squared error cost function instead of inequality constraints in SVM [173]. The LS-SVM uses a set of linear equations instead of quadratic programming in SVM to decrease the computation burden [171] and achieve faster and better classification performance [89].

The LS-SVM classifier has already been used in many biomedical applications that include classification of CAD and normal ECG signals [157], [158], diabetic and normal class RR-interval signals [150] and seizure and seizure-free EEG signals [153], [155]. Moreover, it has also been used on cardiac sound signals for septal defect diagnosis [89] and for classification of cardiac sound signals [174].

6.5 Results and discussions

As each IBI signal of the dataset had atleast seven IMFs, so for uniformity in signal analysis, seven sub-band decomposition was selected. In this study, five non-linear features namely- area of ASR signal, log of area of SODP, RMS value of IMF, Shannon Entropy and Fuzzy Entropy were extracted from seven IMFs of each IBI signal thus leading to extraction of 35 features (5×7=35 features) from IBI signal of every subject. These 35 features are shown in table 6.1 and the values of each feature for baseline non-stressed state and stressed state are expressed in the form of mean$\pm$standard deviation.

6.5.1 Experiment 1- Subject-specific parameter deviation analysis

The key feature of this study is to take into account the distinct stress responses and characteristic cardiovascular behaviour of every individual. Therefore, this method proposes a monitoring technique which takes into account the normal cardiac activity of the individual and measures the deviation from normal cardiac activity due to psychological stress.

As per literature, various studies [59]–[62], [175] used LF/HF power ratio obtained from HRV of ECG signals, to quantify sympathovagal balance. The increase in this index indicates a shift towards sympathetic dominance whereas the decrease of the index indicates a shift towards parasympathetic dominance. This experiment tests the use of PCG-based features which showed deviation during psychological stress from normal baseline values, in comparison with ECG based LF/HF power ratio feature. In this study, the experimental value for every feature of stressed signal category is compared with the respective baseline value of the feature. The features that showed maximum deviation from mean baseline values are shown in table 6.2.

Discussion-

The area of analytic signal representation of intrinsic mode functions is estimated for both the classes (stressed and non-stressed) of signals. It was observed that AASR value of IMF3 showed an increase of 12.56% (average increase in mean value) in 90.62% of cases. Whereas, AASR value of IMF7 showed an increase of 47.35% in 93.75% cases as shown in table 6.2. The mean value of estimated area of ASR is smaller for non-stressed category when compared with stressed category of signals. This could possibly be due to the greater amplitude of these IMF signals for subjects under stress.

The log of area of SODP is computed for both the category of signals. This feature showed an increase of 7.20% in IMF4 for 87.50% of cases. For IMF7, the value of LASODP feature increased by 30.39% in 90.62% of cases. The LASODP feature has smaller value for non-stressed category of signals as compared to stressed category. The increased variability in second-order difference plot of stressed subjects is possibly an indication of changed cardiac activity due to psychological stress.

Table 6.1 Mean and Standard deviation (SD) of features for non-stressed and stressed category of IBI signals

IMF	Feature	Without stress- baseline (Mean±SD)	During stress (Mean±SD)
IMF1	LAASR*	9.492±1.103	9.440±0.622
	LASODP	10.527±1.084	10.522±0.686
	RmsImf	28.580±15.197	26.114±8.873
	ShEnt	8.208±0.046	8.224±0.003
	FzEnt	0.591±0.112	0.649±0.120
IMF2	LAASR*	8.830±1.287	9.187±0.682
	LASODP	8.635±1.152	8.911±0.569
	RmsImf	19.722±10.446	21.465±6.044
	ShEnt	8.208±0.046	8.224±0.003
	FzEnt	0.540±0.045	0.506±0.093
IMF3	LAASR*	8.691±0.788	8.959±0.560
	LASODP	7.164±0.973	7.618±0.569
	RmsImf	17.510±6.539	19.851±4.969
	ShEnt	8.209±0.0484	8.224±0.003
	FzEnt	0.482±0.048	0.506±0.0484
IMF4	LAASR*	8.786±0.743	8.751±0.979
	LASODP	5.731±0.744	6.144±0.703
	RmsImf	16.763±5.129	17.987±7.023
	ShEnt	8.211±0.047	8.225±0.003
	FzEnt	0.301±0.056	0.330±0.064
IMF5	LAASR*	8.451±0.685	8.919±1.399
	LASODP	4.691±0.775	4.622±1.390
	RmsImf	15.914±6.705	22.396±16.953
	ShEnt	8.211±0.049	8.225±0.003
	FzEnt	0.212±0.067	0.174±0.049
IMF6	LAASR*	8.397±0.837	9.317±1.504
	LASODP	3.604±1.265	4.227±1.479
	RmsImf	17.063±7.461	31.755±23.403
	ShEnt	8.210±0.049	8.227±0.003
	FzEnt	0.125±0.046	0.089±0.035
IMF7	LAASR*	8.336±1.758	9.276±1.461
	LASODP	2.464±1.556	3.214±2.0672
	RmsImf	35.965±63.231	38.188±31.53
	ShEnt	8.209±0.049	8.226±0.003
	FzEnt	0.054±0.035	0.054±0.033

*Here log values of AASR feature have been used and are depicted by LAASR

The RMS value of all IMFs is computed for both stressed and non-stressed category signals. A higher value of IMF6 and IMF7 is observed for subjects under stress. The increase of 86.10% in value of IMF6 for 93.75% of signals was observed making it a very powerful indicator of psychological stress. For IMF7, the value of RMS feature increased by 6.18% in 81.25% of cases. This increase in RMS value during psychological stress could be due to greater amplitude of these IMFs during stress.

Table 6.2 Features showing significant deviation from mean baseline values during psychological stress

IMF	Feature Name	Mean baseline (BL) value	Mean value during stress	Change in mean from BL value (%)	Feature suitable for number of subjects (%)
IMF3	AASR	79.277	89.234	12.56 Increase	90.62
IMF7	AASR	229.997	338.889	47.35 Increase	93.75
IMF4	LASODP	5.731	6.144	7.20 Increase	87.50
IMF7	LASODP	2.464	3.214	30.39 Increase	90.62
IMF6	RmsImf	17.063	31.755	86.10 Increase	93.75
IMF7	RmsImf	35.965	38.188	6.18 Increase	81.25
IMF5	FzEnt	0.212	0.174	17.94 Decrease	84.37
IMF6	FzEnt	0.125	0.089	28.98 Decrease	90.62
ECG-HRV	LF/HF ratio	1.026	1.233	20.15 Increase	78.12

The FzEnt feature is computed from IMFs for every subject during stress and is compared with the respective baseline value. This feature for IMF5 recorded a decrease of 17.94% from mean baseline value in 84.37% of cases under consideration and a decrease of 28.98% for IMF6 in 90.62% of cases. The results showed lower mean values of FzEnt for subjects under psychological stress category depicting the lower complexity of PCG

stress category signals. This reduced complexity indicates a stable and periodic behaviour of heart rate under stress. This may be a reflection of reduced parasympathetic activity and thus depicting sympathovagal imbalance.

This experiment also emphasized a very interesting fact that the features showing deviation due to psychological stress were predominantly from higher IMFs namely IMF3, IMF4, IMF5, IMF6 and IMF7 as shown in table 6.2. As per the implementation of EMD technique, the higher IMF signals correspond to lower frequency signals. As most of the information of PCG signals is concentrated at lower frequencies, this justifies the results of this experiment and reason for getting useful information from higher IMF signals.

This experiment identifies features that show maximum deviation from subject-specific template baseline values as shown in table 6.2. The ECG-based LF/HF power ratio feature showed an increase of 20.15% in 78.12% cases. Whereas, the most powerful PCG-based features identified based on findings of experiment 1 are RMS value of IMF6 and AASR from IMF7 which showed 86.10% increase in 93.75% of cases and 47.35% increase in 93.75% of cases respectively. Therefore, this experiment also showed that the features extracted from PCG signals are better indicators of sympathovagal balance than LF/HF power ratio feature of ECG-HRV signal as evident from table 6.2.

6.5.2 Experiment 2-Identifying statistically significant features for psychological stress analysis

The IMFs were derived using EMD technique on IBI of PCG signals from stressed and non-stressed category of signals. These IMFs were arranged in order from high-frequency to low-frequency components. Thereafter, mean and standard deviation values of features obtained from these IMFs are shown in table 6.1. The obtained features were tested for statistical relevance using Kruskal-Wallis non-parametric test. All the features which show *p*-value less than 0.05 are considered to be statistically significant. These features are not subject-specific as they are not obtained by comparison with individual baseline values, but are significant across the subjects. The *p*-values of all five extracted features for IMF1 to IMF7 are computed and are presented in table 6.3. The box-plots for these features are shown in figure 6.6 to figure 6.9.

Table 6.3 *p*-values of extracted features from IMFs for non-stressed and stressed category signals

Feature	IMF1	IMF2	IMF3	IMF4	IMF5	IMF6	IMF7
AASR	7.78×10^{-1}	4.05×10^{-1}	8.78×10^{-2}	7.47×10^{-1}	4.66×10^{-2}	3.26×10^{-2}	4.96×10^{-3}
LASODP	8.09×10^{-1}	3.26×10^{-1}	1.39×10^{-2}	6.96×10^{-2}	6.97×10^{-1}	2.88×10^{-1}	2.00×10^{-2}
RmsImf	8.40×10^{-1}	1.01×10^{-1}	1.70×10^{-1}	4.93×10^{-1}	5.80×10^{-2}	7.18×10^{-3}	1.50×10^{-2}
ShEnt	5.16×10^{-2}	1.76×10^{-2}	4.52×10^{-1}	9.40×10^{-1}	4.35×10^{-1}	2.53×10^{-2}	7.60×10^{-2}
FzEnt	4.10×10^{-2}	6.75×10^{-2}	3.84×10^{-2}	2.94×10^{-2}	8.09×10^{-3}	1.51×10^{-3}	7.88×10^{-1}

Discussion-

Kruskal-Wallis is a non-parametric statistical test and makes no assumption about the distribution of data. This test uses feature-data ranks rather than raw values to evaluate discriminative power of a feature. The *p*-value of a feature is a measure of discriminating ability of the feature in separating two classes and the features with $p < 0.05$ are considered to be statistically significant.

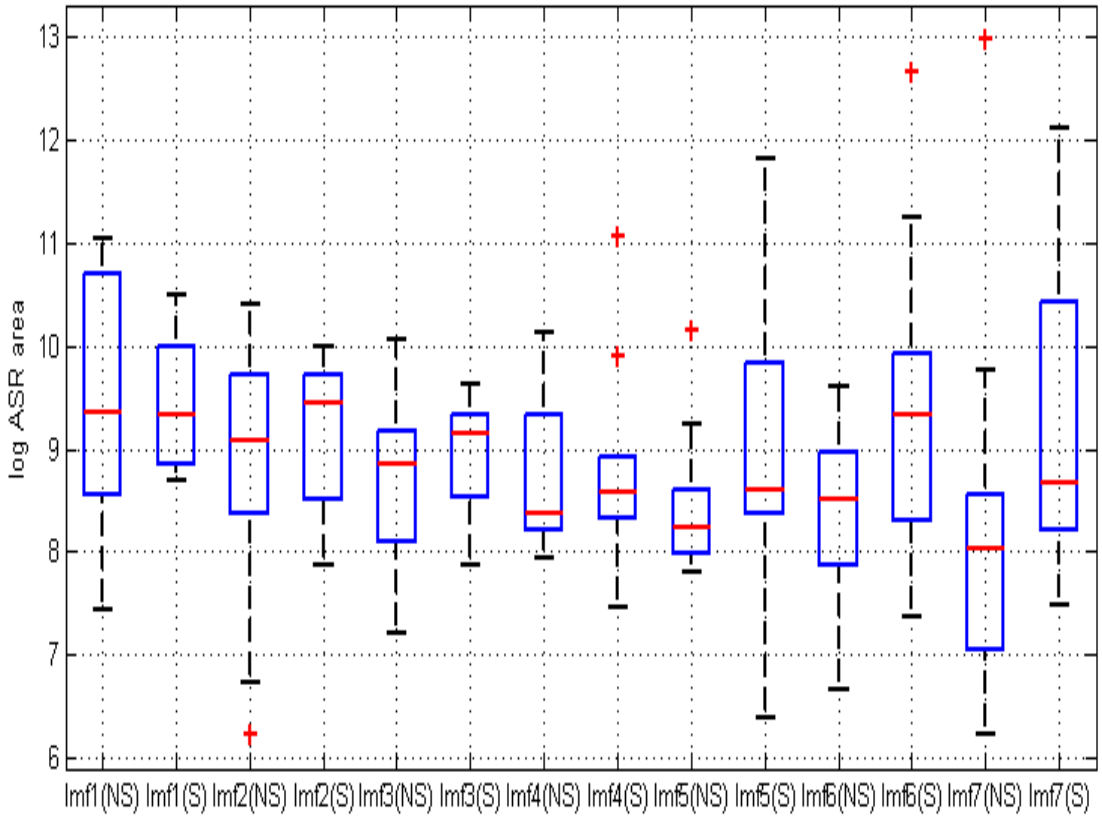

Figure 6.6 Box-plot of log ASR area, IMFn(NS)=nth IMF for Non-stressed baseline state, IMFn(S)= nth IMF for stressed state

The AASR feature is statistically significant ($p < 0.05$) for IMF5, IMF6 and IMF7 as shown in table 6.3. Therefore, IMF5, IMF6 and IMF7 of AASR feature can be used to discriminate stressed and non-stressed categories of signals. This can also be inferred by observing figure 6.6 depicting the box-plots corresponding to AASR feature of first seven IMFs of IBI signals. It can also be observed from the box-plot that the statistically significant IMFs of this features show higher values of AASR in case of stressed category of signals. For rest of the IMFs, *p*-value is not less than 0.05, so they do not provide any significant discrimination between S and NS category of signals.

In case of LASODP feature, $p < 0.05$ is observed in case of IMF3 and IMF7 as depicted in table 6.3. These IMFs of LASODP feature can significantly be used to discriminate S and NS category of signals. The box-plots for LASODP corresponding to IMF1 to IMF7 of NS and S category of signals are shown in figure 6.7.

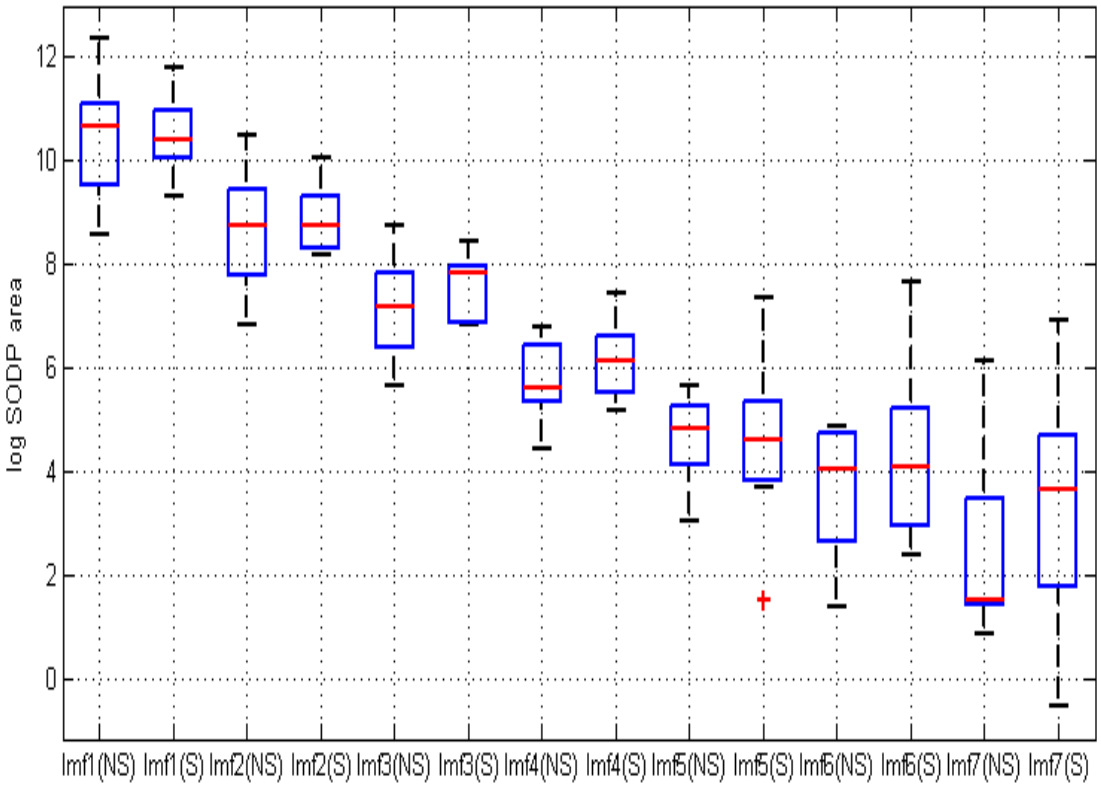

Figure 6.7 Box-plot of log SODP area, IMFn(NS)=nth IMF for Non-stressed baseline state, IMFn(S)= nth IMF for stressed state

The *p*-values for RmsImf feature are significantly lower ($p < 0.05$) for IMF6 and IMF7 as shown in table 6.3 and this can also be inferred by observing box-plot in figure 6.8 as these IMFs show significant separation between two categories of signals. Hence the IMF6 and IMF7 are suitable for discriminating S and NS category of signals. The visual analysis of box-plot of this feature also shows higher values of significant IMFs in stressed category of signals.

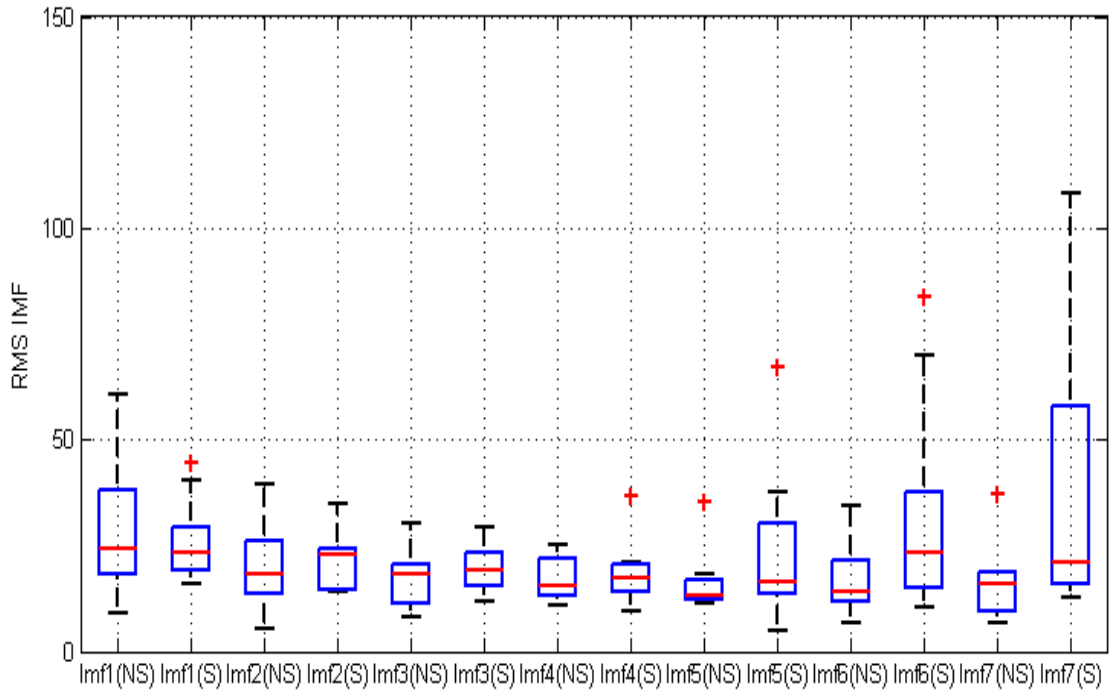

Figure 6.8 Box-plot of RMS, IMFn(NS)=nth IMF for Non-stressed baseline state, IMFn(S)= nth IMF for stressed state

In case of ShEnt feature, the *p*-values for IMF2 and IMF6 are significantly lower ($p < 0.05$), thus making these IMFs suitable for discriminating S and NS categories of signals. Whereas, for FzEnt feature as shown in table 6.3, the significantly lower *p*-values ($p < 0.05$) were observed for IMF1, IMF3, IMF4, IMF5 and IMF6 making them suitable for discrimination of NS and S category of signals. The boxplot for FzEnt is shown in figure 6.9.

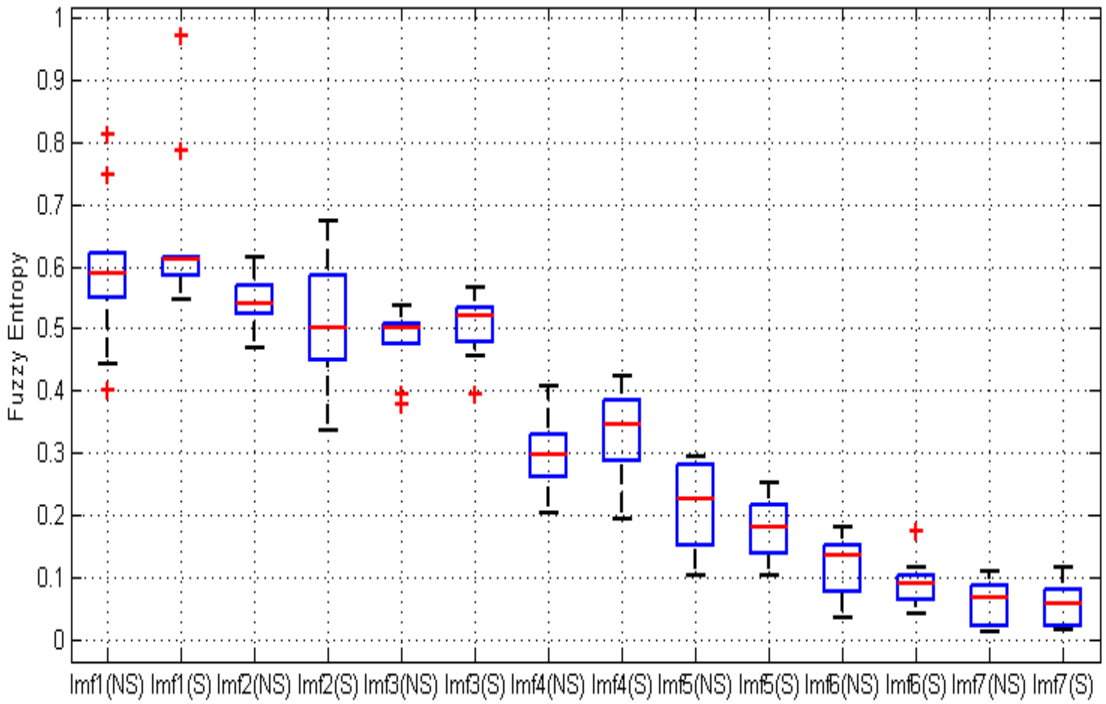

Figure 6.9 Box-plot of Fuzzy Entropy, IMFn(NS)=nth IMF for Non-stressed baseline state, IMFn(S)= nth IMF for stressed state

Table 6.4 Statistically significant features identified using Kruskal-Wallis statistical test ($p < 0.05$)

Feature	IMF
AASR	IMF5, IMF6, IMF7
LASODP	IMF3, IMF7
RmsImf	IMF6, IMF7
ShEnt	IMF2, IMF6
FzEnt	IMF1, IMF3, IMF4, IMF5, IMF6

To summarize experiment 2 of this study, the significant features identified using Kruskal-Wallis statistical test ($p < 0.05$) to discriminate stressed and non-stressed category of signals are shown in table 6.4. These results are also confirmed by box-plots depicted in figure 6.6 to figure 6.9. The features which showed the least *p*-value and thus can be considered as the most significant features are IMF7 of AASR, IMF6 of RmsImf, IMF5 and IMF6 of FzEnt. It is interesting to note that these results support the findings from experiment 1 which showed the most powerful features to be IMF7 of AASR and IMF6 of RMSImf.

The table 6.5 summarizes the features selected from experiment 1 and experiment 2. The results shown in table 6.5 indicate that the results of experiment 2 are supporting the results of experiment 1. There are six significant features that are common in experiment 1 and experiment 2 namely- AASR IMF7, LASODP IMF7, RmsIMF IMF6, RmsIMF IMF7, FzEnt IMF5, FzEnt IMF6. These features are depicted in bold in table 6.5. The presence of these common features in both subject-specific (experiment 1) and across subjects feature analysis (experiment 2) implies that these features give high discrimination between stressed and non-stressed category of signals and are statistically significant.

Table 6.5 List of features significant in experiment 1 and experiment 2 to find common features

Feature Name	Selected features	
	Experiment1	Experiment 2
AASR	IMF3	-
	-	IMF5
	-	IMF6
	IMF7	**IMF7**
LASODP	-	IMF3
	IMF4	-
	IMF7	**IMF7**
RmsImf	**IMF6**	**IMF6**
	IMF7	**IMF7**
ShEnt	-	IMF2
	-	IMF6
FzEnt	-	IMF1
	-	IMF3
	-	IMF4
	IMF5	**IMF5**
	IMF6	**IMF6**

Thereafter, the selected six features are used for training and testing of three classifiers LS-SVM, k-Nearest Neighbour (kNN) and Bayes Net and their classification performance is evaluated. In this study, we have used inbuilt MATLAB function `svmtrain` with least square method and kernel functions linear, quadratic, polynomial (order 3), multi-layer perceptron with default weight 1 and default bias -1 and radial basis function (RBF) with rbf_sigma value 1.05. The optimal kernel parameter is decided on

the basis of trial and error experimentation. The reliability and robustness of classification is ensured using 10-fold cross-validation. The performance of classifiers can be evaluated using parameters namely accuracy (ACC), sensitivity (SEN), specificity (SPE).

In this study, the comparison of LS-SVM with other classifiers in table 6.6 shows high classification accuracy provided by LS-SVM classifier in comparison to other classifiers included in this research work. The LS-SVM classifier with RBF kernel showed highest classification accuracy for PCG-based psychological stress detection. This is the reason for using RBF kernel with LS-SVM. The previous study [174] on cardiac sound signals classification also reported high classification performance by using LS-SVM with RBF kernel. In this study, the average ACC, SEN and SPE achieved on the dataset using LS-SVM classifier with RBF kernel is 93.14%, 92.58% and 93.33% respectively. The summary of performance of classifiers is depicted in table 6.6.

Table 6.6 Performance summary of classifiers for classification between stressed and non-stressed category signals

Features selected	**Classifier**	**Kernel and Kernel parameter**	**ACC (%)**	**SEN (%)**	**SPE (%)**
AASR IMF7 LASODP IMF7 RmsIMF IMF6 RmsIMF IMF7 FzEnt IMF5 FzEnt IMF6	LS-SVM	Linear	68.75	65.63	71.88
		Quadratic	76.56	71.88	81.25
		Polynomial (order 3)	90.45	80.91	98.00
		RBF, ϒ=1.05	**93.14**	**92.58**	**93.33**
		MLP (scale [1 -1])	63.51	54.17	72.50
	kNN	k=1	85.94	81.25	90.63
		k=3	71.88	68.75	75.00
		k=5	64.06	59.38	68.75
	Bayes Net		81.25	72.72	62.50

Thus, the features proposed in this study are significant for psychological stress detection from PCG signals using EMD technique. The discrimination ability of PCG-based features is more on this dataset than ECG-based LF/HF power ratio sympathovagal balance indicator method as shown in experiment 1. The proposed methodology achieved average classification accuracy of 93.14% on the dataset. Therefore, it can be inferred that PCG-based method is a robust, cost-efficient and reasonably better method than ECG-based LF/HF power ratio method for psychological stress detection.

The main finding of this research is the applicability of PCG signals for psychological stress detection using six non-linear features which are sensitive in both subject-specific and across subject analysis. Another finding of this study is that the important features identified for psychological stress detection in this study are- AASR IMF7, LASODP IMF7, RmsIMF IMF6, RmsIMF IMF7, FzEnt IMF5, FzEnt IMF6. It is interesting to note that these features are predominantly from higher IMFs which are lower frequency signals. This research finding is justified as most of the information of PCG signals is concentrated at lower frequencies. The advantage of the study is that the proposed system is automatic and hence, there is no inter-observer and intra-observer variability. Also, the subject-specific template analysis in this study takes into account varied stress responses and characteristic cardiac behaviour of every individual. The proposed system is reliable and robust as 10-fold cross-validation is used. This cost-effective methodology is suitable for home-care and telemedicine. However, the proposed methodology has been tested on a small dataset of age group 18 to 25 years. In order to apply this method for home-care and clinical use, it is necessary to test it on a larger dataset. The use of other kernel functions with different kernel parameters can also enhance the performance of classifier. In addition to this, computing other non-linear features like fractal dimension and Lyapunov exponent and combining them with proposed features may further improve the accuracy.

6.6 Summary

In present work, a novel technique of using PCG signals for psychological stress detection is proposed. This method uses EMD technique suitable for non-linear and non-stationary signal analysis of PCG signals. The use of non-linear features ensures capturing of complex non-linear dynamics of heart sound PCG signals. In this study, the findings of experiment 1 support the findings of experiment 2 for identifying most powerful features for PCG-based psychological stress detection. The common features identified from experiment 1 and experiment 2 of this study for psychological stress detection are- AASR IMF7, LASODP IMF7, RmsIMF IMF6, RmsIMF IMF7, FzEnt IMF5, FzEnt IMF6. The use of these identified common features ensures high discrimination ability between stressed and non-stressed category of signals and statistical significance of features.

The main findings from this study include-

- Applicability of PCG signals for psychological stress detection
- The results on this dataset indicate that PCG-based psychological stress detection method is reasonably better than well-documented ECG-based LF/HF power ratio method
- The important features identified for PCG-based psychological stress detection are predominantly from higher IMFs which are lower frequency signals. This research finding is justified as most of the information of PCG signals is concentrated at lower frequencies

As the features suitable for PCG-based psychological stress detection identified in this study are from low-frequency IMFs, therefore, it becomes vital to preserve low-frequency IMFs of IBI signals. This will ensure effective feature extraction and can improve accuracy in detecting psychological stress. This forms the basis of the proposed method 2 of this research, which is discussed in the next chapter of the thesis.

CHAPTER 7 PROPOSED METHOD 2

7.1 Introduction

The aim of this work is to develop an improved framework for PCG-based psychological stress detection based on the findings of proposed method 1 (discussed in chapter 6). This study explores the potential of non-linear entropy-based features extracted in EMD domain for psychological stress detection. Firstly, simultaneous PCG and ECG signals are acquired from the subjects. The ECG signals are used for ECG-gating to find S1 peak in PCG signals and then used for comparison of the results obtained from PCG-based psychological stress detection (explained in chapter 4). The time interval between consecutive S1 peaks is extracted to form IBI signals (explained in chapter 4). Subsequently, the EMD signal decomposition technique is applied on IBI signal to decompose it into mono-component sub-band IMF signals (explained in chapter 4). In this study, each IBI signal had atleast seven IMFs, so seven sub-band signal decomposition is selected. As per the findings of previous method (proposed method 1 presented in chapter 6), low-frequency IMFs are important and contain significant information for psychological stress detection. So, the low-frequency seven IMFs are retained in this study to prevent information loss at this stage. The next step is to extract non-linear entropy-based features from these IMFs. These features are useful in capturing non-linear subtleties of PCG signals. This PCG-based psychological stress detection method uses entropy-based non-linear features extracted in EMD domain namely- Permutation entropy, Fuzzy entropy and K-NN entropy. The explanation of these features is given in the next section.

The remaining chapter is organized as- section 7.2 describes non-linear feature extraction. The statistical significance and feature ranking are explained in section 7.3. The section 7.4 of this chapter describes classifier used and the results are presented in section 7.5. The discussions of results obtained in this study are provided in section 7.6. The proposed method is summarized in section 7.7 of this chapter.

7.2 Feature extraction

This study uses entropy-based features namely- Permutation entropy, Fuzzy entropy and K-NN entropy to capture the non-linear dynamics of the cardiac sound signal in order to detect psychological stress from PCG signals.

7.2.1 Permutation Entropy

Permutation Entropy (PEn) feature is useful in complexity analysis of the signals. It is chosen as a feature for analysis in this study because of its practical advantages like computational simplicity and robustness to noise [176]. It is computed as [177]:

$$PEn = -\sum_{l=1}^{a!} A_l \log(A_l) \tag{7.1}$$

where a is sequence length and total number of possible permutation patterns are $a!$, A_l is probability of occurrence of l^{th} permutation pattern. This feature is used for ECG signals for diagnosis of atrial fibrillation [178], for detection of focal EEG signals [167] and for detection of congestive heart failure in short term HRV signals [159].

7.2.2 Fuzzy Entropy

Fuzzy Entropy (FzEn) is a measure of the degree of similarity between two vectors of length p from N-sample time series. It is computed as [166]:

$$FzEn(p, q, r, N) = \ln[\varphi^p(q, r)] - \ln[\varphi^{p+1}(q, r)] \tag{7.2}$$

The function $\varphi^p(q,r)$ is defined as:

$$\varphi^p(q,r) = \frac{1}{N-p}\sum_{k=1}^{N-p}\{\frac{1}{N-p-1}\sum_{j=1,j\neq k}^{N-p}(l_{kj}^p)\} \tag{7.3}$$

where, l_{kj} is degree of similarity between two vectors (kth and jth) and q,r control fuzzy boundary. Here, q is gradient and r is width of boundary of fuzzy function and p is the embedding dimension. The advantage of using FzEn feature is that unlike other entropies, it uses soft boundary for similarity measurement which prevents abrupt entropy value changes due to small changes in tolerance limit. More details of fuzzy entropy are discussed in chapter 6.

This feature has been used for CAD diagnosis from HRV signals [158], for detection of congestive heart failure in short-term HRV signals [159], for characterization of surface EMG signal [166] and for detection of focal EEG signals [167].

7.2.3 K-Nearest Neighbour Entropy

K-Nearest Neighbour Entropy (K-NN) measures the scattering of the signal. It can be defined as follows [179]:

$$KNN(x) = -\varphi(K) + \varphi(S) + \log(V_D) + D/S\sum_{j=1}^{S}\log\{\epsilon(j)\} \tag{7.4}$$

where, S is total number of samples, D is dimension of x and $\epsilon(j)$ is distance between jth sample and K-nearest neighbours of x, whereas, V_D represents volume of unit ball of D-dimension and function $\varphi(S)$ is digamma function as explained by [179]. This feature has been used in CAD diagnosis using HRV signals [158] and to identify focal EEG signals [167].

7.3 Statistical significance and feature ranking methods

Biomedical data often does not follow normal distribution and usually has small sample sizes as humans or animals are involved in data acquisition [180]. If the data is not normally distributed or underlying distribution is heavily tailed or skewed, non-

parametric tests are more powerful than parametric counterparts [180]. Kruskal-Wallis non-parametric test showed high Asymptotic Relative Efficiency (ARE) and minimal power loss even when the underlying distribution is normal whereas the power gain is substantial when normality condition is not met [181], [182]. Therefore non-parametric statistical tests are preferred in biomedical signal analysis. Kruskal-Wallis is a non-parametric statistical test and makes no assumption about the distribution of data [183]. The median is central tendency statistic for non-parametric tests [180]. This test uses data ranks rather than the original values to evaluate the discriminative power of the feature. In this study, Kruskal-Wallis non-parametric statistical test is applied on the extracted features to measure the statistical significance of features in terms of *p*-value. The features with p-value < 0.05 are considered to be statistically significant.

In this study, we have used inbuilt MATLAB function `kruskalwallis` to evaluate *p*-values of the features and to draw the box-plots for visual comparison of values of PEn, FzEn and K-NN entropy features for stressed and non-stressed category signals. The boxplots use 5-number summary which consists of– maximum and minimum range values, upper and lower quartiles and median to convey the level, spread and symmetry of data values [184]. The boxplot is exploratory data analysis statistical technique, used to identify patterns that can otherwise be hidden in data [185].

The feature ranking methods are useful in identifying the most significant features by assigning ranks to the extracted features and arranging the features in descending order as per their clinical relevance. Thereafter, the identified features with higher ranks can be used for classification and other lesser significant features can be neglected. The methods are useful in reducing system complexity without affecting the classification performance of the system. The feature ranking methods used in this study include entropy method, Bhattacharya space algorithm, Receiver Operating Characteristic (ROC) method and Wilcoxon method. The entropy feature selection method uses divergence method for measuring class separability of different classes in order to rank the features whereas, the Bhattacharya space algorithm uses Bhattacharya distance for measuring the differentiability of different classes [158], [186]. The ROC method uses area under ROC curve to rank features [186] whereas, the Wilcoxon method ranks the features on the basis of non-parametric test [158]. The highest-ranked features identified using these methods are then used for classification.

7.4 Least-squares support vector machines

The SVM is explained in chapter 6. The LS-SVM method of classification works by constructing separating hyperplanes in higher dimension input space in order to identify different classes of data. Mathematically, LS-SVM is represented as [171]

$$L(x) = sign\left[\sum_{k=1}^{m} \alpha_k s_k P(z, z_k) + b\right] \tag{7.5}$$

where, α_k is Lagrangian multiplier, $P(z, z_k)$ is kernel function, s_k is target class vector, z_k denotes *D*-dimension *k*-th input vector and b represents the bias-term. In this study, LS-SVM with Radial Basis Function (RBF) kernel is used, which is mathematically represented as [172]

$$P(z, z_k) = e^{\frac{-\|z - z_k\|^2}{2\gamma^2}} \tag{7.6}$$

where, γ parameter controls the width of RBF function.

The differences in SVM and LS-SVM and the applications of LS-SVM in biomedical field are mentioned in chapter 6.

7.5 Results

The timing information of consecutive S1 peaks of acquired PCG signals is extracted to form IBI signals. The IBI signals decompose to different number of IMFs on application of EMD technique. Each IBI signal of the dataset had atleast seven IMFs, so for uniformity in signal analysis, seven sub-band decomposition was selected as done in studies [149], [150], [157]. As per the findings of proposed method 1 (chapter 6), the low-frequency IMFs are important and contain significant information for psychological stress detection. The low-frequency IMFs also showed higher correlation with IBI signal. Therefore, the low frequency seven IMFs for each IBI signal were retained and high-frequency IMFs were discarded to avoid information loss at this stage. If we exclude all higher IMFs existing after IMF7, there will be information loss as low-frequency IMFs will be discarded. For this, we reversed the numbering of IMFs to consider significant low-frequency seven IMFs of each signal. Therefore, unlike convention, in this study,

IMF1 has the lowest frequency components, IMF2 has subsequent higher frequency components and IMF7 has highest frequency components as depicted in figure 7.1.

As explained in chapter 4, two readings from each subject- one in baseline state and another in stressed state were acquired for this study and each IBI signal is decomposed to seven IMFs. The experiments in this study were conducted on 420 signals of 30 subjects (30×2×7=420 signals) containing 18,000 beats (30×2×300=18,000 beats). In this research work, three non-linear entropy features namely- Permutation entropy, Fuzzy entropy and K-NN entropy were extracted from seven IMFs of each IBI signal thus leading to extraction of 21 features (3×7=21 features) from each IBI signal of the subject.

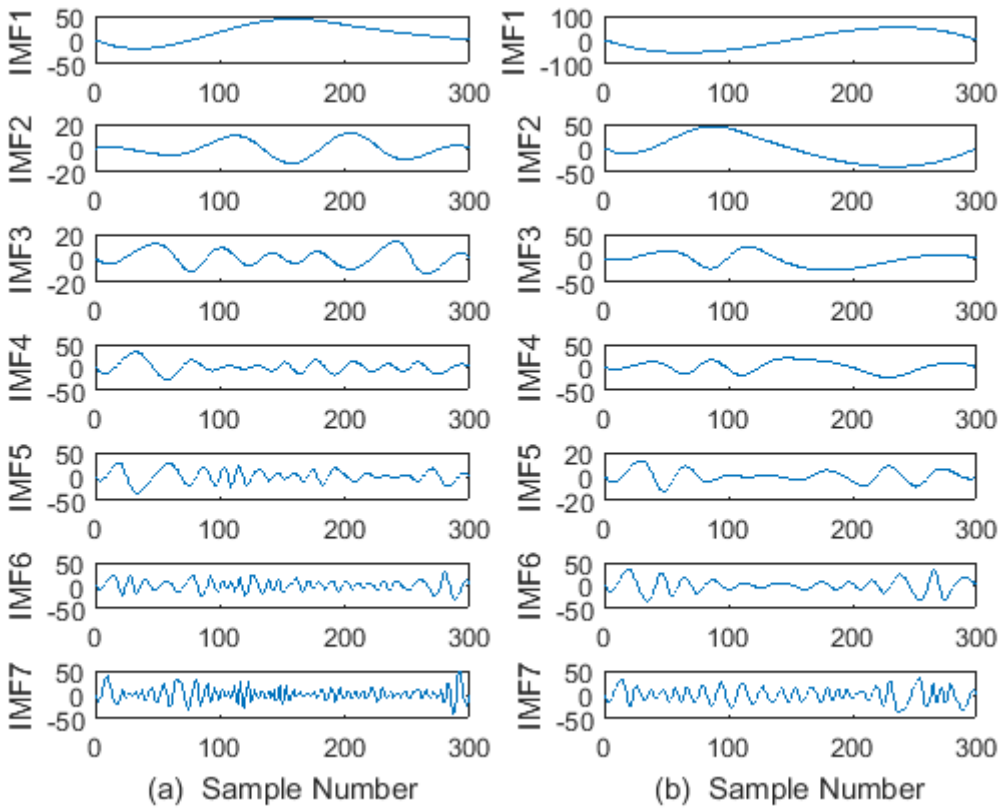

Figure 7.1 Plots of IMFs, IMF1=Lowest frequency, IMF7=Highest frequency a) Baseline state b) Stressed state

Typical values used in this study and parameter selection for features

The EMD technique is applied to decompose IBI signals to IMFs for signal analysis and feature extraction. The EMD technique uses sifting process for signal decomposition. The stopping criterion used for sifting process limits the standard deviation between two consecutive sifting results to typical value of 0.3 [143]. In this study, the essential parameters required for computing PEn, FzEn and KNN entropy parameters are selected in suggested ranges using trial and error experimentation to maximize the classification accuracy. In case of Permutation entropy, for practical purposes, the range suggested for embedding dimension for time series is 3 to 7 [177]. In our study, number of samples in each signal is 300 and is less than 6! so the embedding dimension values 3,4,5 are considered as suggested in [177] and maximum classification accuracy is achieved using values of embedding dimension as 3 and time lag as 1. For FzEn, q is gradient and r is width of fuzzy boundary and p is embedding dimension. If the boundary is too narrow, it results in salient influence from noise, while too broad boundary may result in the loss of information [166]. A study conducted on EMG signal [166], suggested values r=0.2*standard deviation of dataset, q=2 and p=2,3,4,5 for FzEn. The method adopted in the above study is reported to be suitable for other physiological signals. Moreover, the values suggested in above study have also been used for ECG-based HRV signals for detection of congestive heart failure [159]. In this study, we achieved highest classification accuracy using p=4. For K-NN entropy, the number of nearest neighbours used for this study are K=3,5,7 and value K=7 yielded maximum classification accuracy.

The non-linear entropy features are computed from IMF signals of stressed and non-stressed category and their range is shown in table 7.1. The p-values to check the statistical significance of these features are computed using Kruskal-Wallis non-parametric test and are shown in table 7.2. In order to visualize the discriminating power of these features, the boxplots of PEn, FzEn and K-NN are shown in figure 7.2, figure 7.3 and figure 7.4 respectively. The boxplots show five-point summary of extracted features values for stressed and non-stressed category signals and are used for visual comparison and interpretation of results.

Table 7.1 Mean and Standard deviation of features obtained from IMFs of baseline and stressed state signals

Feature	IMF	Baseline-Non-stress (Mean±SD)	Stress (Mean±SD)
PEn	**IMF1**	0.7285±0.0155	0.7258±0.0121
	IMF2	0.7778±0.0295	0.7598±0.0152
	IMF3	0.8049±0.0878	0.7984±0.0329
	IMF4	0.9292±0.0591	0.8723±0.0372
	IMF5	1.0335±0.0890	0.9943±0.0817
	IMF6	1.2189±0.1346	1.1388±0.1258
	IMF7	1.4735±0.1972	1.3567±0.1813
FzEn	**IMF1**	0.0104±0.0058	0.0088±0.0017
	IMF2	0.0358±0.0277	0.0223±0.0101
	IMF3	0.1001±0.0537	0.0605±0.0143
	IMF4	0.1816±0.0654	0.1154±0.0307
	IMF5	0.2679±0.0792	0.2434±0.1027
	IMF6	0.4220±0.1267	0.3643±0.1290
	IMF7	0.5163±0.0816	0.4648±0.1078
K-NN Entropy Estimator	**IMF1**	-2.1890±6.2875	0.3559±5.2630
	IMF2	-3.6729±7.0938	0.5814±3.9141
	IMF3	-5.1779±3.6738	-1.2857±4.4269
	IMF4	-5.3848±1.3413	-1.4626±3.9897
	IMF5	-4.3915±1.4847	-4.3903±4.0141
	IMF6	-4.2954±2.6828	-2.9657±2.3421
	IMF7	-3.9210±4.1166	-3.0132±2.5016

Table 7.2 *p*-values of features from IMFs of baseline and stressed state signals

Feature	IMF1	IMF2	IMF3	IMF4	IMF5	IMF6	IMF7
PEn	3.9×10^{-2}	7.2×10^{-2}	2.3×10^{-1}	3.2×10^{-4}	6.2×10^{-2}	2.4×10^{-2}	3.3×10^{-2}
FzEn	5.0×10^{-1}	2.3×10^{-1}	5.2×10^{-3}	1.1×10^{-4}	3.5×10^{-1}	4.6×10^{-2}	4.6×10^{-2}
K-NN	3.3×10^{-2}	1.4×10^{-3}	1.7×10^{-2}	3.6×10^{-5}	7.9×10^{-1}	4.6×10^{-2}	4.2×10^{-1}

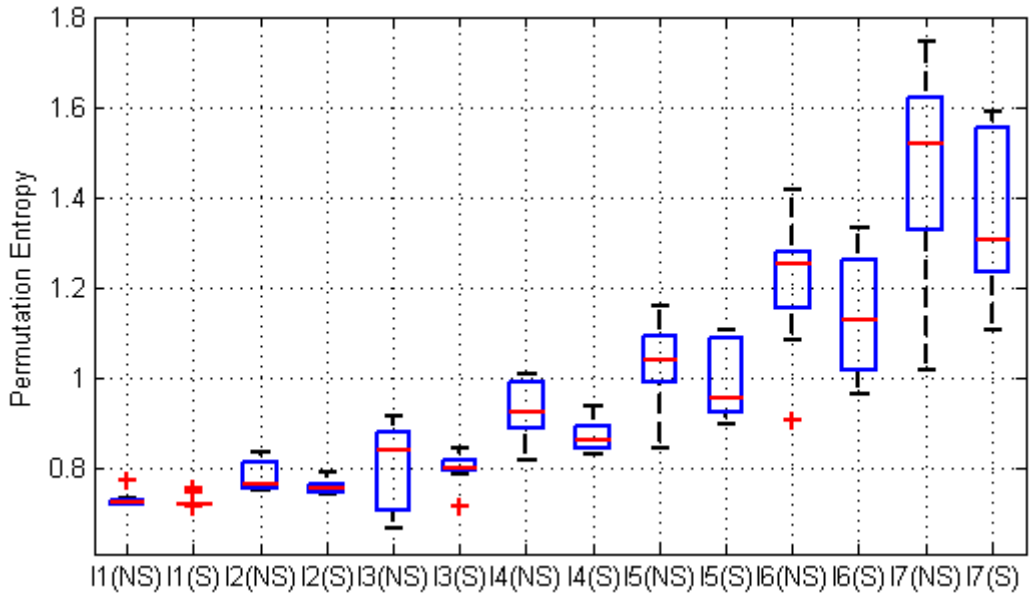

Figure 7.2 Boxplot of Permutation Entropy, In(NS)=nth IMF for Non-stressed baseline state, In(S)= nth IMF for stressed state

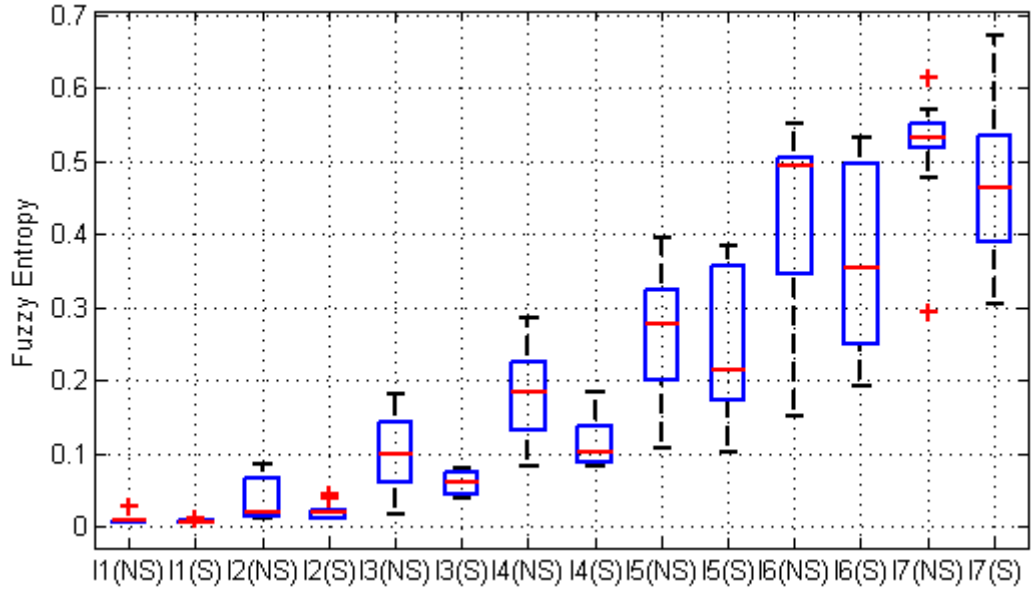

Figure 7.3 Boxplot of Fuzzy Entropy, In(NS)=nth IMF for Non-stressed baseline state, In(S)= nth IMF for stressed state

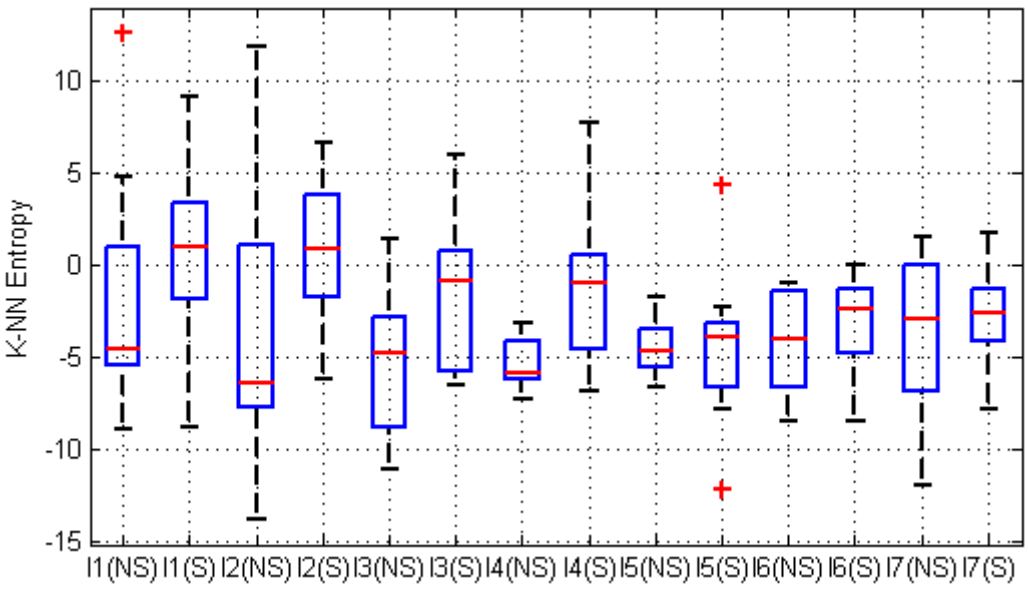

Figure 7.4 Boxplot of K-NN Entropy, In(NS)=nth IMF for Non-stressed baseline state, In(S)= nth IMF for stressed state

All the extracted features may not be significant and can result in a decrease in classification accuracy of the classifier. Therefore, the selection of significant features becomes fundamental. In this study, feature ranking methods namely- Entropy method, Bhattacharya space algorithm, ROC method and Wilcoxon method have been used for feature selection. These ranking methods arrange features in descending order of their statistical significance as shown in table 7.3. The higher ranked features should be used for classification and insignificant lower ranked features can be neglected. In order to obtain maximum classification accuracy using minimum number of feature vectors, these ranked features are fed one by one to LS-SVM classifier with RBF kernel until highest accuracy is obtained. The plot showing number of features versus classification accuracy for various ranking methods is shown in figure 7.5. The highest classification accuracy of 96.67% is achieved using first five features of Bhattacharya space algorithm as shown in figure 7.5.

Table 7.3 Features in descending order of significance according to feature ranking methods

Feature Rank	Entropy method	Bhattacharya Method	ROC method	Wilcoxon Method
1	FzEn IMF3	K-NN IMF4	K-NN IMF4	K-NN IMF4
2	K-NN IMF4	K-NN IMF3	FzEn IMF4	K-NN IMF2
3	FzEn IMF1	K-NN IMF2	PEn IMF4	FzEn IMF4
4	FzEn IMF4	K-NN IMF1	K-NN IMF2	K-NN IMF3
5	FzEn IMF2	FzEn IMF3	FzEn IMF3	PEn IMF4
6	K-NN IMF5	FzEn IMF1	K-NN IMF3	K-NN IMF1
7	PEn IMF3	K-NN IMF6	PEn IMF6	K-NN IMF6
8	PEn IMF4	FzEn IMF2	PEn IMF7	FzEn IMF3
9	PEn IMF2	K-NN IMF5	K-NN IMF1	PEn IMF6
10	K-NN IMF2	PEn IMF3	FzEn IMF6	PEn IMF7
11	K-NN IMF3	FzEn IMF4	FzEn IMF7	K-NN IMF7
12	K-NN IMF7	K-NN IMF7	K-NN IMF6	FzEn IMF6
13	FzEn IMF7	PEn IMF2	PEn IMF5	FzEn IMF7
14	PEn IMF7	PEn IMF4	PEn IMF2	PEn IMF1
15	PEn IMF6	PEn IMF7	PEn IMF3	PEn IMF5
16	K-NN IMF6	FzEn IMF7	FzEn IMF2	PEn IMF2
17	K-NN IMF1	PEn IMF6	FzEn IMF5	K-NN IMF5
18	PEn IMF5	FzEn IMF5	K-NN IMF7	PEn IMF3
19	FzEn IMF5	PEn IMF1	PEn IMF1	FzEn IMF2
20	FzEn IMF6	FzEn IMF6	FzEn IMF1	FzEn IMF5
21	PEn IMF1	PEn IMF5	K-NN IMF5	FzEn IMF1

The LS-SVM classifier with RBF kernel has been used in studies on cardiac sound PCG signals [174], [187]. In this study, the classification of LS-SVM with RBF kernel is compared with linear and quadratic kernel functions using selected first five features of Bhattacharya space algorithm as shown in table 7.4. The optimal kernel parameter is decided on the basis of trial and error experimentation. The reliability and robustness of classification are ensured using 10-fold cross-validation. The classification performance

of the classifier can be evaluated using parameters namely- accuracy (ACC), sensitivity (SEN), specificity (SPE). The performance summary of the proposed system is shown in table 7.4.

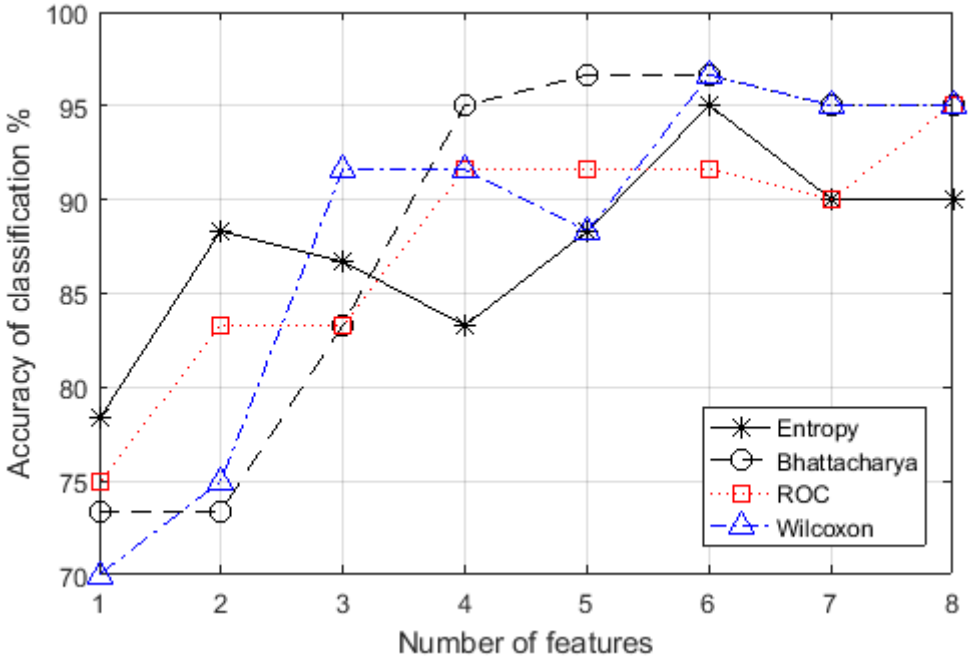

Figure 7.5 Plot depicting accuracy versus number of features using different ranking methods

As per literature, various studies [59]–[62] used ECG-HRV based LF/HF power ratio feature as a standard to quantify sympathovagal balance. The increase in this index indicates a shift towards sympathetic dominance whereas the decrease of the index indicates a shift towards parasympathetic dominance. The proposed methodology for using PCG signals for psychological stress detection showed higher accuracy on our dataset in comparison with ECG based LF/HF power ratio feature as shown in table 7.4 and table 7.5.

Table 7.4 Performance summary of proposed system for classifying baseline and stressed state signals

Features used	**Ranking Method**	**Classifier**	**Kernel and Kernel parameter**	**ACC**	**SEN**	**SPE**
K-NN IMF4 K-NN IMF3 K-NN IMF2 K-NN IMF1 FzEn IMF3	Bhattacharya	LS-SVM	Linear	71.67%	73.33%	70.00%
			Quadratic	83.33%	66.67%	100%
			RBF ϒ=1.05	**96.67%**	**100%**	**93.33%**

Table 7.5 Performance using ECG-based LF/HF power ratio feature

Feature	**Description**	**Used in studies**	**Accuracy**
ECG based LF/HF power ratio	Increase in this feature shows sympathetic dominance whereas, decrease shows parasympathetic dominance	[59]–[62]	80%

Table 7.6 Improvement in classification accuracy with each step of proposed methodology

Features	**Classifier**	**Methodology**	**Accuracy**
Permutation Entropy, Fuzzy Entropy, K-NN Entropy	LS-SVM RBF Kernel ϒ=1.05	Inter-beat Interval (IBI) signal used, No use of EMD technique, Total features used per IBI signal = 3	68.33%
		EMD technique used on IBI signals, No ranking methods used, Total features used per IBI signal = 21	85.00%
		Proposed Methodology Total features used per IBI signal = 5	96.67%

In order to evaluate the efficacy of each step of the proposed methodology, the improvement in classification accuracy at every step using LS-SVM classifier and RBF kernel is evaluated and recorded in table 7.6.

7.6 Discussion

In this work, the methodology for psychological stress detection using PCG signals is proposed. The time-duration between consecutive S1 peaks of the acquired PCG signals is used to form IBI signals. Thereafter, EMD technique is used to decompose IBI signals to IMFs which are mono-component AM-FM signals. The extracted IMFs are shown in figure 7.1, where IMF1 has the lowest frequency components and IMF7 has the highest frequency components. The EMD technique of signal decomposition is suitable for non-linear and non-stationary signals. The complex cardiac dynamics are then captured using three non-linear entropy features namely- PEn, FzEn and K-NN entropy estimator computed from IMFs of IBI signals.

The PEn quantifies the degree of complexity of the time series. The higher values of PEn show high complexity of signals whereas, low values of this feature indicate low complexity of the signals. The mean values of PEn in table 7.1 and the boxplot representation in figure 7.2 indicate lower values of PEn feature for subjects under psychological stress. This depicts the lower complexity of stress category signals as compared to non-stressed category signals. The reduced complexity indicates a stable and periodic behaviour of heart under stress. This may be a reflection of reduced parasympathetic activity and thus depicting sympathovagal imbalance.

The FzEn is used for similarity analysis of time series. The mean values of FzEn in table 7.1 and the boxplot representation in figure 7.3 indicate lower values of FzEn feature for subjects under psychological stress. The smaller values of FzEn feature indicate more regularity of signals. The cardiac signals of subjects under stress show more regular behaviour depicting reduced parasympathetic activity.

The K-NN entropy feature quantifies scattering of a time series. The higher values of this parameter indicate wider scattering. The mean values from table 7.1 and boxplot representation in figure 7.4 show higher values of this feature for subjects under psychological stress. This shows signals for subjects under psychological stress are more scattered as compared to non-stressed subject signals. A study [188] used K-NN entropy to measure scatter (diffusiveness) to characterize divergence from homeostasis and reported similar results. The value of scattering increased in stressed states. This is due to the adjustment of metabolism (dysregulated metabolic behaviour) and coordinated adaptive responses of the organism due to stressor [188].

Thereafter, the extracted features were tested for statistical relevance using Kruskal-Wallis non-parametric test and the *p*-values obtained for the features are reported in table 7.2. The *p*-value is a measure of discriminating ability of the feature in separating two classes and all the features which show *p*-value less than 0.05 are considered to be statistically significant. The PEn feature is statistically relevant ($p < 0.05$) for IMF1, IMF4, IMF6 and IMF7 as evident in table 7.2. In case of FzEn feature, $p < 0.05$ is observed in case of IMF3, IMF4, IMF6 and IMF7 as depicted in table 7.2. The *p*-values for K-NN feature are significantly lower ($p < 0.05$) for IMF1, IMF2, IMF3, IMF4 and IMF6 as shown in table 7.2. Therefore, these IMFs of the extracted features can be used to discriminate stressed and baseline categories of signals. The K-NN IMF4 feature showed lowest *p*-values in table 7.2 and hence can be considered as the most significant feature for psychological stress detection according to statistical test.

The extracted features are arranged in descending order of significance using feature ranking methods namely- Entropy method, Bhattacharya space algorithm, ROC method and Wilcoxon method as shown in table 7.3. The main objective here is to obtain maximum classification accuracy using minimum number of features, therefore, the higher-ranked features are fed one by one to LS-SVM classifier until highest accuracy is obtained. The plot of number of features versus classification accuracy for various ranking methods is shown in figure 7.5 which depicts that the highest classification accuracy of 96.67% is achieved using first five features of Bhattacharya space algorithm. The highest accuracy, sensitivity and specificity achieved using the proposed methodology is 96.67%, 100% and 93.33% respectively using LS-SVM classifier with RBF kernel as shown in table 7.4. It is also interesting that the highest-ranked feature in table 7.4 is K-NN IMF4, which also showed lowest *p*-value in table 7.2. The most significant features used for classification in table 7.4 are- K-NN IMF4, K-NN IMF3, K-NN IMF2, K-NN IMF1 and FzEn IMF3. It can be observed that these most significant features are from low-frequency, lower IMF signals. As most of the information of PCG signals is concentrated at lower frequencies, this justifies the results of this study and the reason for getting useful information from low-frequency IMFs.

The proposed methodology achieved highest classification accuracy of 96.67% on the dataset, whereas the classification accuracy achieved using standard ECG-based LF/HF power ratio method is 80% on this dataset as shown in table 7.5. Therefore, it can be

inferred that the proposed method is a robust, cost-efficient and reasonably better method for psychological stress detection than ECG-based LF/HF power ratio method.

The efficacy and importance of each step of the proposed methodology is depicted in table 7.6 of the study. Firstly, IBI signal is used to compute the entropy features, without the use of EMD technique for signal decomposition. The accuracy of 68.33% is achieved in this case. Secondly, 85.00% accuracy is achieved if all features obtained using EMD technique for signal decomposition of IBI signals are used for classification and hence no ranking methods are used. Finally, if all steps of proposed methodology are followed, the highest accuracy, 96.67% is achieved. This shows that all steps of the proposed methodology are integral to obtain high classification accuracy between non-stressed and stressed psychological states.

The main contribution of this study is the novel methodology to use PCG signals for psychological stress detection instead of EEG or ECG signals. The advantages of using PCG signals over other bio-signals for psychological stress detection are- acquisition process of PCG is simpler, easier and inexpensive, making this method suitable for use in rural areas, developing economies, home-care and other areas where a specialized physician/equipment is not available. Another finding of this study is that the PCG-based features for psychological stress detection are more efficient on the dataset as compared to well-documented ECG-based LF/HF power ratio feature as shown in table 7.4 and table 7.5. As the proposed system is automatic, there is no inter-observer and intra-observer variability. This method requires computation of only five features making it a fast method suitable for real-time psychological stress detection. The proposed system is robust and reliable as 10-fold cross-validation is used. However, fundamental heart sounds segmentation of PCG signals is a cumbersome task but many studies [73], [91], [95], [96] have suggested algorithms for FHS detection without using a reference signal. The limitation of this work is that the proposed methodology is tested on a small dataset. The proposed system needs to be tested on a larger dataset before deployment for homecare and clinical use. The use of other kernel functions with different kernel parameters can also enhance performance of the classifier. The other significant non-linear features can be identified and combined with proposed features to further enhance classification accuracy.

7.7 Summary

In this work, we have retained low-frequency seven IMF signals for feature extraction as inferred from findings of chapter 6 and they also showed higher correlation with IBI signals. This leads to lesser information loss and hence, better classification accuracy. The features extracted in this study are entropy-based non-linear features in EMD domain namely- Permutation Entropy (PEn), Fuzzy Entropy (FzEn) and K-Nearest Neighbour (K-NN) entropy estimator. The results show that K-NN and FzEn features performed better than PEn feature. The highest classification accuracy achieved is 96.67% using first five features of Bhattacharya space algorithm namely- K-NN IMF4, K-NN IMF3, K-NN IMF2, K-NN IMF1 and FzEn IMF3. In this study, unlike convention, IMF1 contains lowest frequency components and IMF7 contains highest frequency components. Therefore, identified most significant features for psychological stress detection are from low-frequency IMF signals, supporting the findings of chapter 6. As most of the information of PCG signals is concentrated at lower frequencies, this justifies the results of this study and the reason for getting useful information from low-frequency IMFs.

CHAPTER 8 CONCLUSION AND FUTURE SCOPE

8.1 Conclusion

This work develops a novel method of using PCG signals for psychological stress detection. The easier acquisition of PCG signals as compared to EEG or ECG signals makes the developed method suitable for rural areas, developing economies, home-care and other areas where a specialized physician/equipment is not available. This study focuses on PCG-based psychological stress detection and the stress used in this study is not laboratory-induced rather real-life examination stress. The data for this study is acquired from students approximately two hours before the institute examination and another reading as baseline is acquired from the same subjects after they return from holidays. The S1 peaks of PCG signals are detected and time duration of consecutive S1 peaks leads to formation of IBI signal. The EMD technique for non-linear and non-stationary signal analysis is applied on IBI signals to form IMFs. The features are then extracted from IMFs for psychological stress detection.

In proposed method 1, the applicability of five non-linear features namely- Area of analytic signal representation (AASR), Log of area of second order difference plot (LASODP), Root Mean Square value of IMF (RmsIMF), Shannon Entropy (ShEnt) and Fuzzy Entropy (FzEnt) for PCG-based psychological stress detection is explored. The analysis has been done in two phases. The subject-specific analysis incorporated the individual characteristic cardiac behaviour and the features that showed maximum deviation from baseline values were identified. The next phase aimed at finding the features for psychological stress analysis that are significant across subjects using

Kruskal-Wallis statistical test. Thereafter, a comparative analysis has been conducted to select the features that were consistent during subject-specific and across subject analysis. A total of six features namely: AASR IMF7, LASODP IMF7, RmsIMF IMF6, RmsIMF IMF7, FzEnt IMF5 and FzEnt IMF6 were identified that were common in both the phases of study. The identified six features from the comparative analysis are used for classification using LS-SVM classifier with RBF kernel. The average accuracy achieved for classification of stressed and non-stressed category of signals is 93.14% using 10-fold cross-validation.

In proposed method 2, the applicability of three non-linear entropy-based features- Permutation entropy (PEn), Fuzzy entropy (FzEn) and K-NN entropy estimator (KNN) for PCG-based psychological stress detection is explored. The non-linear features have been computed for capturing the non-linear characteristics of cardiac PCG signals. The ranking methods have been used for optimizing the classification performance and highest accuracy achieved is 96.67% using first five features of Bhattacharya ranking algorithm. The use of 10-fold cross-validation with LS-SVM and RBF kernel function makes the proposed system reliable and robust. The identified most suitable features for psychological stress detection are- K-NN IMF4, K-NN IMF3, K-NN IMF2, K-NN IMF1 and FzEn IMF3.

This research work also highlights that the features identified from PCG signals provided better results on the dataset as compared to well-documented ECG based LF/HF power ratio feature-based sympathovagal balance indicator method. Therefore, the developed methodology for PCG-based psychological stress detection is efficient to detect psychological stress.

Another conclusion that can be inferred from this study is that the important features identified for psychological stress detection are predominantly from low-frequency IMFs. As most of the information of PCG signals is concentrated at lower frequencies, this justifies the results of this study and reason for getting useful information from low-frequency IMF signals. The proposed methodology for psychological stress detection using PCG signals can be further applied to design a reliable system for home-care and primary health-care centres of rural areas to provide timely diagnosis.

8.2 Major Findings and Contributions

- The **novelty** of this study is the applicability of PCG signals for psychological stress detection
- **The important features identified for psychological stress detection are from lower frequency IMF signals**. As most of the information of PCG signals is concentrated at lower frequencies, this justifies the results of this study and reason for getting useful information from low-frequency IMF signals
- The PCG-based method has reasonably better discrimination ability on the dataset than ECG-based LF/HF power ratio sympathovagal balance indicator method, when STAI self-report questionnaire is taken as a standard
- The subject-specific baseline template used in the study ensures incorporation of the individual cardiovascular characteristic behaviour and stress responses
- This study opened a **new research area** of psychological stress detection using PCG signals

8.3 Advantages of PCG-based stress detection

- Suitable for places where sophisticated equipment like EEG and ECG are not available
- **An important contribution for reducing urban-rural divide in healthcare**
- Cost-effective methodology, easy to acquire PCG signals makes it suitable for home-care, developing economies and telemedicine
- Performed better than standard ECG-based sympathovagal balance indicator method on the dataset
- The developed system is automatic and hence, there is no inter-observer and intra-observer variability
- Can be further developed as a smartphone-based system for psychological stress detection

8.4 Limitations and Future Scope

- The proposed system needs to be tested on a larger dataset comprising of various age-groups before deployment for homecare and clinical use
- The use of other kernel functions with different kernel parameters can also enhance performance of the classifier
- A computer-based optimum criteria for kernel function and kernel parameter selection can be developed
- The other significant non-linear features can be identified and combined with proposed features to further enhance classification accuracy
- Differentiating State-anxiety and Trait-anxiety using PCG signals may form another field of research
- The use of PCG signals for human emotion recognition can also be explored in future works

LIST OF PUBLICATIONS

List of SCI Publications based on thesis work:

- A. Cheema, M. Singh, Psychological stress detection using phonocardiography signal : An empirical mode decomposition approach, Biomed. Signal Process. Control. 49 (2019) 493–505. doi:10.1016/j.bspc.2018.12.028. **Impact Factor- 3.137**.
- A. Cheema, M. Singh, An application of phonocardiography signals for psychological stress detection using non-linear entropy based features in empirical mode decomposition domain, Appl. Soft Comput. J. 77 (2019) 24–33. doi:10.1016/j.asoc.2019.01.006. **Impact factor- 5.472**.
- A. Cheema, M. Singh, Classification of Psychologically Stressed and Non-stressed state from cardiac sound signals using phase space representation analysis of intrinsic mode functions (To be communicated)

List of non-SCI (SCOPUS) publications besides thesis work:

- A. Cheema, M. Singh, A Pre-screening method for cardiac anomalies detection using phonocardiography signals, Indian Journal of Public Health Research & Development 9 (2018) 180-185. doi:10.5958/0976-5506.2018.00717.9

References

[1] World Health Organization, “Promoting mental health: concepts, emerging evidence, practice (Summary report),” 2004.

[2] World Health Organization, “Mental health: strengthening our response,” 2018. [Online]. Available: https://www.who.int/news-room/fact-sheets/detail/mental-health-strengthening-our-response.

[3] World Health Organization, “Constitution of the world Health Organization.” pp. 1–18, 1946.

[4] World Health Organization, “The world health report 2001; Mental health: new understanding, new hope,” 2001.

[5] World Health Organization, “Mental disorders,” 2019.

[6] Á. C. Msw, J. Navarro-pérez, and M.-V. Mestre, “Challenges and barriers in mental healthcare systems and their impact on the family : A systematic integrative review,” *Heal. Soc. care community*, vol. 28, pp. 1366–1379, 2020.

[7] P. S. Wang, S. Aguilar-gaxiola, J. Alonso, M. C. Angermeyer, G. Borges, E. J. Bromet, and R. Bruff, “Use of mental health services for anxiety , mood , and substance disorders in 17 countries in the WHO world mental health surveys,” *Lancet*, vol. 370, pp. 841–850, 2007.

[8] GBD 2017 Disease and Injury Incidence and Prevalence Collaborators, “Global, regional, and national incidence, prevalence, and years lived with disability for 354 diseases and injuries for 195 countries and territories, 1990 – 2017 : a systematic analysis for the Global Burden of Disease Study 2017,” *Lancet*, vol. 392, pp. 1789–858, 2018.

[9] World Health Organisation, “Schizophrenia,” 2019.

[10] A. Lora, R. Kohn, I. Levav, R. Mcbain, S. Saxena, and A. Lora, “Service availability and utilization and treatment gap for schizophrenic disorders : a survey in 50 low- and middle-income countries,” 2012.

[11] World Health Organisation, “Dementia,” 2019.

[12] World Health Organisation, “Autism spectrum disorders,” 2019.

[13] World Health Organisation, “Social determinants of mental health,” 2014.

[14] J. Oliva-Moreno, J. Lopez-Bastida, A. Luis Montejo-Gonzalez, R. Osuna-Guerrero, and B. Duque-Gonzalez, “The socioeconomic costs of mental illness in Spain,” *Eur. J. Heal. Econ.*, vol. 10, pp. 361–369, 2009.

[15] S. Mnookin, A. Kleinman, T. Evans, P. Marquez, S. Saxena, D. Chisholm, A. Becker, P. Collins, M. De Silva, P. Farias, R. Iunes, A. Ito, D. Jamison, Y. Kim, J. Klein, V. Patel, and B. Saraceno, “Out of shadows: Making mental health a global development priority,” 2016.

[16] T. A. Ghebreyesus, “The WHO Special Initiative for Mental Health (2019-2023): Universal Health Coverage for Mental Health,” 2019.

[17] World Health Organization, “Investing in mental health: evidence for action,” 2013.

[18] M. L. Wainberg, P. Scorza, J. M. Shultz, L. Helpman, J. J. Mootz, K. A. Johnson, Y. Neria, J. E. Bradford, M. A. Oquendo, and M. R. Arbuckle, “Challenges and opportunities in global mental health: a research-to-practice perspective,” *Curr. Psychiatry Rep.*, vol. 19, no. 5, 2017.

[19] World Health Organisation, *Mental Health Atlas 2017*. 2017.

[20] G. M. Slavich, *Psychoneuroimmunology of Stress and Mental Health*. 2019.

[21] National Institute of Mental health, “Things You Should Know About Stress.”

[22] H. Selye, “The General Adaptation Syndrome and the diseases of adaptation,” *J. Clin. Endocrinol.*, vol. 6, no. 2, 1946.

[23] L. M. Romero and L. K. Butler, “Endocrinology of Stress,” *Int. J. Comp. Psychol.*, vol. 20, no. 2, pp. 89–95, 2007.

[24] Havard Medical School, “Understanding the stress response,” *Havard Health Publishing*, 2020. [Online]. Available: https://www.health.harvard.edu/staying-

healthy/understanding-the-stress-response.

[25] G. Russell and S. Lightman, “The human stress response,” *Nat. Rev. Endocrinol.*, vol. 15, no. 9, pp. 525–534, 2019.

[26] M. R. Salleh, “Life event, stress and illness,” *Malaysian J. Med. Sci.*, vol. 15, no. 4, pp. 9–18, 2008.

[27] C. Schiweck, D. Piette, D. Berckmans, S. Claes, and E. Vrieze, “Heart rate and high frequency heart rate variability during stress as biomarker for clinical depression . A systematic review,” *Psychol. Med.*, no. August, pp. 1–12, 2018.

[28] World Health Organisation, “Depression,” 2020.

[29] B. E. Leonard, “The concept of depression as a dysfunction of the immune system,” *Curr. Immunol. Rev.*, vol. 6, no. 3, pp. 205–212, 2010.

[30] World Health Organisation, “Depression: What you should know,” 2017. [Online]. Available: https://www.who.int/campaigns/world-health-day/2017/handouts-depression/what-you-should-know/en/.

[31] National Health Service UK, “Symptoms Clinical Depression,” 2019. .

[32] National Health Service UK, “Treatment Clinical depression,” 2019. [Online]. Available: https://www.nhs.uk/conditions/clinical-depression/treatment/.

[33] R. Sagar, R. Dandona, G. Gururaj, R. S. Dhaliwal, A. Singh, A. Ferrari, T. Dua, A. Ganguli, M. Varghese, J. K. Chakma, G. A. Kumar, K. S. Shaji, A. Ambekar, T. Rangaswamy, L. Vijayakumar, V. Agarwal, R. P. Kri, and L. Dandona, “The burden of mental disorders across the states of India: the Global Burden of Disease Study 1990-2017,” *The lancet. Psychiatry*, vol. 7, no. 2, pp. 148–161, Feb. 2020.

[34] A. Gururaj G, Varghese M, Benegal V, Rao GN, Pathak K, Singh LK, Mehta RY, Ram D, Shibukumar TM, Kokane A, Lenin Singh RK, Chavan BS, Sharma P, Ramasubramanian C, Dalal PK, Saha PK , Deuri SP, Giri AK, Kavishvar AB, Sinha VK, Thavody J, Chatterji R and M. R, *National Mental Health Survey of India, 2015-16: Prevalence, Pattern and Outcomes*. 2016.

[35] Hindustan Times, “Let the techers do what they are hired for. The plan to utilise

them as mental health counsellors for students may not work," Chandigarh, p. 10, 28-Aug-2018.

[36] A. B. Dahale, A. Kandasamy, B. AS, C. Kishore, G. Desai, G. SM, H. Angothu, H. Thippeswamy, J. Thirthalli, J. V. Sagar K, K. P. Muliyala, L. P. Sharma, M. Varghese, N. Manjunatha, N. P. Rao, N. Kumar C, N. M. Pai, P. Khadse, P. S. Chandra, P. Jacob, P. Sinha, R. KM, S. Baliga, S. K. Reddi V, S. S. Reddy M, S. S. Arumugham, S. PT, S. Ghosh, S. HH, S. Ganjekar, S. B. Math, T. Sivakumar, T. R, U. Mehta, V. Shanbhag, V. Kumar KG, and Y. Devendran, "COVID-19 Pandemic Guidance for Psychiatrists COVID-19 Pandemic Guidance for Psychiatrists," 2020.

[37] W. Wan, "The coronavirus pandemic is pushing America into a mental health crisis," *The Washington Post*, 2020.

[38] B. Pfefferbaum and C. S. North, "Mental Health and the Covid-19 Pandemic," *N. Engl. J. Med.*, vol. 383, no. 6, pp. 510–512, 2020.

[39] L. Duan and G. Zhu, "Psychological interventions for people affected by the COVID-19 epidemic," *The lancet. Psychiatry*, vol. 7, no. April, pp. 300–302, 2020.

[40] V. Patel, S. Saxena, C. Lund, G. Thornicroft, F. Baingana, P. Bolton, D. Chisholm, P. Y. Collins, J. L. Cooper, J. Eaton, H. Herrman, M. M. Herzallah, Y. Huang, M. J. D. Jordans, A. Kleinman, M. E. Medina-Mora, E. Morgan, U. Niaz, O. Omigbodun, M. Prince, A. Rahman, B. Saraceno, B. K. Sarkar, M. De Silva, I. Singh, D. J. Stein, C. Sunkel, and Jü. UnÜtzer, "The Lancet Commission on global mental health and sustainable development," *Lancet*, vol. 392, no. 10157, pp. 1553–1598, 2018.

[41] G. P. Chrousos, "Stress and disorders of the stress system," *Nat. Publ. Gr.*, vol. 5, no. 7, pp. 374–381, 2009.

[42] B. S. McEwen, *Stress Concepts and Cognition, Emotion, and Behavior*. Elsevier Inc., 2016.

[43] S. Cohen, D. Janicki-Deverts, and G. E. Miller, "Psychological stress and disease," *Jama*, vol. 298, no. 14, pp. 1685–1687, 2007.

[44] World Health Organisation, “WHO Mental Health Action Plan 2013-2020.” p. 48, 2013.

[45] M. E. Tavel, “Cardiac Auscultation,” *Circulation*, vol. 93, no. 6, pp. 1250 – 1253, Mar. 1996.

[46] A. K. Bhoi, K. S. Sherpa, and B. Khandelwal, “Multidimensional analytical study of heart sounds: A review,” *Int. J. Bioautomation*, vol. 19, no. 3, pp. 351–376, 2015.

[47] U. R. Acharya, J. S. Suri, J. A. E. Spaan, and S. M. Krishnan, *Advances in Cardiac Signal Processing*. 2007.

[48] F. Shaffer, R. Mccraty, and C. L. Zerr, “A healthy heart is not a metronome : an integrative review of the heart’s anatomy and heart rate variability,” *Front. Psychol.*, vol. 5, no. September, pp. 1–19, 2014.

[49] M. Kumar, “Automated diagnosis methods for heart diseases using flexible analytic wavelet transform,” 2018.

[50] L. Cromwell, F. J. Weibell, and E. A. Pfeiffer, *Biomedical instrumentation and measurements*, Second. 2011.

[51] G. Seemann, C. Höper, F. B. Sachse, O. Dössel, and A. V Holden, “Heterogeneous three-dimensional anatomical and electrophysiological model of human atria,” *Philos. Trans. R. Soc. A*, vol. 364, pp. 1465–1481, 2006.

[52] C. Ahlström, “Processing of the Phonocardiographic Signal − Methods for the Intelligent Stethoscope,” 2006.

[53] S. W. Porges, “Vagal tone : A physiologic marker of stress vulnerability,” *Pediatrics*, vol. 90, pp. 498–504, 1992.

[54] A. N. Syamsunder, G. K. Pal, P. Pal, C. S. Kamalanathan, S. C. Parija, and N. Nanda, “Association of sympathovagal imbalance with cardiovascular risks in overt hypothyroidism.,” *N. Am. J. Med. Sci.*, vol. 5, no. 9, pp. 554–561, Sep. 2013.

[55] R. McCraty and F. Shaffer, “Heart Rate Variability : New Perspectives on Physiological Mechanisms , Assessment of Self-regulatory Capacity , and Health

Risk," *Glob. Adv. Heal. Med.*, vol. 4, no. 1, pp. 46–61, 2015.

[56] R. Soufer, H. Jain, and A. J. Yoon, "Heart – Brain Interactions in Mental Stress – Induced Myocardial Ischemia," *Nucl. Cardiol.*, vol. 11, pp. 133–140, 2009.

[57] R. M. Carney, K. E. Freedland, and R. C. Veith, "Depression, the Autonomic Nervous System, and Coronary Heart Disease," *Psychosom. Med. 67*, vol. 33, no. 1, pp. 29–33, 2005.

[58] M. Marek, "Guidelines Heart rate variability," *Eur. Heart J.*, vol. 17, pp. 354–381, 1996.

[59] M. Pagani, F. Lombardi, S. Guzzetti, G. Sandrone, O. Rimoldi, G. Malfatto, S. Cerutti, and A. Malliani, "Power spectral density of heart rate variability as an index of sympatho-vagal interaction in normal and hypertensive subjects.," *J. Hypertens. Suppl.*, vol. 2, no. 3, pp. 383–385, Dec. 1984.

[60] M. Pagani, F. Lombardi, S. Guzzetti, O. Rimoldi, R. Furlan, P. Pizzinelli, G. Sandrone, G. Malfatto, S. Dell'Orto, and E. Piccaluga, "Power spectral analysis of heart rate and arterial pressure variabilities as a marker of sympatho-vagal interaction in man and conscious dog.," *Circ. Res.*, vol. 59, no. 2, pp. 178–193, Aug. 1986.

[61] A. Malliani, M. Pagani, F. Lombardi, and S. Cerutti, "Cardiovascular neural regulation explored in the frequency domain.," *Circulation*, vol. 84, no. 2, pp. 482–492, Aug. 1991.

[62] A. Azhari, A. Truzzi, P. Rigo, M. H. Bornstein, and G. Esposito, "Putting salient vocalizations in context: Adults' physiological arousal to emotive cues in domestic and external environments," *Physiol. Behav.*, vol. 196, no. August, pp. 25–32, 2018.

[63] K. Shafqat, S. K. Pal, S. Kumari, and P. A. Kyriacou, "Empirical mode decomposition analysis of HRV data from patients undergoing local anaesthesia (brachial plexus block)," *Physiol. Meas.*, vol. 32, no. 4, pp. 483–497, 2011.

[64] G. Parati, G. Mancia, M. Di Rienzo, and P. Castiglioni, "Point: Counterpoint: Cardiovascular variability is/is not an index of autonomic control of circulation," *J.*

Appl. Physiol., vol. 101, no. 2, pp. 676–682, 2006.

[65] G. E. Billman, "Cardiac autonomic neural remodeling and susceptibility to sudden cardiac death: effect of endurance exercise training," *Am. J. Physiol. Circ. Physiol.*, vol. 297, no. 4, pp. H1171–H1193, 2009.

[66] G. E. Billman, "The LF/HF ratio does not accurately measure cardiac sympatho-vagal balance," *Front. Physiol.*, vol. 4, p. 26, 2013.

[67] M. Malik, "Guidelines Heart rate variability Standards of measurement, physiological interpretation, and clinical use," *Eur. Heart J.*, vol. 17, pp. 354–381, 1996.

[68] S. Kofman, A. Bickel, A. Eitan, A. Weiss, N. Gavriely, and N. Intrator, "Discovery of multiple level heart-sound morphological variability resulting from changes in physiological states," *Biomed. Signal Process. Control*, vol. 7, no. 4, pp. 315–324, 2012.

[69] V. N. Varghees and K. I. Ramachandran, "Effective Heart Sound Segmentation and Murmur Classification Using Empirical Wavelet Transform and Instantaneous Phase for Electronic Stethoscope," *IEEE Sens. J.*, vol. 17, no. 12, pp. 3861–3872, 2017.

[70] G. Amit, N. Gavriely, and N. Intrator, "Cluster analysis and classification of heart sounds," *Biomed. Signal Process. Control*, vol. 4, pp. 26–36, 2009.

[71] J. Herzig, A. Bickel, A. Eitan, and N. Intrator, "Monitoring Cardiac Stress Using Features Extracted From S1 Heart Sounds," *IEEE Trans. Biomed. Eng.*, vol. 62, no. 4, pp. 1169–1178, 2015.

[72] C. Spiers, "Cardiac auscultation," *Br. J. Card. Nurs.*, vol. 6, no. 10, pp. 482–486, 2011.

[73] D. B. Springer, L. Tarassenko, and G. D. Clifford, "Logistic Regression-HSMM-Based Heart Sound Segmentation," *IEEE Trans. Biomed. Eng.*, vol. 63, no. 4, pp. 822–832, 2016.

[74] "Heart murmurs and heart sounds." [Online]. Available: https://www.practicalclinicalskills.com/heart-murmurs.

[75] K. K. Sharma, P. Gupta, and S. D. Joshi, “Baseline wander removal of electrocardiogram signals using multivariate empirical mode decomposition,” *Healthc. Technol. Lett.*, vol. 2, no. 6, pp. 164–166, 2015.

[76] F. Kovacs, M. Torok, and I. Habermajer, “A rule-based phonocardiographic method for long-term fetal heart rate monitoring,” *IEEE Trans. Biomed. Eng.*, vol. 47, no. 1, pp. 124–130, 2000.

[77] R. J. Lehner and R. M. Rangayyan, “A Three-Channel Microcomputer System for Segmentation and Characterization of the Phonocardiogram,” *IEEE Trans. Biomed. Eng.*, vol. 34, no. 6, pp. 485–489, 1987.

[78] L. Khadra, M. Matalgah, B. El Asir, and S. Mawagdeh, “The Wavelet transform and its applications to phonocardiogram signal analysis,” *Med. Informatics*, vol. 16, no. 3, pp. 271–277, 1991.

[79] X. Zhang, L. Durand, L. Senhadji, H. C. Lee, and J. L. Coatrieux, “Time-Frequency Scaling Transformation of the Phonocardiogram Based of the Matching Pursuit Method,” *IEEE Trans. Biomed. Eng.*, vol. 45, no. 8, pp. 972–979, 1998.

[80] S. Guillén, M. T. Arredondo, V. Traver, J. M. García, and C. Fernández, “Multimedia telehomecare system using standard TV set,” *IEEE Trans. Biomed. Eng.*, vol. 49, no. 12, pp. 1431–1437, 2002.

[81] R. Ortiz, R. Gonza, M. A. Pen, and C. Vargas, “Differences in foetal heart rate variability from phonocardiography and abdominal electrocardiography,” *J. Med. Eng. Technol.*, vol. 26, no. 1, pp. 39–45, 2002.

[82] P. Várady, L. Wildt, Z. Benyó, and A. Hein, “An advanced method in fetal phonocardiography,” *Comput. Methods Programs Biomed.*, vol. 71, no. 3, pp. 283–296, 2003.

[83] Z. Syed, D. Leeds, D. Curtis, F. Nesta, R. A. Levine, and J. Guttag, “A framework for the analysis of acoustical cardiac signals,” *IEEE Trans. Biomed. Eng.*, vol. 54, no. 4, pp. 651–662, 2007.

[84] H. Tang, T. Li, and T. Qiu, “Noise and Disturbance Reduction for Heart Sounds in Cycle-Frequency Domain Based on Nonlinear Time Scaling,” *IEEE Trans.*

Biomed. Eng., vol. 57, no. 2, pp. 325–333, 2010.

[85] H. Tang, T. Li, and T. Qiu, "Separation of Heart Sound Signal from Noise in Joint Cycle Frequency – Time – Frequency Domains Based on Fuzzy Detection," *IEEE Trans. Biomed. Eng.*, vol. 57, no. 10, pp. 2438–2447, 2010.

[86] S. Mandal, K. Basak, M. Mahadevappa, K. Mandana, A. Ray, and J. Chatterjee, "Development of Cardiac Prescreening Device for Rural Population Using Ultralow - Power Embedded System," *IEEE Trans. Biomed. Eng.*, vol. 58, no. 3, pp. 745–749, 2011.

[87] F. Kovacs, C. Horváth, Á. Balogh, and G. Hosszú, "Extended Noninvasive Fetal Monitoring by Detailed Analysis of Data Measured With Phonocardiography," *IEEE Trans. Biomed. Eng.*, vol. 58, no. 1, pp. 64–70, 2011.

[88] S. Patidar and R. B. Pachori, "Segmentation of cardiac sound signals by removing murmurs using constrained tunable-Q wavelet transform," *Biomed. Signal Process. Control*, vol. 8, no. 6, pp. 559–567, 2013.

[89] S. Patidar, R. Bilas, and N. Garg, "Automatic diagnosis of septal defects based on tunable- Q wavelet transform of cardiac sound signals," *Expert Syst. Appl.*, vol. 42, no. 7, pp. 3315–3326, 2015.

[90] K. Watanabe, Y. Kurihara, K. Watanabe, T. Azami, S. Nukaya, and H. Tanaka, "Biosignals sensing by novel use of bidirectional microphones in a mobile phone for ubiquitous healthcare monitoring," *IEEE Trans. Human-Machine Syst.*, vol. 44, no. 4, pp. 545–550, 2014.

[91] C. D. Papadaniil and L. J. Hadjileontiadis, "Efficient Heart Sound Segmentation and Extraction Using Ensemble Empirical Mode Decomposition and Kurtosis Features," *IEEE J. Biomed. Heal. Informatics*, vol. 18, no. 4, pp. 1138–1152, 2014.

[92] S. E. Schmidt, C. Holst-Hansen, C. Graff, E. Toft, and J. J. Struijk, "Segmentation of heart sound recordings by a duration-dependent hidden Markov model," *Physiol. Meas.*, vol. 31, no. 4, pp. 513–529, Mar. 2010.

[93] C. Liu, D. Springer, Q. Li, B. Moody, F. Castells, M. Roig, and I. Silva, "An open access database for the evaluation of heart sound algorithms," *Physiol. Meas.*, vol.

37, pp. 2181–2213, 2016.

[94] W. Zhang, J. Han, and S. Deng, “Heart sound classification based on scaled spectrogram and partial least squares regression,” *Biomed. Signal Process. Control*, vol. 32, pp. 20–28, 2017.

[95] W. Zhang, J. Han, and S. Deng, “Heart sound classification based on scaled spectrogram and tensor decomposition,” *Expert Syst. Appl.*, vol. 84, pp. 220–231, 2017.

[96] T. Chen, S. Yang, L. Ho, K. Tsai, Y. Chen, Y. Chang, Y. Lai, S. Wang, Y. Tsao, and C. Wu, “S1 and S2 Heart Sound Recognition Using Deep Neural Networks,” *IEEE Trans. Biomed. Eng.*, vol. 64, no. 2, pp. 372–380, 2017.

[97] S. Latif, M. Usman, R. Rana, and J. Qadir, “Phonocardiographic Sensing Using Deep Learning for Abnormal Heartbeat Detection,” *IEEE Sens. J.*, vol. 18, no. 22, pp. 9393–9400, 2018.

[98] T. Omari and F. Bereksi-Reguig, “A new approach for blood pressure estimation based on phonocardiogram,” *Biomed. Eng. Lett.*, vol. 9, pp. 395–406, 2019.

[99] S. K. Ghosh, R. K. Tripathy, R. N. Ponnalagu, and R. B. Pachori, “Automated Detection of Heart Valve Disorders from PCG Signal using Time-Frequency Magnitude and Phase Features,” *IEEE Sensors Lett.*, vol. 3, no. 12, pp. 1–4, 2019.

[100] P. Thanaraj, K. Parvathavarthini, and B. Snekhalatha, “Automated heart sound classification system from unsegmented phonocardiogram (PCG) using deep neural network,” *Phys. Eng. Sci. Med.*, vol. 43, no. 2, pp. 505–515, 2020.

[101] Y.-R. Chien, K.-C. Hsu, and H.-W. Tsao, “Phonocardiography Signals Compression with Deep Convolutional Autoencoder for Telecare Applications,” *Appl. Sci.*, vol. 10, no. 17, 2020.

[102] M. Altuve, L. Suárez, and J. Ardila, “Fundamental heart sounds analysis using improved complete ensemble EMD ScienceDirect Fundamental heart sounds analysis using improved complete ensemble EMD with adaptive noise,” *Biocybern. Biomed. Eng.*, vol. 40, no. June, pp. 426–439, 2020.

[103] L. Lin, D. Guan, D. Zhang, J. Feng, and L. Xu, “Refined analysis of heart sound

based on Hilbert-Huang transform," in *IEEE International Conference on Information and Automation, ICIA 2012*, 2012, no. June, pp. 100–105.

[104] G. Giannakakis, D. Grigoriadis, K. Giannakaki, O. Simantiraki, A. Roniotis, and M. Tsiknakis, "Review on psychological stress detection using biosignals," *IEEE Trans. Affect. Comput.*, 2019.

[105] V. Shusterman and O. Barnea, "Sympathetic nervous system activity in stress and biofeedback relaxation," *IEEE Engineering in Medicine and Biology Magazine*, vol. 24, no. 2, pp. 52–57, 2005.

[106] J. Zhai, A. B. Barreto, C. Chin, and C. Li, "Realization of stress detection using psychophysiological signals for improvement of human -computer interactions," in *IEEE SoutheastCon*, 2005, pp. 415–420.

[107] M. Kumar, M. Weippert, R. Vilbrandt, S. Kreuzfeld, and R. Stoll, "Fuzzy Evaluation of Heart Rate Signals for Mental Stress Assessment," *IEEE Trans. Fuzzy Syst.*, vol. 15, no. 5, pp. 791–808, 2007.

[108] J. Choi and R. Gutierrez-osuna, "Removal of Respiratory Influences From Heart Rate Variability in Stress Monitoring," *IEEE Sens. J.*, vol. 11, no. 11, pp. 2649–2656, 2011.

[109] H. Li, S. Kwong, L. Yang, D. Huang, and D. Xiao, "Hilbert-Huang Transform for Analysis of Heart Rate Variability in Cardiac Health," *IEEE/ACM Trans. Comput. Biol. Bioinforma.*, vol. 8, no. 6, pp. 1557–1567, 2011.

[110] N. Sharma, A. Dhall, T. Gedeon, and R. Goecke, "Modeling Stress Using Thermal Facial Patterns : A Spatio-Temporal Approach," in *Humaine Association Conference on Affective Computing and Intelligent Interaction*, 2013, pp. 387–92.

[111] T. Chen, P. Yuen, M. Richardson, G. Liu, and Z. She, "Detection of Psychological Stress Using a Hyperspectral Imaging Technique," *IEEE Trans. Affect. Comput.*, vol. 5, no. 4, pp. 391–405, 2014.

[112] A. Lanata, G. Valenza, A. Greco, C. Gentili, R. Bartolozzi, F. Bucchi, F. Frendo, and E. P. Scilingo, "How the Autonomic Nervous System and Driving Style Change With Incremental Stressing Conditions During Simulated Driving," *IEEE*

Trans. Intell. Transp. Syst., vol. 16, no. 3, pp. 1505–1517, 2015.

[113] F. Al-Shargie, M. Kiguchi, N. Badruddin, S. C. Dass, A. F. M. Hani, and T. B. Tang, "Mental stress assessment using simultaneous measurement of EEG and fNIRS," *Biomed. Opt. Express*, vol. 7, no. 10, pp. 3882–3898, 2016.

[114] S. Baltaci and D. Gokcay, "Stress Detection in Human–Computer Interaction: Fusion of Pupil Dilation and Facial Temperature Features," *Int. J. Hum. Comput. Interact.*, vol. 32, no. 12, pp. 956–966, 2016.

[115] G. Giannakakis, M. Pediaditis, D. Manousos, E. Kazantzaki, F. Chiarugi, P. G. Simos, K. Marias, and M. Tsiknakis, "Stress and anxiety detection using facial cues from videos," *Biomed. Signal Process. Control*, vol. 31, pp. 89–101, 2017.

[116] A. A S, J. Joy, P. S P, J. Joseph, and M. Sivaprakasam, "Physiological Signal Based Work Stress Detection Using Unobtrusive Sensors," *Biomed. Phys. Eng. Express*, vol. 4, no. 6, 2018.

[117] L. Xia, A. S. Malik, and A. R. Subhani, "A physiological signal-based method for early mental-stress detection," *Biomed. Signal Process. Control*, vol. 46, pp. 18–32, 2018.

[118] A. Asif, M. Majid, and S. M. Anwar, "Human stress classification using EEG signals in response to music tracks," *Comput. Biol. Med.*, vol. 107, pp. 182–196, 2019.

[119] R. Castaldo, L. Montesinos, P. Melillo, C. James, and L. Pecchia, "Ultra-short term HRV features as surrogates of short term HRV : a case study on mental stress detection in real life," *BMC Med. Inform. Decis. Mak.*, vol. 19, no. 12, 2019.

[120] E. M. Mejia, K. Budidha, T. Y. Abay, J. M. May, and P. A. Kyriacou, "Heart Rate Variability (HRV) and Pulse Rate Variability (PRV) for the Assessment of Autonomic Responses," *Front. Physiol.*, vol. 11, 2020.

[121] M. Zubair and C. Yoon, "Multilevel mental stress detection using ultra-short pulse rate variability series," *Biomed. Signal Process. Control*, vol. 57, p. 101736, 2020.

[122] S. Chandra, A. K. Jaiswal, R. Singh, D. Jha, and A. P. Mittal, "Mental stress: Neurophysiology and its regulation by Sudarshan Kriya Yoga," *Int. J. Yoga*, vol.

10, no. 2, pp. 67–72, 2017.

[123] Garmin, “Stress score.” [Online]. Available: https://www8.garmin.com/manuals/webhelp/fenix3/EN-US/GUID-20E035CE-CA52-40D0-B202-13403D6FAA51.html.

[124] Samsung, “What does the heart rate sensor measure?” [Online]. Available: https://www.samsung.com/us/heartratesensor/.

[125] Apple Inc., “Monitor your heart rate with Apple Watch,” 2020. [Online]. Available: https://support.apple.com/en-in/HT204666.

[126] Muse, “Muse Translates Your Brainwaves Into the Guiding Sounds of Weather.” [Online]. Available: https://choosemuse.com/how-it-works/).

[127] Y. Said, B. Arnrich, and C. Ersoy, “Stress detection in daily life scenarios using smart phones and wearable sensors : A survey,” *J. Biomed. Inform.*, vol. 92, no. August 2018, pp. 1–22, 2019.

[128] G. D. Clifford and S. C. College, “Signal Processing Methods for Heart Rate Variability,” 2002.

[129] P. D. Stein, H. N. Sabbah, J. B. Lakier, D. J. Magilligan, and D. Goldstein, “Frequency of the first heart sound in the assessment of stiffening of mitral bioprosthetic valves,” *Circulation*, vol. 63, no. 1, pp. 200–203, 1981.

[130] S. Chauhan, P. Wang, C. Sing Lim, and V. Anantharaman, “A computer-aided MFCC-based HMM system for automatic auscultation,” *Comput. Biol. Med.*, vol. 38, no. 2, pp. 221–233, 2008.

[131] D. Lucini, G. Norbiato, M. Clerici, and M. Pagani, “Hemodynamic and autonomic adjustments to real life stress conditions in humans,” *Hypertension*, vol. 39, no. 1, pp. 184–188, 2002.

[132] P. Melillo, M. Bracale, and L. Pecchia, “Nonlinear Heart Rate Variability features for real-life stress detection. Case study: students under stress due to university examination,” *Biomed. Eng. Online*, vol. 10, no. 1, p. 96, 2011.

[133] D. A. Dimitriev, A. D. Dimitriev, Y. D. Karpenko, and E. V Saperova, “Influence

of examination stress and psychoemotional characteristics on the blood pressure and heart rate regulation in female students," *Hum. Physiol.*, vol. 34, no. 5, pp. 617–624, 2008.

[134] N. L. Corah, E. N. Gale, and S. J. Illig, "Psychological Stress Reduction During Dental Procedures," *J. Dent. Res.*, vol. 58, no. 4, pp. 1347–1351, 1979.

[135] J. Mccarthy and R. Goffin, "Measuring job interview anxiety: Beyond weak knees and sweaty palms," *Pers. Psychol.*, vol. 57, pp. 607–637, 2004.

[136] A. K. Jaryal, N. Selvaraj, J. Santhosh, S. Anand, and K. K. Deepak, "Monitoring of cardiovascular reactivity to cold stress using digital volume pulse characteristics in health and diabetes," *J. Clin. Monit. Comput.*, vol. 23, no. 2, pp. 123–130, 2009.

[137] U. Panjwani, S. B. Singh, K. Harinath, D. K. Yadav, and W. Selvamurthy, "Effect of stress on somatosensory evoked potentials," *Stress Med.*, vol. 15, no. 1, pp. 35–40, 1999.

[138] D. A. Dimitriev, E. V Saperova, and A. D. Dimitriev, "State Anxiety and Nonlinear Dynamics of Heart Rate Variability in Students.," *PLoS One*, vol. 11, no. 1, 2016.

[139] O. Kwon, J. Jeong, H. Bin Kim, I. H. Kwon, S. Y. Park, J. E. Kim, and Y. Choi, "Electrocardiogram Sampling Frequency Range Acceptable for Heart Rate Variability Analysis," *Healthc. Inform. Res.*, vol. 24, no. 3, pp. 198–206, 2018.

[140] C. D. Spielberger, R. L. Gorsuch, R. Lushene, P. R. Vagg, and G. A. Jacobs, *State-Trait Anxiety Inventory for Adults, Manual, Instrument and Scoring Guide*. 1983.

[141] C. E. R. Warlar, "Integer coefficient bandpass filter for the simultaneous removal of baseline wander, 50 and 100 Hz interference from the ECG," *Med. Biol. Eng. Comput.*, vol. 29, no. 3, pp. 333–336, 1991.

[142] J. Pan and W. J. Tompkins, "A Real-Time QRS Detection Algorithm," *IEEE Trans. Biomed. Eng.*, vol. BME-32, no. 3, pp. 230–236, 1985.

[143] N. E. Huang, Z. Shen, S. R. Long, M. C. Wu, H. H. Shih, Q. Zheng, C. C. Tung, H. H. Liu, and P. R. S. L. A, "The empirical mode decomposition and the Hilbert spectrum for nonlinear and non-stationary time series analysis analysis," *R. Soc.*,

vol. 454, pp. 903–995, 1998.

[144] S. Dutta, M. Singh, and A. Kumar, “Classification of non-motor cognitive task in EEG based brain-computer interface using phase space features in multivariate empirical mode decomposition domain,” *Biomed. Signal Process. Control*, vol. 39, pp. 378–389, 2018.

[145] L. Cohen, “Time-frequency distributions-a review,” *Proc. IEEE*, vol. 77, no. 7, pp. 941–981, 1989.

[146] C. Chui, *An Introduction to Wavelets*, vol. 1. 1992.

[147] O. T. Inan, L. Giovangrandi, and G. T. A. Kovacs, “Robust neural-network-based classification of premature ventricular contractions using wavelet transform and timing interval features,” *IEEE Trans. Biomed. Eng.*, vol. 53, no. 12, pp. 2507–2515, 2006.

[148] T. Ince, S. Kiranyaz, and M. Gabbouj, “A Generic and Robust System for Automated Patient-Specific Classification of ECG Signals,” *IEEE Trans. Biomed. Eng.*, vol. 56, pp. 1415–1426, 2009.

[149] R. B. Pachori, P. Avinash, K. Shashank, R. Sharma, and U. R. Acharya, “Application of empirical mode decomposition for analysis of normal and diabetic RR-interval signals,” *Expert Syst. Appl.*, vol. 42, no. 9, pp. 4567–4581, 2015.

[150] R. B. Pachori, M. Kumar, P. Avinash, K. Shashank, and U. R. Acharya, “An improved online paradigm for screening of Diabetic patients using RR-interval signals,” *J. Mech. Med. Biol.*, vol. 16, no. 1, pp. 1–23, 2016.

[151] R. . Thuraisingham, Y. Tran, P. Boord, and A. Craig, “Analysis of eyes open , eye closed EEG signals using second-order difference plot,” *Med. Biol. Eng. Comput.*, vol. 45, no. 12, pp. 1243–1249, 2007.

[152] R. B. Pachori and V. Bajaj, “Analysis of normal and epileptic seizure EEG signals using empirical mode decomposition empirical mode decomposition,” *Comput. Methods Programs Biomed.*, vol. 104, no. April 2011, pp. 373–381, 2011.

[153] V. Bajaj and R. B. Pachori, “Classification of Seizure and Nonseizure EEG Signals Using Empirical Mode Decomposition,” *IEEE Trans. Inf. Technol. Biomed.*, vol.

16, no. 6, pp. 1135–1142, 2012.

[154] V. Bajaj and R. B. Pachori, “Epileptic Seizure Detection Based on the Instantaneous Area of Analytic Intrinsic Mode Functions of EEG Signals,” *Biomed. Eng. Lett.*, vol. 3, pp. 17–21, 2013.

[155] R. B. Pachori and S. Patidar, “Epileptic seizure classification in EEG signals using second-order difference plot of intrinsic mode functions,” *Comput. Methods Programs Biomed.*, vol. 113, no. 2, pp. 494–502, 2013.

[156] S. Ari and G. Saha, “Classification of heart sounds using empirical mode decomposition based features,” *Int. J. Med. Eng. Informatics*, vol. 1, no. 1, 2008.

[157] S. Sood, M. Kumar, R. B. Pachori, and U. R. Acharya, “Application of empirical mode decomposition – based features for analysis of normal and CAD heart rate signals,” *J. Mech. Med. Biol.*, vol. 16, no. 1, pp. 1–20, 2016.

[158] M. Kumar, R. B. Pachori, and U. Rajendra Acharya, “An efficient automated technique for CAD diagnosis using flexible analytic wavelet transform and entropy features extracted from HRV signals,” *Expert Syst. Appl.*, vol. 63, pp. 165–172, 2016.

[159] M. Kumar, R. B. Pachori, and U. R. Acharya, “Use of Accumulated Entropies for Automated Detection of Congestive Heart Failure in Flexible Analytic Wavelet Tranform Framework Based on Short-Term HRV Signals,” *Entropy*, vol. 19, no. 92, pp. 1–21, 2017.

[160] M. Cohen, D. Hudson, and P. Deedwania, “Applying Continuous Chaotic Modeling to Cardiac Signal Analysis,” *IEEE Eng. Med. Biol. Mag.*, vol. 15, no. 2, pp. 97–102, 1996.

[161] R. B. Pachori, D. J. Hewson, H. Snoussi, and J. Duchene, “Analysis of center of pressure signals using Empirical Mode Decomposition and Fourier-Bessel expansion,” in *TENCON 2008 - 2008 IEEE Region 10 Conference*, 2008, pp. 1–6.

[162] J. García, L. Sörnmo, S. Olmos, and P. Laguna, “Automatic Detection of ST-T Complex Changes on the ECG Using Filtered RMS Difference Series : Application to Ambulatory Ischemia Monitoring,” *IEEE Trans. Biomed. Eng.*, vol. 47, no. 9,

pp. 1195–1201, 2000.

[163] S. Lin, C. Chen, C. Lin, W. Yang, and C. Chiang, “Individual identification based on chaotic electrocardiogram signals during muscular exercise,” *Inst. Eng. Technol. Biometrics*, vol. 3, no. 4, pp. 257–266, 2014.

[164] C. M. Lim, U. R. Acharya, and S. Puthusserypady, “Entropies for detection of epilepsy in EEG,” *Comput. Methods Programs Biomed.*, vol. 80, pp. 187–194, 2006.

[165] R. Sharma, R. B. Pachori, and U. R. Acharya, “Application of Entropy Measures on Intrinsic Mode Functions for the Automated Identification of Focal Electroencephalogram Signals,” *Entropy*, vol. 17, pp. 669–691, 2015.

[166] W. Chen, Z. Wang, H. Xie, and W. Yu, “Characterization of Surface EMG Signal Based on Fuzzy Entropy,” *IEEE Trans. Neural Syst. Rehabil. Eng.*, vol. 15, no. 2, pp. 266–272, 2007.

[167] R. Sharma, M. Kumar, R. B. Pachori, and U. R. Acharya, “Decision support system for focal EEG signals using tunable-Q wavelet transform,” *J. Comput. Sci.*, vol. 20, pp. 52–0, 2017.

[168] A. Cord, C. Ambroise, and J. P. Cocquerez, “Feature selection in robust clustering based on Laplace mixture,” *Pattern Recognit. Lett.*, vol. 27, no. 6, pp. 627–635, 2006.

[169] S. Patidar, R. Bilas, and U. R. Acharya, “Automated diagnosis of coronary artery disease using tunable-Q wavelet transform applied on heart rate signals,” *Knowledge-Based Syst.*, vol. 82, pp. 1–10, 2015.

[170] K. S. Chua, “Efficient computations for large least square support vector machine classifiers,” *Pattern Recognit. Lett.*, vol. 24, pp. 75–80, 2003.

[171] J. A. K. Suykens and J. Vandewalle, “Least Squares Support Vector Machine Classifiers,” *Neural Process. Lett.*, vol. 9, no. 3, pp. 293–300, 1999.

[172] A. H. Khandoker, D. T. H. Lai, R. K. Begg, and M. Palaniswami, “Wavelet-Based Feature Extraction for Support Vector Machines for Screening Balance Impairments in the Elderly,” *IEEE Trans. Neural Syst. Rehabil. Eng.*, vol. 15, no.

4, pp. 587–597, 2007.

[173] H. Wang and D. Hu, “Comparison of SVM and LS-SVM for regression,” in *International Conference on Neural Networks and Brain*, 2005, no. 5, pp. 279–283.

[174] S. Patidar and R. B. Pachori, “Classification of cardiac sound signals using constrained tunable-Q wavelet transform,” *Expert Syst. Appl.*, vol. 41, no. 16, pp. 7161–7170, 2014.

[175] M. G. Poddar, V. Kumar, and Y. P. Sharma, “Heart rate variability based classification of normal and hypertension cases by linear-nonlinear method,” *Def. Sci. J.*, vol. 64, no. 6, pp. 542–548, 2014.

[176] L. Zunino, F. Olivares, F. Scholkmann, and O. A. Rosso, “Permutation entropy based time series analysis : Equalities in the input signal can lead to false conclusions,” *Phys. Lett. A*, vol. 381, no. 22, pp. 1883–1892, 2017.

[177] C. Bandt and B. Pompe, “Permutation entropy - a complexity measure for time series,” *Phys. Rev. Lett.*, vol. 88, no. 17, p. 174102, 2002.

[178] M. Kumar, R. B. Pachori, and U. R. Acharya, “Automated diagnosis of atrial fibrillation ECG signals using entropy features extracted from flexible analytic wavelet,” *Biocybern. Biomed. Eng.*, no. April, 2018.

[179] A. Kraskov, H. Stögbauer, and P. Grassberger, “Estimating mutual information,” *Phys. Rev. E - Stat. Physics, Plasmas, Fluids, Relat. Interdiscip. Top.*, vol. 69, no. 6, p. 16, 2004.

[180] C. M. R. Kitchen, “Nonparametric versus parametric tests of location in biomedical research,” *Am. J. Ophthalmol.*, vol. 147, no. 4, pp. 571–572, 2010.

[181] W. J. Dixon, “Power Under Normality of Several Nonparametric Tests,” *Ann. Math. Stat.*, vol. 25, no. 3, pp. 610–614, 1954.

[182] J. L. Hodges and E. L. Lehmann, “The Efficiency of Some Nonparametric Competitors of the t-Test,” *Ann. Math. Stat.*, vol. 27, no. 2, pp. 324–335, 1956.

[183] W. H. Kruskal and W. A. Wallis, “Use of Ranks in One-Criterion Variance

Analysis," *J. Am. Stat. Assoc.*, vol. 47, no. 260, pp. 583–621, 1952.

[184] K. Potter, "Methods for Presenting Statistical Information : The Box Plot," *Vis. Large Unstructured Data Sets*, vol. 4, pp. 97–106, 2006.

[185] D. F. Williamson, R. A. Parker, and J. S. Kendrick, "The box plot: A simple visual method to interpret data," *Ann. Intern. Med.*, vol. 110, no. 11, pp. 916–921, 1989.

[186] S. Theodoridis and K. Koutroumbas, *Pattern Recognition*, Second. San Diego, USA: Academic Press, 2003.

[187] W. Kao and C. Wei, "Automatic phonocardiograph signal analysis for detecting heart valve disorders," *Expert Syst. Appl.*, vol. 38, no. 6, pp. 6458–6468, 2011.

[188] K. A. Veselkov, V. I. Pahomov, J. C. Lindon, V. S. Volynkin, D. Crockford, G. S. Osipenko, D. B. Davies, R. H. Barton, J. W. Bang, E. Holmes, and J. K. Nicholson, "A metabolic entropy approach for measurements of systemic metabolic disruptions in patho-physiological states," *J. Proteome Res.*, vol. 9, no. 7, pp. 3537–3544, 2010.